The book cover features a dark blue background with a vertical red stripe on the left side. The title is printed in white text in the upper right quadrant. The author's name is printed in red text in the lower right quadrant, which is also a red area. The bottom right corner of the cover is missing, showing a white surface.

**Pseudospin Models
of
Boson Systems**

Dirk Jan Bukman

5 JAN 1982

BIBLIOTHEK
KONSTANTIN LORANTZ
an der Theologischen Fakultät
Postfach 2306 - 2300 LA Lüneburg
Niedersachsen

[Faint handwritten text]

PSEUDOSPIN MODELS
OF
BOSON SYSTEMS

PROOFSCRIPT

THE VERBODING VAN DE GRAD VAN DOCTOR AAN
DE RIJKSUNIVERSITEIT TE LEIDEN OP VERZAG VAN
DE RECTOR MAGISTRUS DR. A. L. F. DE VRIES, HOOG-
LERaar EN DECANUS DER FACULTEIT DER GODGELEERDHEID,
VOLGENS BESLUIT VAN HET COLLEGE VAN DEKANUS
TE VIERDAGEN OP DONNERSDAG 11 FEBRUARI 1964
TE KLOKKE 14.30 UUR.

DOOR

DIRK JAN BUKMAN

GENEEN TE AMSTERDAM IN 1963.

PSEUDOSPIN MODELS
OF
BOSON SYSTEMS

PSEUDOSPIN MODELS OF BOSON SYSTEMS

PROEFSCHRIFT

TER VERKRIJGING VAN DE GRAAD VAN DOCTOR AAN
DE RIJKSUNIVERSITEIT TE LEIDEN, OP GEZAG VAN
DE RECTOR MAGNIFICUS DR. L. LEERTOUWER, HOOG-
LERAAR IN DE FACULTEIT DER GODGELEERDHEID,
VOLGENS BESLUIT VAN HET COLLEGE VAN DEKANEN
TE VERDEDIGEN OP DONDERDAG 13 FEBRUARI 1992
TE KLOKKE 14.15 UUR

DOOR

DIRK JAN BUKMAN

GEBOREN TE AMSTELVEEN IN 1965

PSEUDOSPICY MODELS
OF
BOSON SYSTEMS

Promotiecommissie:

Promotor: Prof. dr. J.M.J. van Leeuwen
Overige leden: Prof. dr. C.W.J. Beenakker
Prof. dr. H.J. Habing
Prof. dr. H.J. Hilhorst
Dr. J.O. Indekeu
Prof. dr. ir. W. van Saarloos

VERKLARING
DE VERKLARING VAN DE DEEL VAN DOCTOR AAN
DE UNIVERSITEIT TE LEIJDE, OP DEN 14 JAN
DE RECTOR MAGISTRUS DR. J. L. DE GROOT, HEDER
LEZARE IN DE FACULTEIT DER GODGELEERDHEIT
VOLGENS BEVELT VAN HET COLLEGE VAN HOOGERE
LEZERS OP ZONDAG 11 FEBRUARI 1966
IN FLORES 144 016

DOOS

DIRK JAN BUKMAN

GEBOREN TE AMSTERDAM IN 1941

Part of this research was supported by the "Stichting voor Fundamenteel Onderzoek der Materie (FOM)" which is financially supported by the "Stichting Nederlands Wetenschappelijk Onderzoek (NWO)".

Contents

1	Introduction	1
2	Preliminary considerations	5
2.1	The interacting boson system	5
2.2	The pseudospin model	6
2.3	Some real-space renormalization approaches	10
2.3.1	Migdal-Kadanoff renormalization	11
2.3.2	Cumulant and cluster methods	12
3	Cluster variation approach to the spin- $\frac{1}{2}$ XXZ model	15
3.1	Introduction	15
3.2	The cluster variation method	17
3.3	The two-spin cluster	19
3.4	The minimization of \mathcal{F}	26
3.4.1	The phases without x - y order	26
3.4.2	The phases with x - y order	28
3.5	Results	29
3.6	Discussion	35
3.A	Appendix	37
4	The phase diagram of the XXZ model for slab and layered geometries	41
4.1	Introduction	41
4.2	General theory	43
4.3	The spatially anisotropic geometry	47
4.3.1	The calculation of M^p	48
4.3.2	Results	50
4.4	The slab geometry	52
4.4.1	The calculation of M^p	53
4.4.2	The case $H = 0$	54
4.4.3	Results	58
4.5	Discussion	60
4.A	Appendix	63

5	Mean field renormalization group for the spin-$\frac{1}{2}$ XXZ model	69
5.1	Introduction	69
5.2	The mean field renormalization group	70
5.3	Results of the two-cluster method	72
5.3.1	The triangular lattice	74
5.3.2	The square lattice	76
5.3.3	The three-dimensional lattices	77
5.4	Results of the three-cluster method	78
5.5	Discussion	80
6	The t-matrix for collisions of hard spheres in a layer geometry	85
6.1	Introduction	85
6.2	The hard sphere t -matrix	88
6.3	A layer of infinite width	90
6.4	A layer of zero width	91
6.5	A finite layer with periodic boundary conditions	93
6.5.1	The case $w < a$	93
6.5.2	The case $w \geq a$	98
6.6	A finite layer with zero boundary conditions	101
6.7	Discussion	104
6.A	Bessel functions	105
6.B	The continuity equations at $r = w$	106
	Samenvatting	109
	Curriculum vitae	113

1. General Introduction	1
2. Theoretical Foundations	10
3. Experimental Methods	20
4. Results and Discussion	30
5. Conclusions	40
6. Acknowledgments	45
7. References	50
8. Appendix	60
9. Bibliography	70
10. Index	80
11. Glossary	90
12. Summary	100
13. Bibliography	110
14. Index	120
15. Glossary	130
16. Summary	140
17. Bibliography	150
18. Index	160
19. Glossary	170
20. Summary	180
21. Bibliography	190
22. Index	200
23. Glossary	210
24. Summary	220
25. Bibliography	230
26. Index	240
27. Glossary	250
28. Summary	260
29. Bibliography	270
30. Index	280
31. Glossary	290
32. Summary	300
33. Bibliography	310
34. Index	320
35. Glossary	330
36. Summary	340
37. Bibliography	350
38. Index	360
39. Glossary	370
40. Summary	380
41. Bibliography	390
42. Index	400
43. Glossary	410
44. Summary	420
45. Bibliography	430
46. Index	440
47. Glossary	450
48. Summary	460
49. Bibliography	470
50. Index	480
51. Glossary	490
52. Summary	500
53. Bibliography	510
54. Index	520
55. Glossary	530
56. Summary	540
57. Bibliography	550
58. Index	560
59. Glossary	570
60. Summary	580
61. Bibliography	590
62. Index	600
63. Glossary	610
64. Summary	620
65. Bibliography	630
66. Index	640
67. Glossary	650
68. Summary	660
69. Bibliography	670
70. Index	680
71. Glossary	690
72. Summary	700
73. Bibliography	710
74. Index	720
75. Glossary	730
76. Summary	740
77. Bibliography	750
78. Index	760
79. Glossary	770
80. Summary	780
81. Bibliography	790
82. Index	800
83. Glossary	810
84. Summary	820
85. Bibliography	830
86. Index	840
87. Glossary	850
88. Summary	860
89. Bibliography	870
90. Index	880
91. Glossary	890
92. Summary	900
93. Bibliography	910
94. Index	920
95. Glossary	930
96. Summary	940
97. Bibliography	950
98. Index	960
99. Glossary	970
100. Summary	980
101. Bibliography	990
102. Index	1000

Chapter 1

Introduction

The two relevant isotherms of the present system are those of ^{20}Ne and ^{22}Ne . These are the only isotherms that at several pressures remain liquid down to the absolute zero temperature. It would be likewise presumed at least to hold for neon in general. The cause of this behavior is the combination of the delocalization giving rise to a large zero-point energy, and the weakness of the interatomic attraction, which is overcome by the large zero-point motion. These features of a two-quantum fluid, in the case of ^{20}Ne and ^{22}Ne , are qualitatively similar to those of ^4He and ^3He at the low temperature. Since the first observation of liquid helium, by H. Kamerlingh Onnes in 1908, there has been continuous research concerning its peculiar macroscopic properties.

The most spectacular manifestation of such quantum behavior of atoms is the superfluidity of ^4He , discovered in 1937, which at several pressures exists below 4.2 K in one flow without dissipation, and has many other anomalous properties that cannot possibly have their classical origin, that is, that cannot be explained by the classical hydrodynamics. The most striking characteristic of the superfluidity of ^4He was probably its frictionless motion, which was first observed as a specific mechanical effect and later confirmed by the experiment of Onsager (1954). This unusual, non-dissipative, liquid ^4He , which consists of bosons, does not behave superficially in this way.

If one wants to understand the behavior of liquid ^4He one can consider the phase diagram based on the properties of the constituent particles, the microscopic structure of the atoms, which is the same as that of the other noble gases, and the nature of the interatomic forces, which are the same as those of the other noble gases.

*'Tis pleasant, sure, to see one's name in print;
A book's a book, although there's nothing in't.*

Byron

This can be done by using perturbation theory, by the method of Feynman diagrams, which is the way the interaction potential is treated. This can be done for a system of bosons, but it is not obtained when the attractive forces are the largest strong in magnitude. The hard sphere does not give the same results as one

The present, says, is not a time to
A look a look, although there's nothing in it.

1915

Chapter 1

Introduction

In nature, two different isotopes of the element helium are found, ^3He and ^4He . These are the only substances that, at normal pressure, remain liquid down to the absolute zero of temperature. To solidify helium, a pressure of at least $25 \cdot 10^5$ Pa must be applied. The cause of this behaviour is the small mass of the helium atoms, giving rise to a large zero-point energy, and the weakness of the interparticle attraction, which is overpowered by the large zero-point motion. Thus, helium is a true quantum fluid, in the sense that, at low temperatures, quantum effects have a large influence on its behaviour. Since the first observation of liquid helium, by H. Kamerlingh Onnes in 1908, there has been continuous interest in studying its quantum mechanical properties.

The most spectacular manifestation of such quantum mechanical effects is the superfluidity of ^4He . Superfluid ^4He , which at normal pressure exists below 2.18 K, can flow without dissipation, and has many other extraordinary properties that distinguish it from the normal liquid that exists above 2.18 K. Theoretically, superfluidity is interpreted as Bose-Einstein condensation of the ^4He atoms. This is a purely quantum mechanical effect that only occurs in systems composed of bosons (like ^4He atoms). And indeed, liquid ^3He , which consists of fermions, does not become superfluid in this way.

If one wants to understand the behaviour of liquid ^4He (e.g. to calculate the phase diagram) based on the properties of the constituent particles, the microscopic properties of the atoms, which are well known, must be translated into macroscopic properties of the fluid. This cannot be done exactly, except in the case of an ideal, non-interacting Bose gas, where the description of Bose-Einstein condensation is not very difficult. But this ideal system is rather artificial and unphysical, and certainly not a good model for a real fluid like ^4He . To give a good description of this fluid one must take into account the interaction between the helium atoms, especially the strong short-range repulsion between them.

This can be done by using perturbation theory; by that method one can systematically improve the way the interaction potential is treated. This has been done for a system of bosonic hard spheres, which is obtained when the attraction between the helium atoms is neglected. The hard sphere Bose gas has many features in com-

mon with real ${}^4\text{He}$. From this perturbative approach a number of low temperature properties of ${}^4\text{He}$ are correctly found. However, this approach is only justified at low density, and not at densities like that of liquid ${}^4\text{He}$. Also, the complexity of the calculation increases rapidly with the improvement of the approximation. Particularly for systems in non-trivial geometries, like thin layers of ${}^4\text{He}$, it is hard to obtain results in this way. This is apparent from chapter 6, where an essential quantity in the description of many-particle systems, the t -matrix, is examined. In particular its behaviour in a slab geometry and the cross-over from two to three dimensions are considered.

A different approach, and the one that is mainly used in this thesis, is to study a simplified model that still, one expects, contains the essential ingredients of the real ${}^4\text{He}$ fluid. In this way one can get insight into the behaviour of this system, if not quantitatively then at least qualitatively, without having to deal with all the complexities of the real liquid. The model with which most of this thesis is concerned consists of bosonic particles that move on a lattice instead of moving freely through space. Their motion is further restricted to hops from one lattice site to an adjacent one. The interparticle interaction is represented by an interaction between two particles on neighbouring lattice points. The hard core of the potential is taken care of by preventing two particles from occupying the same lattice site. To study this model one can use the many techniques that have been developed for dealing with lattice models. The fact that both the movement of the particles and the interaction between particles are localized, further facilitates the problem of calculating the properties of this system. Even so, it is impossible to treat this simplified model exactly, and approximations have to be made in order to extract information from it.

Before doing this, in chapter 2 we discuss the relation between the description of the real system of ${}^4\text{He}$ particles, and the lattice model discussed above. It is shown how the model of interacting bosons in free space is transformed into the lattice model, and how the properties of the helium atoms correspond with the parameters of that model. Also, the lattice model is rephrased in terms of quantum spins, which is exactly equivalent to the original description. The correspondence between the spin- $\frac{1}{2}$ XXZ model and the lattice model is discussed. The reason for introducing this pseudospin model is twofold. First, the wealth of knowledge about magnetic spin models can now also be applied to the lattice boson model. Second, it is, at least for the author of this thesis, easier to think about problems in terms of spins than in terms of particles. Since there is an exact, one-to-one correspondence between the two, this is largely a matter of taste. A major part of this thesis is devoted to the calculation of some of the properties of this model in two approximations.

In chapter 3 we apply the pair approximation of the so-called cluster variation method to the spin model. This is a well-known method to find the phase diagram of statistical systems, and its results are usually quite good. This is also the case for our spin model, although the fact that we are dealing with quantum spins gives rise to some complications. Nevertheless, in most cases the method works satisfactorily.

In chapter 4 we apply the same method to spin models on a lattice with a more complicated geometry, like a slab that has a finite width in one direction. The cluster variation method is able to deal with these geometries very well, and the results are again quite good. Also, for this inhomogeneous geometry we find expressions for the profile of, e.g., the order parameter in the slab.

Chapter 5 concerns another method, the mean field renormalization group, which is again applied to the XXZ model. It appears that the simplest version of this method gives the same results as the pair approximation of the cluster variation method. This turns out to be a coincidence, and as the method is further refined the connection with the cluster variation method is lost. The mean field renormalization method does not always work well when dealing with quantum spins, but it does produce meaningful results for the phase transitions.

Chapter 2

Preliminary considerations

2.1 The interacting boson system

A system of interacting bosons of mass m , with an interparticle potential $\phi(\mathbf{r}, \mathbf{r}')$, has the following Hamiltonian in terms of the field operators $\psi(\mathbf{r})$ and $\psi^\dagger(\mathbf{r})$

$$\begin{aligned} \mathcal{H}_B = & -\frac{\hbar^2}{2m} \int d^3r \psi^\dagger(\mathbf{r}) \nabla^2 \psi(\mathbf{r}) \\ & -\frac{1}{2} \int \int d^3r d^3r' \psi^\dagger(\mathbf{r}) \psi^\dagger(\mathbf{r}') \phi(\mathbf{r}, \mathbf{r}') \psi(\mathbf{r}') \psi(\mathbf{r}). \end{aligned} \quad (2.1.1)$$

The field operators $\psi(\mathbf{r})$ and $\psi^\dagger(\mathbf{r})$ satisfy Bose commutation relations

$$\begin{aligned} [\psi^\dagger(\mathbf{r}'), \psi(\mathbf{r})] &= \delta(\mathbf{r}' - \mathbf{r}), \\ [\psi^\dagger(\mathbf{r}'), \psi^\dagger(\mathbf{r})] &= [\psi(\mathbf{r}'), \psi(\mathbf{r})] = 0. \end{aligned} \quad (2.1.2)$$

To study the thermodynamics of such a system with a variable number of particles, one should consider the grand partition function, given by

$$\Xi = \text{Tr} e^{-\beta(\mathcal{H}_B - \mu \mathcal{N})}, \quad (2.1.3)$$

with $\beta = 1/k_B T$, μ the chemical potential, and \mathcal{N} the number operator given by

$$\mathcal{N} = \int d^3r \psi^\dagger(\mathbf{r}) \psi(\mathbf{r}). \quad (2.1.4)$$

In the case of ^4He particles the interaction potential $\phi(\mathbf{r}, \mathbf{r}')$ depends only on the distance $|\mathbf{r} - \mathbf{r}'|$, and to a reasonable approximation it is given by the Lennard-Jones 6-12 potential,

$$\phi(r) = -4\epsilon \left\{ \left(\frac{\sigma}{r} \right)^6 - \left(\frac{\sigma}{r} \right)^{12} \right\}, \quad (2.1.5)$$

with $\sigma = 0.256$ nm and $\epsilon = 14.11 \cdot 10^{-23}$ J. Other systems will, of course, have different interaction potentials.

The phenomenon of superfluidity in a boson system is signalled by the appearance of so-called off-diagonal long-range order (ODLRO) in the one-particle reduced density matrix, $\rho^{(1)}(\mathbf{r}_1, \mathbf{r}_2) \equiv \langle \psi^\dagger(\mathbf{r}_1)\psi(\mathbf{r}_2) \rangle$ [1]. (The average $\langle \dots \rangle$ must be taken in an ensemble that allows the gauge symmetry corresponding to the conservation of the number of particles to be broken; e.g. the η -ensemble introduced by Hohenberg and Martin [2].) A system has ODLRO when the off-diagonal elements of $\rho^{(1)}$ are non-zero in the limit $|\mathbf{r}_1 - \mathbf{r}_2| \rightarrow \infty$. The value they approach is in fact $\langle \psi^\dagger(\mathbf{r}_1) \rangle \langle \psi(\mathbf{r}_2) \rangle$. Hence, the presence of ODLRO is equivalent to a non-zero expectation value $\langle \psi(\mathbf{r}) \rangle$, and $\langle \psi(\mathbf{r}) \rangle$ is the order parameter of the superfluid phase. It is also the macroscopic wave function of the superfluid condensate, and its square is the density of the condensate, $|\langle \psi(\mathbf{r}) \rangle|^2 = n_0(\mathbf{r})$.

One can approximate the potential $\phi(\mathbf{r})$ by a hard sphere potential with a radius σ . The attraction between the atoms is then replaced by a uniform background potential which gives the system its density [3]. The resulting gas of hard spheres has many of the properties of the ^4He system, including a superfluid phase. This gas has been examined with perturbational methods [4]. The approximations made are only valid for $n\sigma^3 \ll 1$, where n is the density of the hard sphere gas. A number of low temperature features of ^4He , like the linear slope of the energy spectrum, are correctly obtained by this method. But for parameters in the range of those appropriate for ^4He the above inequalities are not satisfied, and so the perturbative approach is not well founded. Therefore we turn to a different method to deal with the boson system under consideration.

2.2 The pseudospin model

In order to make the system described by the Hamiltonian (2.1.1) more manageable, we make some simplifications. First, we discretize space so that the bosons are restricted to move on a lattice. Second, we cut off the interaction potential $\phi(\mathbf{r})$ such that only particles that are nearest neighbours on the lattice interact, with an interaction strength ϕ_0 . The hard core repulsion of the interaction is incorporated by limiting the number of particles that can occupy a lattice site to one[†].

The creation and annihilation operators for a particle at a lattice site i are a_i^\dagger and a_i . They are related to the field operators by

$$\psi^{(t)}(\mathbf{r}_i) \rightarrow \frac{1}{\sqrt{v_0}} a_i^{(t)}, \quad (2.2.1)$$

where v_0 is the volume of the cell surrounding a lattice site. All integrals over space are changed into sums through

[†]Instead of particles moving on a lattice, one can also think of cells in space that are, or are not, occupied by a particle.

$$\int d^3r \rightarrow v_0 \sum_{i=1}^N. \quad (2.2.2)$$

Here, N is the total number of lattice sites. The operators a_i^\dagger and a_i have Bose commutation relations for different lattice sites,

$$[a_i^\dagger, a_j] = [a_i^\dagger, a_j^\dagger] = [a_i, a_j] = 0, \quad (i \neq j), \quad (2.2.3)$$

and Fermi anticommutation relations for the same site in order to exclude double occupancy of a lattice site,

$$\begin{aligned} \{a_i^\dagger, a_i\} &= 1, \\ \{a_i^\dagger, a_i^\dagger\} &= \{a_i, a_i\} = 0. \end{aligned} \quad (2.2.4)$$

The number operator for site i is given by

$$n_i = a_i^\dagger a_i, \quad (2.2.5)$$

and has eigenvalues 0 and 1.

To find the lattice version of the Hamiltonian (2.1.1), we discretize the kinetic energy term \mathcal{K} , which gives [5]

$$\mathcal{K} = -\frac{\hbar^2 d}{mz a^2} \sum_{i=1}^N a_i^\dagger \sum_{\delta} (a_{i+\delta} - a_i), \quad (2.2.6)$$

with d the dimension, z the coordination number, a the lattice constant, and the sum \sum_{δ} running over vectors connecting site i with its nearest neighbours. The discrete version of the total Hamiltonian used in the grand canonical ensemble is then

$$\mathcal{H}_B - \mu \mathcal{N} = -\frac{\hbar^2 d}{mz a^2} \sum_{\langle ij \rangle} (a_i^\dagger a_j + a_j^\dagger a_i) - \phi_0 \sum_{\langle ij \rangle} a_i^\dagger a_i a_j^\dagger a_j - \bar{\mu} \sum_{i=1}^N a_i^\dagger a_i, \quad (2.2.7)$$

with $\bar{\mu} = \mu - \hbar^2 d / ma^2$.

The operators a_i and a_i^\dagger with the commutation relations given above are isomorphic to a system of Pauli spins [6]. By defining

$$\begin{aligned} a_j^\dagger &= \frac{1}{2}(\sigma_j^x + i\sigma_j^y) \\ a_j &= \frac{1}{2}(\sigma_j^x - i\sigma_j^y) \\ a_j^\dagger a_j &= \frac{1}{2}(1 + \sigma_j^z), \end{aligned} \quad (2.2.8)$$

we can rewrite (2.2.7) as a spin Hamiltonian

$$\begin{aligned}\mathcal{H}_B - \mu N &= \mathcal{H} + E_0 \\ &= -J \sum_{\langle ij \rangle} (\sigma_i^x \sigma_j^x + \sigma_i^y \sigma_j^y) - J_z \sum_{\langle ij \rangle} \sigma_i^z \sigma_j^z - H \sum_{i=1}^N \sigma_i^z + E_0,\end{aligned}\quad (2.2.9)$$

with

$$\begin{aligned}J &= \frac{\hbar^2 d}{2mza^2}, & J_z &= \frac{\phi_0}{4}, \\ H &= \frac{\mu}{2} - \frac{\hbar^2 d}{2ma^2} + \frac{z\phi_0}{4}, \\ E_0 &= N \left(-\frac{\mu}{2} + \frac{\hbar^2 d}{2ma^2} - \frac{z\phi_0}{8} \right).\end{aligned}\quad (2.2.10)$$

The correspondence between the two systems is given by the fact that the grand partition function Ξ of the lattice gas is, apart from a trivial factor, equal to the partition function of the spin system,

$$\Xi = e^{-\beta E_0} Z, \quad (2.2.11)$$

with

$$Z = \text{Tr} e^{-\beta \mathcal{H}}. \quad (2.2.12)$$

The thermodynamics of these systems now follows from the free energy of the spin system,

$$F = -k_B T \ln Z, \quad (2.2.13)$$

which corresponds to the pressure in the lattice gas,

$$pV = k_B T \ln \Xi = -E_0 - F. \quad (2.2.14)$$

The number density $\langle n_i \rangle$ of the lattice gas is, according to (2.2.8), given by

$$\langle n_i \rangle = \frac{1}{2} (1 + \langle \sigma_i^z \rangle). \quad (2.2.15)$$

It can be seen from (2.2.10) that the interparticle interaction ϕ_0 gives rise to the coupling J_z of the z -components of the spins, which is ferromagnetic (antiferromagnetic) for an attractive (repulsive) interaction. The x - y interaction arises from the quantum kinetic energy (2.2.6), and it is always ferromagnetic. The magnetic field H , which controls the magnetization $\langle \sigma_i^z \rangle$, roughly corresponds to the chemical potential μ governing the density of the lattice gas.

The ordered phases of the spin model depend on the specific values of the coupling constants J and J_z . If J_z is positive and larger than J , there is an Ising-like ferromagnetic phase, with the magnetization $\langle \sigma_i^z \rangle$ as the order parameter. For $J > J_z > 0$, the system will develop a magnetization in the x - y plane¹, with $\langle \sigma_i^z \rangle \neq 0$. On bipartite lattices, for $-J_z > |J|$, an antiferromagnetic phase forms with a non-zero staggered magnetization, $\langle \sigma_a^z \rangle - \langle \sigma_b^z \rangle$ (a and b are the two sublattices of the bipartite lattice). In this case the sign of J is irrelevant, since for such a lattice the cases $J > 0$ and $J < 0$ are related by a global spin reversal on one sublattice.

In the lattice gas the ferromagnetic Ising phase transition can be interpreted as a gas-liquid transition, since the order parameter is the density $\langle n_i \rangle$. The x - y ordered phase, where $\langle \sigma_i^z \rangle$ is non-zero, corresponds to a phase with a non-zero expectation value for the creation and annihilation operators, $\langle a_i^\dagger \rangle = \langle a_i \rangle \neq 0$, and hence $\langle \psi(\mathbf{r}) \rangle \neq 0$. This phase, exhibiting ODLRO, is the superfluid phase of the lattice gas. The antiferromagnetic phase of the spin model corresponds to a phase where the bosons, due to a repulsive interaction, preferentially occupy one sublattice. For the study of a lattice gas or liquid, where the interactions are usually attractive (as is the case for ⁴He), this phase seems to be of less relevance.

The relative importance of quantum effects can be expressed as the ratio J/J_z ,

$$J/J_z = \frac{2h^2d}{mza^2\phi_0} = \frac{d}{2z\pi^2}\Lambda^2, \quad (2.2.16)$$

where the de Boer parameter Λ is given by

$$\Lambda = \frac{h}{\sqrt{m\phi_0 a^2}}. \quad (2.2.17)$$

For a system of hard spheres we have $\Lambda = \infty$, and this extreme quantum case thus corresponds to a pure x - y interaction ($J_z = 0$). Since the x - y ordered phase corresponds to the superfluid phase, the lattice version of the hard sphere gas has such a phase. This confirms the assertion that a hard sphere gas is a good model for liquid ⁴He. However, if we try to find realistic values for J and J_z for ⁴He by substituting the values $m = 4 \cdot 1.67 \cdot 10^{-27}$ kg, $\phi_0 = 14.11 \cdot 10^{-23}$ J, and $a = 0.256$ nm, we find $\Lambda = 2.67$, and consequently $J/J_z = 0.18$ in the case of a simple cubic lattice. So even though ⁴He has one of the highest known values for Λ , it is not high enough to make $J/J_z > 1$. Hence the corresponding spin model does not have an x - y ordered phase, and the lattice fluid does not have a superfluid phase. To find a ratio J/J_z that is larger than one, Λ should be larger than 6. So, by going from the continuum to the lattice in this way, one loses the possibility of accurately modelling real fluids. This is not surprising, since the nearest neighbour lattice model can never be more

¹In two dimensions there can be no magnetization, and there is a phase with topological order instead. The methods we use cannot reproduce this, and give a phase with a finite magnetization, even in two dimensions. Therefore we cannot consider the subtleties associated with the so-called Kosterlitz-Thouless phase transition.

than a very simplified model of a real system. Still, as the case of the hard sphere gas shows, the lattice model does contain the essential physics of a quantum fluid.

Another objection to the lattice model is the observation that it can never have both a gas-liquid transition and a superfluid transition in the same system. The competition between J and J_z forces the system to choose between these possibilities and does not allow a combination of the two. In the case of the hard sphere gas this is not a problem, because in the absence of an attractive interaction between the particles there is no gas-liquid phase transition. If one uses the model for describing ^4He , the best it can do is give a qualitative description of some aspects of its behaviour, like the superfluid transition. It will not reproduce the phase diagram in full.

The lattice model should be better suited for describing systems where the quantum kinetic energy dominates over the interaction potential. A candidate for such a system is the gas of vacancies that exists in ^4He crystals [7]. They are bosons, and they clearly have a hard-core repulsion (two vacancies cannot sit at the same lattice site). Due to their small effective mass and the weak interaction between vacancies the kinetic term is much more important than the interaction term. An additional bonus is the fact that the vacancies move on a real lattice, namely the hcp lattice of the helium crystal. The lattice model is also often used in theories for high temperature superconductors that assume the existence of real-space electron pairs [8, 9]. Lastly, results obtained for the pseudospin model can, of course, also be applied to spin models for real magnetic systems.

2.3 Some real-space renormalization approaches

Real-space renormalization is a powerful technique that has been applied to many physical systems [10, 11]. The idea behind this approach is to eliminate the original degrees of freedom (e.g. spins) in a system, and replace them by degrees of freedom on a coarser scale (e.g. the block spins introduced by Kadanoff [12]), while leaving the partition function of the system invariant. This procedure leads to a transformation between systems at different length scales. The transformation has a fixed point if the coupling constants of the system are chosen such that it is invariant under the transformation. For a system with a phase transition there are usually two trivial, attractive fixed points at $T = 0$ and $T = \infty$ governing its behaviour at low and high temperatures, and a repulsive fixed point corresponding to the critical point at $T = T_c$. Most applications of this technique concerned classical models, but several real-space renormalization group methods have also been applied to quantum spin models.

In this section we briefly review two of these applications. First we discuss a simple technique introduced by Migdal and Kadanoff, and subsequently a more general class of real-space renormalization techniques. In both instances, the quantum nature of the spins gives rise to two complications. The first is the fact that the terms in the

Hamiltonian do not commute. This must be neglected when eliminating the original spins, and this is an approximation that is only valid at high temperatures. The second, more important problem is that the ground state of a cluster of quantum spins is generally not preserved in the decimation process. So if the original spin system is in the ground state, the new system of block spins, obtained after the decimation, is not. The effect of this is that the $T = 0$ fixed point is destroyed.

As a result of these two facts, real-space renormalization procedures are of limited use for quantum spins. In the region of the phase diagram where the z coupling is positive and larger than the x - y coupling, the ground state is preserved, so that the renormalization method gives reasonable results for the Ising part of the phase transition. In those systems where the x - y interaction dominates, or where the z interaction is antiferromagnetic, the validity of real-space renormalization methods is doubtful.

2.3.1 Migdal-Kadanoff renormalization

One of the simplest renormalization techniques is the Migdal-Kadanoff method [13, 14, 15]. Because of its simplicity it has been used to get a qualitative picture of the phase diagrams of many classical lattice systems. Its application to quantum spin models [16], which we discuss here, is more problematic.

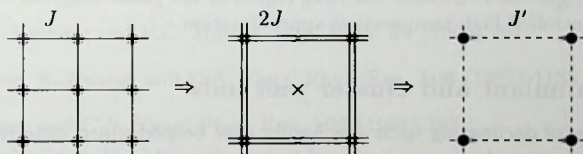


Fig. 2.1. The two steps of the Migdal-Kadanoff renormalization procedure for a rescaling factor 2. First, bonds (representing the coupling J between nearest neighbour spins (dots)) are moved in order to decouple the spins that are to be decimated (crosses). The coupling constant of the remaining bonds is consequently doubled. Next, the decimation of the spins is performed, giving a new, rescaled lattice, and a new coupling constant J' .

The renormalization procedure consists of two steps (see figure 2.1). First, a potential moving scheme introduced by Kadanoff [14] is applied. The result of this is a lattice with less, but stronger, couplings between the spins, which makes it easier to eliminate some of the spins in the next step. In the second step, a number of spins is summed out, so that the remaining spins form a lattice that is identical to the original one, but rescaled by a factor. The coupling constants for this new lattice are calculated from the original ones through the decimation of the spins. By iterating

this procedure, and looking for fixed points, an approximation for the critical point and the critical exponents of the spin model can be obtained.

For classical spins, the strength of this method lies in the fact that it is exact in both the high and low temperature limits, and can thus be expected to give a reasonably good interpolation for intermediate temperatures. In particular near the lower critical dimension d_c , where T_c is low, it should be a good approximation. For quantum systems, this is only the case for systems with $J_z \geq J > 0$ because of the two problems mentioned above [17]. Only then does the bond moving procedure preserve the ground state of the quantum spin system. For other values of J and J_z the system at $T = 0$ is mapped onto a finite temperature, or onto the $T = 0$ fixed point corresponding to a different symmetry class.

The effect of this is apparent in the calculation for the XXZ model. The ferromagnetic Ising phase is described well, and the lower critical dimension of the Heisenberg model is correctly given as 2. The rest of the phase diagram is less convincing. There, the renormalization flow for different symmetry classes of the Hamiltonian is directed towards the same $T = 0$ fixed point. Also, spurious fixed points appear at low temperature. In short, the low temperature behaviour of the transformation is not reliable here (for more details see [18]). Since the success of the Migdal-Kadanoff approximation rests upon the fact that it is an interpolation between correct procedures at high and low temperatures, it is questionable what its value is if one of these limits is no longer valid. Outside the Ising region of the phase diagram it is no more than an uncontrolled high temperature approximation.

2.3.2 Cumulant and cluster methods

The procedure of decimating spins can hardly ever be performed exactly. Therefore an approximate procedure must be found to transform the old system into the new, rescaled system by replacing the spins inside certain cells by block spins. Apart from the Migdal-Kadanoff method, two other approximation schemes are widely used to perform the decimation [19, 20, 21, 22]. The cumulant approximation treats the couplings within the basic cells exactly, and perturbation theory is used for the couplings between the cells. This use of perturbation theory is rather dangerous, since the inter-cell couplings are generally of equal strength to the intracell couplings. Consequently the convergence of this method is not very good. In the cluster approximation the decimation is performed exactly for finite clusters. This method does give better results as the cluster size is increased, at the price of an increasing amount of book-keeping that has to be done to keep track of the contributions of the various clusters.

For quantum spins, both approximations involve a mapping of the 2^N states of a subsystem of N spins onto $2^{N'}$ states of a smaller subsystem of N' spins. In order to have a well-behaved renormalization transformation, there should at least be the usual fixed points at $T = 0$ and $T = \infty$. The $T = \infty$ fixed point is always there, but to have a fixed point at $T = 0$ the ground state of the larger cluster should be mapped

onto the ground state of the smaller one. Because one has considerable freedom in choosing the details of the transformation, this can usually be arranged for a simple model. But if one tries to apply one single transformation to a model like the XXZ model, for arbitrary ratios J_z/J , this is only possible in the region $J_z \geq J > 0$. In the rest of the phase diagram such a transformation cannot be found. On the contrary, if one wants the transformation to preserve the different symmetries of the Hamiltonian of such a model, then this puts extra constraints on the properties of the transformation [23]. It is not possible to find a renormalization transformation that satisfies all these demands for the whole phase diagram. One is now faced with the choice between artificially limiting the parameter space of the system one considers, by, e.g., constructing a transformation for a single, fixed ratio of J_z/J , or, on the other hand, using a general transformation that does not have fixed points at $T = 0$ in a large part of the parameter space. Neither of these choices is satisfactory; the conclusion is again that outside the Ising region, real-space renormalization is not very useful for quantum spin systems.

References

- [1] See, e.g., K. Huang, *Statistical Mechanics* (2nd edition), Wiley, New York, 1987, Chap. 12
- [2] P.C. Hohenberg and P.C. Martin, *Ann. Phys.* **34** (1965) 291
- [3] T.D. Lee, K. Huang, and C.N. Yang, *Phys. Rev.* **106** (1957) 1135
- [4] K. Huang and C.N. Yang, *Phys. Rev.* **105** (1957) 767
- [5] J. Stephenson, in: *Physical Chemistry*, Vol. VIII B (H. Eyring, D. Henderson, and W. Jost, eds.), Academic Press, New York, 1971
- [6] T. Matsubara and H. Matsuda, *Prog. Theor. Phys.* **16** (1956) 569;
H. Matsuda and T. Matsubara, *Prog. Theor. Phys.* **17** (1957) 19
- [7] G.A. Lengua and J.M. Goodkind, *J. Low Temp. Phys.* **79** (1990) 251
- [8] L.J. de Jongh, *Physica C* **161** (1989) 631
- [9] R. Micnas, J. Ranninger, and S. Robaszkiewicz, *Rev. Mod. Phys.* **62** (1990) 113
- [10] Th. Niemeijer and J.M.J. van Leeuwen, in: *Phase Transitions and Critical Phenomena*, Vol. 6 (C. Domb and M.S. Green, eds.), Academic Press, London, 1976
- [11] *Real Space Renormalization* (T.W. Burkhardt and J.M.J. van Leeuwen, eds.), Springer, Berlin, 1982

- [12] L.P. Kadanoff, *Physics* **2** (1966) 263
- [13] A.A. Migdal, *Sov. Phys. JETP* **42** (1976) 743
- [14] L.P. Kadanoff, *Ann. Phys.* **100** (1976) 359
- [15] T.W. Burkhardt, in [11]
- [16] H. Takano and M. Suzuki, *J. Stat. Phys.* **26** (1981) 635
- [17] M. Barma, D. Kumar, and R.B. Pandey, *J. Phys. C* **12** (1979) L283, L909
- [18] C. Castellani, C. Di Castro, and J. Ranninger, *Nucl. Phys. B* **200** [FS4] (1982) 45
- [19] J. Rogiers and R. Dekeyser, *Phys. Rev.* **B13** (1976) 4886
- [20] D.D. Betts and M. Plischke, *Can. J. Phys.* **54** (1976) 1553
- [21] R. Dekeyser, M. Reynaert, A.L. Stella, and F. Toigo, *Phys. Rev. B* **18** (1978) 3486
- [22] A.L. Stella, C. Vanderzande, and R. Dekeyser, *Phys. Rev. B* **27** (1983) 1812
- [23] R.C. Brower, F. Kuttner, M. Nauenberg, and K. Subbarao, *Phys. Rev. Lett.* **38** (1977) 1231

Chapter 3

Cluster variation approach to the spin- $\frac{1}{2}$ XXZ model[†]

3.1 Introduction

Magnetic spin models have been extensively discussed in the literature. Interest in these models derives not only from the need to describe magnetic materials in a simplified way, but also from the fact that certain many-particle systems can be mapped onto such spin models. For instance, simple lattice gas models for classical [1, 2] and quantum [3] fluids have been shown to be equivalent to Ising and XXZ spin models, respectively. Also, the extended Hubbard Hamiltonian can, in the limit of strong attraction, be mapped onto an XXZ spin Hamiltonian [4, 5]. Because of the assumed connection between high- T_c superconductivity and the Hubbard model, this has caused renewed interest in these spin models.

In this paper we will examine the spin- $\frac{1}{2}$ XXZ Hamiltonian

$$\mathcal{H} = -J \sum_{\langle i,j \rangle} (\sigma_i^x \sigma_j^x + \sigma_i^y \sigma_j^y) - J_z \sum_{\langle i,j \rangle} \sigma_i^z \sigma_j^z - h \sum_{i=1}^N \sigma_i^z. \quad (3.1.1)$$

The sum $\langle i,j \rangle$ runs over all nearest neighbour pairs in the N -spin system, and the σ_i^α are Pauli matrices. We will only consider bipartite lattices, thus excluding the possibility of frustration. In that case the coupling constant in the x - y plane, J , can always be taken to be positive (i.e. ferromagnetic), because the cases $J > 0$ and $J < 0$ can be mapped onto each other by a rotation of spins on one sublattice. The coupling constant J_z can assume both positive and negative values.

To make the connection with the extended Hubbard model we consider a system of electrons moving on a lattice, with interactions between electrons both on the same site and on neighbouring sites. Its Hamiltonian is given by

$$\mathcal{H} = t \sum_{\langle i,j \rangle, \sigma} (c_{i\sigma}^\dagger c_{j\sigma} + c_{j\sigma}^\dagger c_{i\sigma}) + U \sum_i n_{i\uparrow} n_{i\downarrow} + W \sum_{\langle i,j \rangle, \sigma\sigma'} n_{i\sigma} n_{j\sigma'} - \mu \sum_{i\sigma} n_{i\sigma}, \quad (3.1.2)$$

[†]Apart from some modifications, this chapter has appeared in Phys. Rev. B 43 (1991) 13352

where $c_{i\sigma}^{(\dagger)}$ is the annihilation (creation) operator for an electron of spin σ on site i , while $n_{i\sigma}$ is the number operator $n_{i\sigma} = c_{i\sigma}^\dagger c_{i\sigma}$. The hopping term contains the transfer integral t , the strength of the on-site interaction between the electrons is given by U , and of the inter-site interaction by W ; the number of electrons is controlled by the chemical potential μ .

In the limit of strong on-site attraction, $U = -|U|$ with $|U| \gg t, W$, strongly bound pairs of electrons are formed, and (3.1.2) can be reduced to a Hamiltonian in which singly occupied sites are excluded [5]. This Hamiltonian can be cast into the form (3.1.1) as a pseudospin Hamiltonian, and to second order in $t/|U|$ this leads to the following expressions for the coupling constants:

$$J = \frac{t^2}{|U|}, \quad J_z = -\frac{t^2}{|U|} - W, \quad h = \mu + \frac{1}{2}|U| - zW, \quad (3.1.3)$$

where z is the coordination number of the lattice. The pseudospin operators are then given by

$$\begin{aligned} \sigma_i^x &= c_{i1}c_{i1} + c_{i1}^\dagger c_{i1}^\dagger \\ \sigma_i^y &= ic_{i1}c_{i1} - ic_{i1}^\dagger c_{i1}^\dagger \\ \sigma_i^z &= n_{i1} + n_{i1} - 1. \end{aligned} \quad (3.1.4)$$

The last equation implies a relation between the average magnetization and the electron density $n = \langle n_1 + n_{\bar{1}} \rangle$:

$$n = \langle \sigma^z \rangle + 1. \quad (3.1.5)$$

There are some special cases of the Hamiltonian (3.1.1), like the Ising and the isotropic Heisenberg models, about which much is known, both from analytical results and from approximations of different degrees of sophistication that have been applied to these models. But about the Hamiltonian in its full anisotropic form far less is known, and practically the only general method dealing with the properties of (3.1.1) is the mean field approximation. In the mean field approximation the correlations between fluctuations are ignored. In classical spin models such correlations can be incorporated quite accurately by the cluster variation method (CVM). The CVM has the intrinsic drawback that it can not account properly for the critical fluctuations, but it is quite successful in calculating phase diagrams. Moreover, by the coherent-anomaly method non-classical critical phenomena can also be incorporated [6].

We have applied the cluster variation method to the Hamiltonian (3.1.1), confining ourselves to its simplest form, which only uses two-spin clusters. As a first improvement over the mean field approximation, this already gives significantly different results. It turns out to be possible to derive analytical expressions for the boundaries between most of the phases, while the behaviour of the system and the location of all phase boundaries can also be examined numerically. The CVM has earlier been applied to this Hamiltonian by Kulik and Pedan [7]. They made however

additional assumptions on the density matrices which cause their results to be quite different from what we obtain in this paper.

Using the cluster variation method we obtain global phase diagrams for arbitrary ratios J_z/J , both ferromagnetic and antiferromagnetic, and for arbitrary fields h . Lattices with different values of the correlation number z are considered. We will examine these phase diagrams both in the context of a spin model and in connection with the Hubbard model, and compare them with the results of other approximations, and with exact results where available. Despite the fact that this method behaves unphysically at low temperatures, which make its results unreliable in some cases, in these cases where this behaviour does not interfere with the rest of the phase diagram its results are quite accurate.

3.2 The cluster variation method

The basic ingredient of the CVM [8, 9] is the variational principle of statistical mechanics which states that the density matrix describing a system in equilibrium can be found by minimizing the free-energy functional \mathcal{F} . This functional has the form

$$\mathcal{F} = \text{Tr}(\rho\mathcal{H}) + k_B T \text{Tr}(\rho \ln \rho), \quad (3.2.1)$$

where $\rho = \rho(j_1, \dots, j_N)$ is a trial density matrix of a system of spins j_1, \dots, j_N that satisfies the constraint

$$\text{Tr} \rho = 1. \quad (3.2.2)$$

The free energy F is then given by

$$F = \min \mathcal{F} = \text{Tr}(\rho_0 \mathcal{H}) + k_B T \text{Tr}(\rho_0 \ln \rho_0) = E - TS, \quad (3.2.3)$$

where the density matrix that minimizes \mathcal{F} is

$$\rho_0 = \frac{e^{-\beta \mathcal{H}}}{\text{Tr} e^{-\beta \mathcal{H}}}. \quad (3.2.4)$$

The advantage of the formulation (3.2.3) is that one can write \mathcal{F} as an infinite series of terms, each of which corresponds to a cluster containing a certain number of lattice points. One expects the importance of these terms to decrease as the cluster size increases, and an approximation can be made by neglecting all contributions except those corresponding to a limited number of small clusters.

To make an expansion for \mathcal{F} in this way, we express it in terms of the reduced density matrices corresponding to the different clusters,

$$\rho_{i_1, \dots, i_n}^{(n)} \equiv \text{Tr}_{j_1, \dots, j_{N-n}} \rho(i_1, \dots, i_n, j_1, \dots, j_{N-n}), \quad (3.2.5)$$

where all spins except the ones contained in the cluster, i_1, \dots, i_n , are traced out. For a Hamiltonian of the form (3.1.1), that only contains on-site and nearest neighbour interactions, the first term of (3.2.1) can be expressed in the reduced density matrices as

$$\text{Tr}(\rho\mathcal{H}) = \sum_i \text{Tr}(\rho_i^{(1)} h_i^{(1)}) + \sum_{(i,j)} \text{Tr}(\rho_{i,j}^{(2)} h_{i,j}^{(2)}), \quad (3.2.6)$$

where $h_i^{(1)}$ is the on-site interaction of spin i and $h_{i,j}^{(2)}$ is the interaction between spins i and j :

$$\begin{aligned} h_i^{(1)} &= -h\sigma_i^z \\ h_{i,j}^{(2)} &= -J(\sigma_i^x\sigma_j^x + \sigma_i^y\sigma_j^y) - J_z\sigma_i^z\sigma_j^z \end{aligned} \quad (3.2.7)$$

Now it remains to write the entropy term in (3.2.1) in terms of the reduced density matrices. A quantity that is convenient from a calculational point of view, as it involves only one reduced density matrix, is the cluster entropy S , defined by

$$S_{j_1, \dots, j_n}^{(n)} = -k_B \text{Tr}(\rho_{j_1, \dots, j_n}^{(n)} \ln \rho_{j_1, \dots, j_n}^{(n)}). \quad (3.2.8)$$

These cluster entropies can be expressed in terms of the so-called cumulants \tilde{S} as follows

$$S_{j_1, \dots, j_n}^{(n)} = \sum_i \tilde{S}_i^{(1)} + \sum_{i < j} \tilde{S}_{i,j}^{(2)} + \dots + \tilde{S}_{j_1, \dots, j_n}^{(n)}. \quad (3.2.9)$$

These relations implicitly define the \tilde{S} , and inverting them gives

$$\begin{aligned} \tilde{S}_i^{(1)} &= S_i^{(1)} \\ \tilde{S}_{i,j}^{(2)} &= S_{i,j}^{(2)} - S_i^{(1)} - S_j^{(1)} \\ &\vdots \end{aligned} \quad (3.2.10)$$

Since obviously the second term in (3.2.1) is $-TS^{(N)}$, the functional \mathcal{F} can be written as

$$\begin{aligned} \mathcal{F} &= \text{Tr}(\rho\mathcal{H}) + k_B T \text{Tr}(\rho \ln \rho) \\ &= \sum_i \text{Tr}(\rho_i^{(1)} h_i^{(1)}) + \sum_{(i,j)} \text{Tr}(\rho_{i,j}^{(2)} h_{i,j}^{(2)}) \\ &\quad - T \left\{ \sum_i \tilde{S}_i^{(1)} + \sum_{i < j} \tilde{S}_{i,j}^{(2)} + \dots + \tilde{S}_{j_1, \dots, j_N}^{(N)} \right\}. \end{aligned} \quad (3.2.11)$$

This expression is still exact, and an approximation can be made by making an ansatz for the density matrix that in some way truncates the expansion in cumulants. For example, taking all reduced density matrices as products of the 1-spin reduced

density matrix $\rho_i^{(1)}$ causes all cumulants except $\tilde{S}_i^{(1)}$ to vanish, and leads to the mean field approximation. An improved approximation is obtained by also taking into account the 2-spin reduced density matrix $\rho_{i,j}^{(2)}$, where spins i and j are nearest neighbours. This is exact for the energy term in (3.2.11), and accounts for the correlations between neighbouring spins that are included in the term $\tilde{S}_{i,j}^{(2)}$. Higher cumulants in expression (3.2.11) are ignored in this approximation, and the entropy term becomes, for a lattice with coordination number z ,

$$\begin{aligned} k_B T \text{Tr}(\rho \ln \rho) &= -T \left\{ \sum_i \tilde{S}_i^{(1)} + \sum_{(i,j)} \tilde{S}_{i,j}^{(2)} \right\} \\ &= -T \left\{ \sum_i (1-z) S_i^{(1)} + \sum_{(i,j)} S_{i,j}^{(2)} \right\}. \end{aligned} \quad (3.2.12)$$

This is the approximation we will be using in this paper.

3.3 The two-spin cluster

To apply the CVM, one has to express the functional \mathcal{F} in terms of variational parameters, which is done by choosing a form for the trial density matrix. For a spin- $\frac{1}{2}$ system one can always express the reduced density matrices in Pauli spin matrices. The coefficients of these matrices are the variational parameters of the problem. In order to be able to describe antiferromagnetic phases it is necessary to introduce, for a bipartite lattice, two 1-spin reduced density matrices, $\rho_a^{(1)}$ and $\rho_b^{(1)}$, one for each of the two sublattices a and b . The 2-spin reduced density matrix is of course always of the form $\rho_{ab}^{(2)} \equiv \rho^{(2)}$.

Thus one can write

$$\rho_i^{(1)} = \frac{1}{2} \{ 1 + c_i^x \sigma_i^x + c_i^y \sigma_i^y + c_i^z \sigma_i^z \} \quad (i = a, b). \quad (3.3.1)$$

It is easy to see that $c_i^x = \text{Tr}(\rho_i^{(1)} \sigma_i^x) = \langle \sigma_i^x \rangle$, and similarly for c_i^y and c_i^z . Also expression (3.3.1) satisfies the constraint (3.2.2). For $\rho^{(2)}$ we write

$$\rho^{(2)} = \frac{1}{4} \left\{ 1 + \sum_{i,\alpha} c_i^\alpha \sigma_i^\alpha + \sum_{\alpha,\beta} c^{\alpha\beta} \sigma_a^\alpha \sigma_b^\beta \right\} \quad (\alpha, \beta = x, y, z), \quad (3.3.2)$$

with $c^{\alpha\beta} \equiv c_{ab}^{\alpha\beta} = \langle \sigma_a^\alpha \sigma_b^\beta \rangle$. The parameters c_i^α , $c^{\alpha\beta}$ must now be chosen such as to minimize \mathcal{F} .

In order to explicitly incorporate the bipartite nature of the lattice, which is of importance in the antiferromagnetic phase, we replace the sublattice magnetizations c_i^α by the total magnetization m ,

$$m \equiv \frac{1}{2}(c_a^z + c_b^z), \quad (3.3.3)$$

and the staggered magnetization \bar{m} ,

$$\bar{m} \equiv \frac{1}{2}(c_a^z - c_b^z). \quad (3.3.4)$$

An additional advantage in introducing these parameters is that, instead of viewing them both as variational parameters as one would do when considering a spin model, it is also possible to fix m at an externally prescribed value, which would be desirable from the viewpoint of a Hubbard model with a given electron density (see (3.1.5)).

Before giving detailed expressions for the reduced density matrices we first examine the symmetry aspects of the problem; this is useful both for gaining insight into the behaviour one should expect, and also into the structure of the matrices ρ . Considering the Hamiltonian (3.1.1) of the spin system, we find that it has the following symmetries:

- \mathcal{H} is symmetric under exchange of the sublattice labels a and b . This translation symmetry will be denoted by T_{ab} .
- \mathcal{H} is invariant under rotations of the spins in the x - y plane around the z -axis; we will denote this symmetry by R_{xy} .
- If the field h is zero, \mathcal{H} is symmetric under a rotation of the spins through an angle π around any axis in the x - y plane. Choosing the line $x = y$ in the plane $z = 0$ for the rotation axis, the result of this spin flip symmetry is $(\sigma^x, \sigma^y, \sigma^z) \rightarrow (\sigma^y, \sigma^x, -\sigma^z)$. We will denote this symmetry by F .
- Lastly, \mathcal{H} is invariant under a reflection of the spins in any plane containing the z -axis. If we take the plane $x = y$ as the mirror plane then this symmetry operation, which we will call I , is the product of time reversal (which lets $\sigma \rightarrow -\sigma$), a spin flip F as described above and a rotation R_{xy} . Whereas the first three symmetries all correspond to unitary operators, this one is antiunitary because it contains a time reversal.

The presence or absence of these symmetries can be used to classify the different phases of the system. Since the symmetry of the phase is reflected in the form of the reduced density matrix, it can also be used to reduce the number of independent variational parameters. Namely, the only parameters that can be non-zero are those that correspond to operators that are invariant under the symmetries of the phase. For instance, the disordered phase has the full symmetry of the Hamiltonian, and this requirement causes all but a few parameters in the reduced density matrix to be zero. In the different ordered phases one (or more) of the symmetries of the Hamiltonian is spontaneously broken, and some of the parameters that were required to be zero by this symmetry assume a non-zero value. The most important of these

operators	symmetries			
	T_{ab}	R_{xy}	F	I
$\sigma_a^x + \sigma_b^x, \sigma_a^y + \sigma_b^y$	each	-	sum	sum
$\sigma_a^x + \sigma_a^y, \sigma_b^x + \sigma_b^y$	sum	-	each	each
σ_a^z, σ_b^z	sum	each	-	each
$\sigma_a^x \sigma_b^x, \sigma_a^y \sigma_b^y$	each	sum	sum	sum
$\sigma_a^x \sigma_b^z$	x	x	x	x
$\sigma_a^x \sigma_b^y, \sigma_a^y \sigma_b^x$	sum	diff.	sum	sum
$\sigma_a^x \sigma_b^z + \sigma_a^z \sigma_b^x, \sigma_a^y \sigma_b^z + \sigma_a^z \sigma_b^y$	each	-	-	sum
$\sigma_a^x \sigma_b^z, \sigma_a^y \sigma_b^z$	-	-	diff.	sum
$\sigma_a^z \sigma_b^x, \sigma_a^z \sigma_b^y$	-	-	diff.	sum

Table 3.1. The operators that are invariant under the symmetries of the Hamiltonian. It is indicated whether the operators are (x) or are not (-) invariant under the symmetries mentioned in the text; if two operators are listed together it is indicated whether each one is conserved individually, or only their sum or difference.

parameters is of course the order parameter of the phase in question, but in general any parameter with the same symmetry can and will become non-zero. Table 3.1 displays the operators that are invariant under the symmetries of the Hamiltonian.

We will now list the properties of the phases that constitute the phase diagram.

- The disordered phase (D)

As can be seen from table 3.1, the only operators that are invariant under all four symmetries of the Hamiltonian are $\sigma_a^x \sigma_b^x + \sigma_a^y \sigma_b^y$ and $\sigma_a^z \sigma_b^z$. Consequently the properties of the disordered phase in zero field are fully described by the two parameters c^{xx} ($= c^{yy}$) and c^{zz} . In the case that $h \neq 0$, so that the Hamiltonian is not invariant under the spin flip F , one must add m as a third parameter, since $\sigma_a^z + \sigma_b^z$ is invariant under the remaining three symmetries.

- The ferromagnetic Ising phase (FI)

In the ferromagnetically ordered Ising phase the spin flip symmetry F is spontaneously broken, so we again have the three parameters c^{xx} , c^{zz} , and m to describe this phase. The difference with the previous case is that, instead of being induced by a field, m is now a spontaneous magnetization, which is the order parameter of this phase. If the Ising symmetry is absent because of an applied magnetic field h the phase transition is destroyed.

near the boundary of these phases, and we are allowed to treat it as a perturbation to ρ_0 in this region.

Since it is rotationally invariant (commutes with S_{tot}^z), ρ_0 has a block diagonal form, only coupling states with the same eigenvalue for S_{tot}^z . This makes it relatively easy to diagonalize exactly, finding its eigenvalues λ_i^0 and eigenvectors \mathbf{x}_i . One can then calculate the free energy functional \mathcal{F} in terms of the parameters m , \bar{m} , c^{xz} , and c^{zz} , using

$$\text{Tr } \rho \ln \rho = \sum_i \lambda_i^0 \ln \lambda_i^0, \quad (3.3.9)$$

and thus exactly solve the minimization equations throughout the phases D, FI, and AI.

Turning to the phases where rotation symmetry is broken, we must also consider the matrix ρ_1 , which does not commute with S_{tot}^z . We use a standard perturbation expansion to calculate the eigenvalues of ρ to second order in ρ_1 :

$$\begin{aligned} \lambda_i &= \lambda_i^0 + \lambda_i^1 + \lambda_i^2 + \dots \\ &= \lambda_i^0 + \mathbf{x}_i^T \cdot \rho_1 \cdot \mathbf{x}_i + \sum_j \frac{\mathbf{x}_i^T \cdot \rho_1 \cdot \mathbf{x}_j \mathbf{x}_j^T \cdot \rho_1 \cdot \mathbf{x}_i}{\lambda_i^0 - \lambda_j^0} + \dots \end{aligned} \quad (3.3.10)$$

The first order term λ_i^1 is zero because ρ_1 only couples states with different eigenvalues for S_{tot}^z , while ρ_0 only couples equal values of S_{tot}^z . We are then left with the second order term, which is bilinear in the parameters c_i^z , c^{xz} , c^{zz} , and c^{zz} . To second order in these parameters the traces in (3.3.7) are

$$\begin{aligned} \text{Tr } \rho \ln \rho &= \sum_i \lambda_i^0 \ln \lambda_i^0 + \lambda_i^2 \ln \lambda_i^0 + \lambda_i^2 \\ &= \sum_i (\lambda_i^0 + \lambda_i^2) \ln \lambda_i^0. \end{aligned} \quad (3.3.11)$$

The last equality holds because $\text{Tr } \rho = \sum_i \lambda_i^0 = 1$, and so $\sum_i \lambda_i^2 = 0$.

We will now compute the eigenvalues of the matrices (3.3.5) in this way. For $\rho_i^{(1)}$ we find for the unperturbed eigenvalues

$$\begin{aligned} \mu_{a1}^0 &= \frac{1}{2}(1 + m + \bar{m}) & \mu_{b1}^0 &= \frac{1}{2}(1 + m - \bar{m}) \\ \mu_{a2}^0 &= \frac{1}{2}(1 - m - \bar{m}) & \mu_{b2}^0 &= \frac{1}{2}(1 - m + \bar{m}). \end{aligned} \quad (3.3.12)$$

The second order corrections to this are

$$\begin{aligned} \mu_{a1}^2 &= \frac{c_a^{x^2}}{2(m + \bar{m})} & \mu_{b1}^2 &= \frac{c_b^{x^2}}{2(m - \bar{m})} \\ \mu_{a2}^2 &= -\frac{c_a^{x^2}}{2(m + \bar{m})} & \mu_{b2}^2 &= -\frac{c_b^{x^2}}{2(m - \bar{m})}. \end{aligned} \quad (3.3.13)$$

Consequently,

$$\begin{aligned} \sum_{i=a,b} \text{Tr}(\rho_i^{(1)} \ln \rho_i^{(1)}) &= \frac{1}{2} \left\{ (1+m+\bar{m}) \ln(1+m+\bar{m}) \right. \\ &+ (1-m-\bar{m}) \ln(1-m-\bar{m}) + (1+m-\bar{m}) \ln(1+m-\bar{m}) \\ &+ (1-m+\bar{m}) \ln(1-m+\bar{m}) - 4 \ln 2 + \frac{c_a^{x^2}}{m+\bar{m}} \ln \frac{1+m+\bar{m}}{1-m-\bar{m}} \\ &\left. + \frac{c_b^{x^2}}{m-\bar{m}} \ln \frac{1+m-\bar{m}}{1-m+\bar{m}} \right\} + \text{higher order terms.} \end{aligned} \quad (3.3.14)$$

Proceeding analogously for $\rho^{(2)}$ we find

$$\begin{aligned} \lambda_1^0 &= \frac{1}{4} (1+2m+c^{xx}) \\ \lambda_2^0 &= \frac{1}{4} \left(1+2\bar{m} \left(1+\frac{c^{xx^2}}{\bar{m}^2} \right)^{1/2} - c^{xx} \right) \\ \lambda_3^0 &= \frac{1}{4} \left(1-2\bar{m} \left(1+\frac{c^{xx^2}}{\bar{m}^2} \right)^{1/2} - c^{xx} \right) \\ \lambda_4^0 &= \frac{1}{4} (1-2m+c^{xx}). \end{aligned} \quad (3.3.15)$$

The second order terms are

$$\lambda_i^2 = \frac{1}{8(1+\xi^2)} \left\{ \frac{P_{ij}}{\lambda_i^0 - \lambda_j^0} + \frac{P_{ik}}{\lambda_i^0 - \lambda_k^0} \right\} \quad (3.3.16)$$

with $j=2, k=3$ for $i=1, 4$ and $j=1, k=4$ for $i=2, 3$, and where ξ is defined by

$$\xi \equiv \frac{\bar{m}}{c^{xx}} \left\{ \left(1+\frac{c^{xx^2}}{\bar{m}^2} \right)^{1/2} - 1 \right\}. \quad (3.3.17)$$

The P_{ij} are given by

$$\begin{aligned} P_{12} &= P_{21} = (c_a^x + c^{xx} + \xi(c_a^x + c^{xx}))^2 \\ P_{13} &= P_{31} = (c_a^x + c^{xx} - \xi(c_a^x + c^{xx}))^2 \\ P_{24} &= P_{42} = (c_a^x - c^{xx} + \xi(c_a^x - c^{xx}))^2 \\ P_{34} &= P_{43} = (c_a^x - c^{xx} - \xi(c_a^x - c^{xx}))^2. \end{aligned} \quad (3.3.18)$$

Then we have for the last term in (3.3.7)

$$\begin{aligned} \text{Tr}(\rho^{(2)} \ln \rho^{(2)}) &= \sum_{i=1}^4 \lambda_i^0 \ln \lambda_i^0 + \frac{1}{2(1+\xi^2)} \{ P_{12} \ell_{12} + P_{13} \ell_{13} + \\ &P_{24} \ell_{24} + P_{34} \ell_{34} \} + \text{higher order terms,} \end{aligned} \quad (3.3.19)$$

where

$$\ell_{ij} \equiv \frac{\ln(\lambda_i^0/\lambda_j^0)}{4(\lambda_i^0 - \lambda_j^0)}. \quad (3.3.20)$$

3.4 The minimization of \mathcal{F}

Collecting all information from the previous sections and scaling \mathcal{F} with $Nk_B T$ we find for the functional to be minimized

$$\Phi \equiv \frac{\mathcal{F}}{Nk_B T} = \quad (3.4.1)$$

$$-z(Kc^{xx} + \frac{1}{2}K_z c^{zz}) - mH + \frac{1-z}{2} \sum_{i=a,b} \text{Tr}(\rho_i^{(1)} \ln \rho_i^{(1)}) + \frac{z}{2} \text{Tr}(\rho^{(2)} \ln \rho^{(2)}),$$

where

$$K = \frac{J}{k_B T}, \quad K_z = \frac{J_z}{k_B T}, \quad H = \frac{h}{k_B T}. \quad (3.4.2)$$

3.4.1 The phases without x - y order

We will first consider the phases which do not have x - y order (D, FI, and AI). In these phases the parameters c_i^x , c^{xz} , and c^{zz} are zero, and we only need to take into account the terms in (3.3.14) and (3.3.19) that are due to ρ_0 . This leads to an expression for Φ that only involves the unperturbed eigenvalues: $\Phi = \Phi_0$. The minimization can then be done exactly, and we find expressions describing the behaviour of the system throughout these phases.

Minimizing Φ_0 with respect to the four relevant parameters we find

$$\frac{\partial \Phi_0}{\partial c^{xx}} = -zK + \frac{zc^{xx}}{4\bar{m}} \left(1 + \frac{c^{xx2}}{\bar{m}^2}\right)^{-1/2} \ln \frac{\lambda_2^0}{\lambda_3^0} = 0 \quad (3.4.3)$$

$$\frac{\partial \Phi_0}{\partial c^{zz}} = -\frac{z}{2}K_z + \frac{z}{8} \ln \frac{\lambda_1^0 \lambda_4^0}{\lambda_2^0 \lambda_3^0} = 0 \quad (3.4.4)$$

$$\frac{\partial \Phi_0}{\partial m} = -H + \frac{1-z}{4} \ln \frac{(1+m+\bar{m})(1+m-\bar{m})}{(1-m+\bar{m})(1-m-\bar{m})} + \frac{z}{4} \ln \frac{\lambda_1^0}{\lambda_4^0} = 0 \quad (3.4.5)$$

$$\frac{\partial \Phi_0}{\partial \bar{m}} = \frac{1-z}{4} \ln \frac{(1+m+\bar{m})(1-m+\bar{m})}{(1+m-\bar{m})(1-m-\bar{m})} + \frac{z}{4} \left(1 + \frac{c^{xx2}}{\bar{m}^2}\right)^{-1/2} \ln \frac{\lambda_2^0}{\lambda_3^0} = 0. \quad (3.4.6)$$

We will now apply these equations to the three phases D, FI, and AI.

3.4.1.1 The disordered phase

In the disordered phase we can set $\bar{m} = 0$ in equations (3.4.3), (3.4.4), and (3.4.5), while (3.4.6) does not apply. From (3.4.3) and (3.4.4) we then find

$$4K = \ln \frac{1+2c^{xx}-c^{zz}}{1-2c^{xx}-c^{zz}} \quad (3.4.7)$$

$$4K_z = \ln \frac{(1 + 2m + c^{zz})(1 - 2m + c^{zz})}{(1 + 2c^{zz} - c^{zz})(1 - 2c^{zz} - c^{zz})}. \quad (3.4.8)$$

It follows from (3.4.7) that

$$2c^{zz} = (1 - c^{zz}) \tanh(2K). \quad (3.4.9)$$

Defining $\sigma = e^{4K_z}$, (3.4.8) reduces to

$$\sigma = \frac{(1 + 2m + c^{zz})(1 - 2m + c^{zz})}{(1 + 2c^{zz} - c^{zz})(1 - 2c^{zz} - c^{zz})}, \quad (3.4.10)$$

and combined with (3.4.9) this gives an expression for c^{zz}

$$c^{zz} = \frac{\sigma + \theta - 2(\sigma\theta + m^2(\theta^2 - \sigma\theta))^{1/2}}{\sigma - \theta}, \quad (3.4.11)$$

where we have defined $\theta \equiv \cosh^2 2K$.

From (3.4.5) we find

$$4H = 2(1 - z) \ln \frac{1 + m}{1 - m} + z \ln \frac{1 + 2m + c^{zz}}{1 - 2m + c^{zz}}. \quad (3.4.12)$$

Combined with (3.4.11) this gives m implicitly for given values of K , K_z and H or, when m is viewed as an externally controlled parameter (like the electron density in the Hubbard model), it gives the field (or the chemical potential in the Hubbard model) that is required to obtain a certain value for m .

These equations completely determine the parameters that play a role in the disordered phase. Next we will consider the two Ising ordered phases.

3.4.1.2 The ferromagnetic Ising phase

If the external field H is zero, m is the order parameter for the ferromagnetically ordered Ising phase, which does not exist outside the $H = 0$ plane. Putting the field equal to zero in (3.4.12), one finds to first order in m

$$m(1 - z + \frac{z}{1 + c^{zz}}) = 0. \quad (3.4.13)$$

The solution $m = 0$ corresponds to the high-temperature phase, and the point where the expression in brackets becomes zero, allowing a non-zero value for m , signals the onset of the ordered phase. The phase boundary is thus given by

$$c^{zz} = \frac{1}{z - 1}. \quad (3.4.14)$$

On the other hand, on the boundary with the disordered phase c^{zz} is also given by (3.4.11), and m is zero by continuity. Then (3.4.11) reduces to

$$c^{xz} = \frac{e^{2K_x} - \cosh 2K}{e^{2K_x} + \cosh 2K}. \quad (3.4.15)$$

From (3.4.14) and (3.4.15) the equation for the boundary of the ferromagnetic Ising phase is found to be

$$K_x = \frac{1}{2} \left(\ln \frac{z}{z-2} + \ln \cosh 2K \right). \quad (3.4.16)$$

3.4.1.3 The antiferromagnetic Ising phase

To examine the antiferromagnetic Ising phase one also needs to take the staggered magnetization into account. Thus one needs all four equations (3.4.3) to (3.4.6) to describe this phase. An expression giving the phase boundary can be found by combining (3.4.3) and (3.4.6) to give

$$c^{xz} = \frac{4zK}{z-1} \bar{m} \left(\ln \frac{(1+m+\bar{m})(1-m+\bar{m})}{(1+m-\bar{m})(1-m-\bar{m})} \right)^{-1}. \quad (3.4.17)$$

Then taking the limit $\bar{m} \rightarrow 0$ this is

$$c^{xz} = \frac{1-m^2}{z-1} zK. \quad (3.4.18)$$

For $\bar{m} = 0$ we can also use (3.4.9) and (3.4.11), and together these three equations determine the boundary of the antiferromagnetic Ising phase.

3.4.2 The phases with x - y order

For the phases that do have x - y order (XY and M) we use the perturbation expansion (3.3.10), and so we can only find the boundaries where the order vanishes. As can be seen from (3.3.14) and (3.3.19) Φ now consists of the unperturbed term Φ_0 , plus a term due to the inclusion of ρ_1 to second order, which is bilinear in c_i^x , c^{xz} , and c^{zx} . So we can write $\Phi = \Phi_0 + c^T \cdot M \cdot c$, where the vector c is $(c_a^x, c_b^x, c^{xz}, c^{zx})^T$ and M is a symmetric 4 by 4 matrix. Taking the derivative with respect to the parameters c then leads to the matrix equation $M \cdot c = 0$. The trivial solution $c = 0$ is valid in the phases without x - y order, and the point where $\det M = 0$, which allows a non-zero solution for c , indicates the phase boundary.

3.4.2.1 The x - y ordered phase

First considering the x - y ordered phase, the matrix M can be simplified by using the sublattice symmetry, which is still unbroken in this phase. This allows us to set $\bar{m} = 0$, which implies $\xi = 1$ (where we take $\bar{m} \downarrow 0$ in (3.3.17)). Also, of the four parameters in c only two are independent: $c_a^x = c_b^x$ and $c^{xz} = c^{zx}$. We are then left with a 2 by 2 determinant,

$$\det M = \left| \begin{array}{cc} \frac{1-z}{2m} \ln \frac{1+m}{1-m} + \frac{z}{2}(\ell_{12} + \ell_{24}) & \frac{z}{2}(\ell_{12} - \ell_{24}) \\ \frac{z}{2}(\ell_{12} - \ell_{24}) & \frac{z}{2}(\ell_{12} + \ell_{24}) \end{array} \right| = 0, \quad (3.4.19)$$

where the ℓ_{ij} are defined in (3.3.20). This leads to the following equation

$$\frac{1-z}{m} \ln \frac{1+m}{1-m} + 4z \frac{\ell_{12}\ell_{24}}{\ell_{12} + \ell_{24}} = 0. \quad (3.4.20)$$

By substituting (3.4.9) and (3.4.11) into this equation one can find the boundary between the disordered and the x - y ordered phases.

3.4.2.2 The mixed phase

In the mixed phase the sublattice symmetry is also broken. Consequently, \bar{m} is not zero, while we have four independent parameters in c : c_a^x , c_b^x , c^{xz} , and c^{xy} . This means that we have to solve the full 4 by 4 determinant $\det M$. The expression one finds for M , as well as the equation it leads to, is rather cumbersome and unenlightening, which is why it has been moved to appendix 3.A. Still, the equation $\det M = 0$ in combination with the equations (3.4.3) to (3.4.6), that hold in the AI phase, does give an analytic expression for the boundary between the antiferromagnetic Ising and mixed phases.

In contrast, the boundary between the mixed and x - y ordered phases cannot be found within our approximation. This is due to the fact that on both sides of this line the parameters c_a^x , c_b^x , c^{xz} , and c^{xy} are non-zero, nor are they small in this region. Therefore the expansion (3.3.10) is not valid here. Nevertheless, to get an idea of the location of the boundary we used a numerical algorithm. This algorithm minimizes Φ as a function of the full set of parameters as they are included in (3.3.5). The results of this algorithm were also used as a check on the analytical calculations in the preceding sections.

Remark that our method treats all clusters as equivalent; therefore the magnetization m is constant throughout the system. Thus the mixed phase is stable when one insists on a homogeneous magnetization. This need not be so when the system is allowed to phase separate into regions with different values of m . The mixed phase disappears when one does not choose a fixed value for m , but fixes the field H instead, leaving m as a free variational parameter. It collapses onto a single line, forming a first order transition between the AI and XY phases, with m changing discontinuously across this line.

3.5 Results

Using the results of section 3.4 we can now construct phase diagrams for different values of z . We will first discuss the significant features of one specific example,

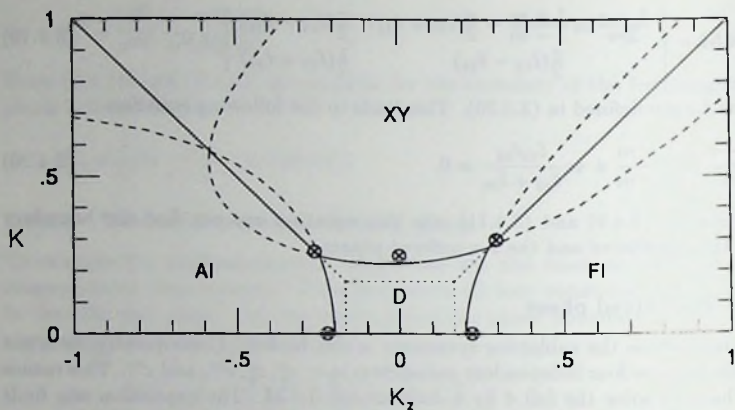


Fig. 3.1. The phase diagram for $z = 6$ and $H = 0$. The phase boundaries according to the CVM are indicated by continuous lines. The dashed lines are those parts of the curves calculated in section 3.4 that do not correspond to a phase transition. The dotted lines are the phase boundaries as they are given by the mean field approximation. The circled crosses show the location of the phase transition for some special cases according to series expansion calculations.

which is more or less representative for the general case. After that we will point out the differences and similarities with other phase diagrams. We start by considering the case $z = 6$, which corresponds to a simple cubic lattice (note that the plane triangular lattice, which also has $z = 6$, is not bipartite, and thus does not fall within the scope of our treatment). The phase diagram should of course be considered in a three-dimensional space, as a function of K , K_z , and H . But we will first look at the plane $H = 0$, and later consider what happens as a magnetic field is turned on.

In figure 3.1 we have plotted the three curves corresponding to equations (3.4.16), (3.4.18), and (3.4.20). These equations are only valid for the boundaries between the ordered phases (FI, AI, and XY) on the one hand, and the disordered phase (D) on the other hand. Therefore only certain segments of the curves (the full curves in figure 3.1) have physical relevance. They represent second order transitions between the ordered phases and the disordered phase. Their location should be compared to the mean field approximation, which gives $K_c = K_{zc} = 1/z$ (the dotted box in figure 3.1), and to the results from series expansions for certain special ratios of K and K_z (the circled crosses in the figure) [10, 11, 12]. The results of the CVM turn out to be in quite good agreement with the series expansion values, and in any case they are a substantial improvement over the mean field approximation. For some special

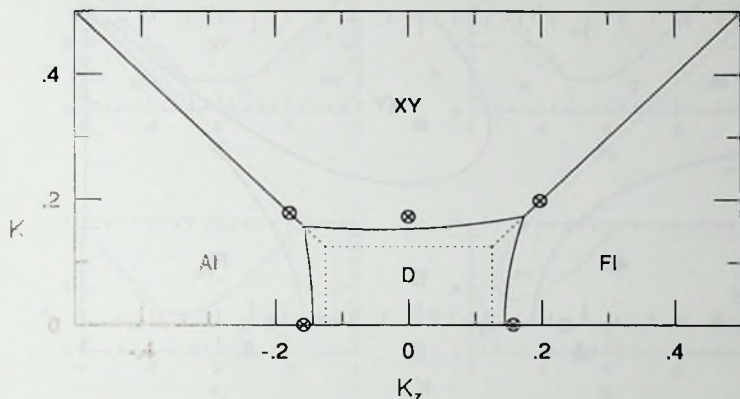


Fig. 3.2. The phase diagram for $z = 8$, $H = 0$. The same description applies as given for figure 3.1. Those parts of the curves that do not correspond to a phase transition (dashed in figure 3.1) are omitted for clarity; they look qualitatively the same as in figure 3.1.

cases, like the ferromagnetic and antiferromagnetic Ising and Heisenberg models, our results agree with those of earlier calculations with the CVM [13], and of the constant coupling method [14], which can be shown to be equivalent to our method.

As for the boundaries between the ordered phases, they do not follow from equations (3.4.16), (3.4.18), and (3.4.20). If $H = 0$ it is obvious from symmetry considerations that the AI-XY boundary lies on the line $K_z = -K$. The FI-XY boundary only exists for $H = 0$ and, again for symmetry reasons, it is immediately evident that it must lie on the line $K_z = K$. Thus the sections of the curves (dashed in figure 3.1) that extend across those lines into a different ordered phase, like the part of the XY curve that lies inside the AI phase, have no physical relevance, because the equations that describe them do not apply inside the ordered phases.

However, the same can not be said about the parts of the XY and AI boundaries that curve back after crossing the line $K_z = -K$ for a second time (also dashed in figure 3.1). These curves again represent a continuous phase transition between the ordered and disordered phases. This implies that the system, after entering the ordered phase at a certain temperature T_c , becomes disordered again at a lower temperature T'_c , and remains so down to $T = 0$. This artifact of the approximation was already noted by Kasteleyn and Van Kranendonk for the Heisenberg antiferromagnet [14]. It indicates that the 2-spin CVM approach fails at low temperature, possibly because the nearest neighbour correlations it takes into account are too short ranged

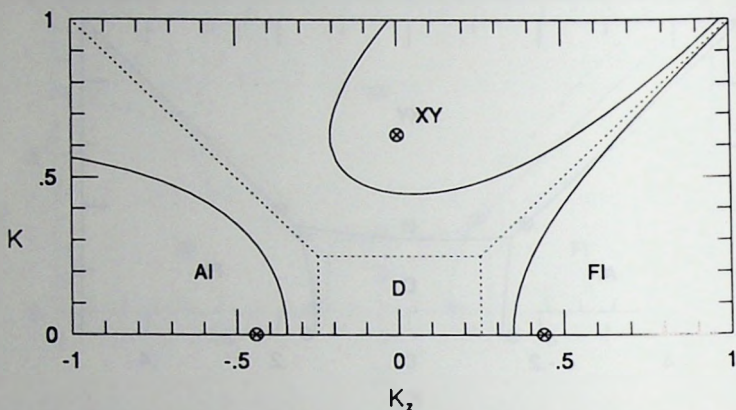


Fig. 3.3. The phase diagram for $z = 4$ and $H = 0$. Again the description given for figure 3.1 applies. In this case the curves calculated in section 3.4 have been entirely drawn as continuous lines, since it is impossible to divide them into real and unphysical phase boundaries in a meaningful way.

to describe long wavelength spin-waves, which play a role at low T [15]. Nevertheless, as long as one can make a clear distinction between the high temperature range, where the results of the approximation are acceptable, and the low temperature region where the unphysical disordering takes place, this method is still a useful approach for obtaining phase diagrams. From figure 3.1 one would conclude that this is indeed the case for $z = 6$ and $H = 0$.

Turning to higher values of z , we see that figure 3.2, which is for $z = 8$ (a bcc lattice) and $H = 0$, presents essentially the same features as the previous one. The irrelevant and unphysical parts of the curves have been omitted for clarity; they are qualitatively the same as for $z = 6$. Again, the 2-spin CVM is a substantial improvement over the mean field approximation where the boundary of the disordered phase is concerned, and the unphysical disordered phase (not shown in the figure) lies at sufficiently low T . If z is increased further, the results of our method become more and more like the mean field ones, which are exact for $z = \infty$.

Lowering z , we see that the case $z = 4$, for the two-dimensional square lattice, presents a different picture (figure 3.3). The part with $K_z > 0$ is acceptable, with the ferromagnetic Heisenberg transition shifted to $K = \infty$ as it should be. But the region with $K_z < 0$ seems rather problematic. A gap has opened around the line $K_z = -K$, connecting the "physical" disordered phase at high T with the "unphysical" one at low T . This makes it impossible to clearly distinguish between the high temperature

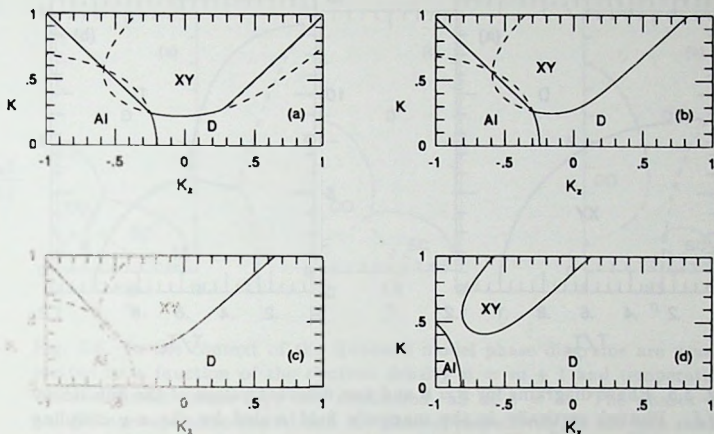


Fig. 3.4. The phase diagrams for $z = 6$ and various values of H . The same description applies as for the previous figures. a: $H = 0.01$; b: $H = 1$; c: $H = 2$; d: $H = 5$.

region where the approximation is valid and the low temperature regime where it fails. Hence one does not know how to interpret this part of the phase diagram for $z = 4$, and it seems that the limit of applicability of the approximation has been reached.

We will now consider the changes in the phase diagram when a magnetic field H is turned on. We will only consider the case $z = 6$, as it is representative for other values of z as well. Figure 3.4 shows 4 cross-sections of the three-dimensional phase diagram (containing K , K_x , and H) at certain values of H . The first thing that happens as soon as one turns on a field is the disappearance of the FI phase (figure 3.4 a, where $H = 0.01$). The transition in the ferromagnetic Heisenberg model is also destroyed. The curve giving the XY phase boundary, which for $H = 0$ crosses the line $K_x = K$ at the critical coupling for the Heisenberg model, is now split into two separate parts on different sides of this line. The part where $K > K_x$ still indicates the XY phase boundary, which now runs very close to the line $K_x = K$, while the part with $K_x > K$ is irrelevant and does not indicate a phase boundary. The remainder of the figure is not perceptibly changed by the small field $H = 0.01$.

On increasing H some trends become apparent (figures 3.4 b to d). The XY boundary shifts away from the line $K_x = K$, while the irrelevant part on the other side of this line moves to higher and higher K values, and disappears from the figure. In the other half of the phase diagram we see that the boundary of the AI phase is

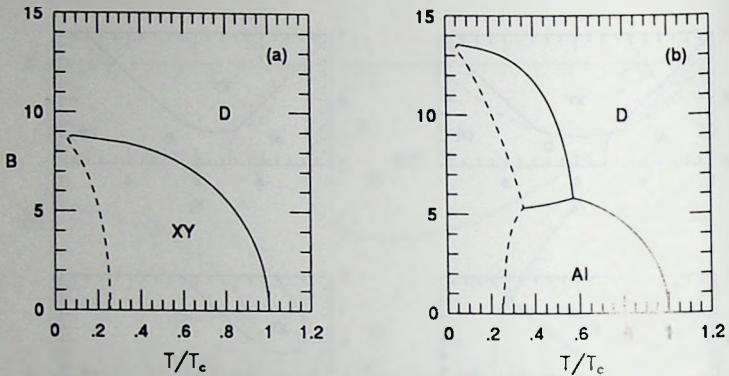


Fig. 3.5. Phase diagrams for $z = 6$ and two different values of the anisotropy J_z/J . Plotted vertically is the magnetic field scaled by the x - y coupling constant, $B = h/J$. The solid lines again indicate the phase boundaries and the dashed lines the unphysical disordering at low T . a: $J_z = -J/2$; b: $J_z = -1.3J$.

shifted towards larger values of $|K_x|$, and also changes in shape slightly. Combined with the narrowing of the XY region this leads to a shift in the boundary between the XY and AI phases, which leaves the line $K_x = -K$, where it was located for $H = 0$, and moves into the region $-K_x > K$. This phase boundary now becomes first order, with m changing discontinuously when it is crossed. If the field is increased still further, the XY and AI boundaries no longer intersect (figure 3.4 d), and the same situation arises described earlier for $z = 4$ and $H = 0$. Again the approximation ceases to be valid beyond this point.

Another conventional way of drawing the phase diagram of a magnetic system is presented in figure 3.5. Here we have fixed the anisotropy J_z/J , and then plot $T/T_c = K_c/K$ versus the scaled field $B = h/J = H/K$ (we again take $z = 6$). If the x - y coupling is predominant the picture is rather simple (figure 3.5 a, where $J_z = -J/2$). One finds the boundary between the disordered and the x - y ordered phases, with a critical temperature that decreases with increasing field, and at lower T the "unphysical" transition back into the disordered phase. A more interesting result is obtained for a model where the z coupling dominates (figure 3.5 b, $J_z = -1.3J$). For low fields B there is an antiferromagnetically ordered phase, while for higher fields x - y order takes over. These two phases are separated by a first order transition. At low T there is again a return to the disordered phase.

Finally, we replot the data in a way appropriate for the Hubbard model. As was pointed out earlier, the externally imposed parameter in the Hubbard model is m ,

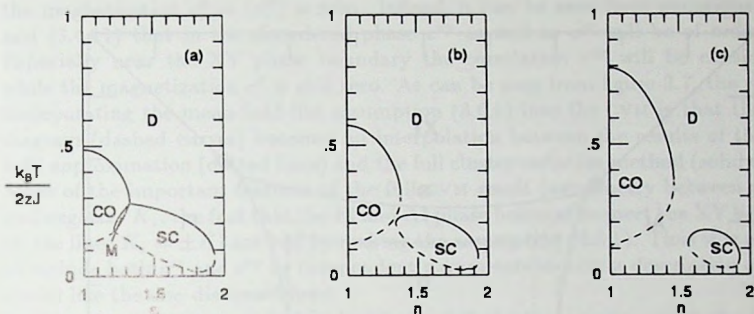


Fig. 3.6. In the context of the Hubbard model phase diagrams are usually plotted as a function of the electron density $n = m + 1$ and temperature. Three different ratios J_z/J are considered, all at $z = 6$. The phases CO and SC correspond to the AI and XY phases, respectively, in the spin model. a: $J_z = -1.3J$; b: $J_z = -1.5J$; c: $J_z = -2J$.

corresponding to the electron density $n = m + 1$ (see (3.1.5)), instead of the field. This leads to the possibility of finding the mixed phase M in place of the first order transition between the AI and XY phases. Figure 3.6 shows the phase diagrams for different ratios J_z/J , and again we have taken $z = 6$. The phase diagrams are symmetric around $n = 1$, because of the up-down symmetry in the spin model. In figure 3.6 we only show the half with $n > 1$. The region around $n = 1$ is an AI phase, which in this context is associated with a charge ordered phase (CO) (for $-J_z > J$ one sees from (3.1.3) that the intersite interaction W is repulsive; in the charge ordered phase the electron density is distributed unevenly among the two sublattices so as to minimize the energy due to this repulsion). This phase is flanked by an XY phase, associated with the superconducting phase of the Hubbard model (SC). In figure 3.6 a there is a thin slice of the mixed phase in between these two phases, exhibiting both charge order and superconducting order. The boundary between the phases M and SC has been calculated with the numerical procedure mentioned in section 3.4.2.2. For larger values of $|J_z/J|$ the two phases become disconnected, and the mixed phase disappears. This is again an example of the limitations of the approximation, since the unphysical phase at low T links up with the high T part of the phase diagram.

3.6 Discussion

We have applied the cluster variation method to the spin- $\frac{1}{2}$ XXZ model, using clusters containing 2 spins. For the phases without x - y order we have derived the equations

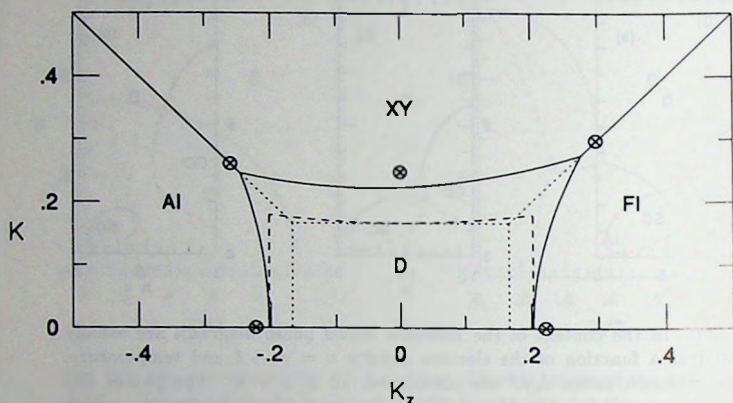


Fig. 3.7. A comparison between the CVM results with and without the assumption (3.6.1). The phase boundaries shown in figure 3.1 are reproduced, so again we have $z = 6, H = 0$. The solid lines are the result of the full CVM, and the dotted lines those of the mean field approximation. The dashed lines that form an interpolation between these two are the result of incorporating assumption (3.6.1) into the CVM.

that follow from minimizing the free energy functional. These equations describe the behaviour of the system in the disordered and the (anti)ferromagnetic Ising phases, and give analytic expressions for the boundaries between these phases. For the phases with x - y order we have made an expansion in the parameters that are associated with this order. This makes it possible also to find analytic expressions for the boundaries between phases with and without x - y order. To examine the behaviour of the system inside the x - y ordered phases, and to find the boundary between phases that both have x - y order, a numerical algorithm was used that performs a minimization of the free energy functional without any further approximation.

As was mentioned in the introduction, Kulik and Pedan [7] have also studied some of the properties of a Hamiltonian equivalent to (3.1.1) with the CVM. But instead of considering both $c^{xz} (= \langle \sigma_a^x \sigma_b^z \rangle)$ and $c^{zz} (= \langle \sigma_a^z \sigma_b^z \rangle)$ as independent variational parameters in the free energy functional \mathcal{F} , they make the assumption

$$c^{xz} \propto c^{zz}, \tag{3.6.1}$$

while keeping c^{zz} as an independent parameter. This assumption does not seem to be justified, since one would expect that for any finite temperature there exists a correlation between both the x - and z -components of neighbouring spins, even if

the magnetization $c_i^z = \langle \sigma_i^z \rangle$ is zero. Indeed, it can be seen from equations (3.4.9) and (3.4.11) that in the disordered phase c^{xz} as well as c^{zz} will be of order $\mathcal{O}(1)$. Especially near the XY phase boundary the correlation c^{xz} will be considerable, while the magnetization c_i^z is still zero. As can be seen from figure 3.7, the result of incorporating the mean-field-like assumption (3.6.1) into the CVM is that the phase diagram (dashed curves) becomes an interpolation between the results of the mean field approximation (dotted lines) and the full cluster variation method (solid curves). Some of the important features of the full CVM result (asymmetry between positive and negative K_z , the fact that the FI and AI phase boundaries meet the XY boundary on the lines $K_z = \pm K$) are lost by making the assumption (3.6.1). Thus it is essential to include both c^{xz} and c^{zz} as independent parameters in a CVM description of a spin model like the one discussed here.

The phase diagrams calculated with the full cluster variation method are, for a certain range of parameters ($z \geq 6$, H not too large), a substantial improvement over the mean field approximation, and agree quite well with the results of series expansion methods. The cluster variation method does behave unphysically at low temperatures, predicting a second disordered phase below the ordered phases, but for this range of parameters this does not interfere with the high-temperature part of the phase diagram.

However, for $z \leq 4$ and/or large values of H the disordered phase at low T links up with the one at high T . This makes the phase diagram calculated with our method unreliable in some regions, especially around $J_z = -J$. Other methods that have been used to study the phase diagram of the XXZ model also suffer from this difficulty in dealing with the antiferromagnetic sector. Some real-space renormalization group approaches that work well for the ferromagnetic Ising sector and the isotropic Heisenberg model turn out to be unable to deal with the rest of the phase diagram in an acceptable manner [16, 17]. Despite its shortcomings, the full cluster variation method seems to be a useful tool to examine the phase diagram of the XXZ model. It is considerably more sophisticated than the mean field approximation, and gives qualitatively better and quite accurate results over a range of parameters.

Appendix

As was pointed out in section 3.4.2.2, to find the boundary separating the AI and M phases one needs to take into account all four parameters c_a^z , c_b^z , c^{xz} , and c^{zz} . Then one finds the following expression for $\det M$

$$\det M = \begin{vmatrix} Q_1 + A_1 & C_1 & A_2 & C_2 \\ C_1 & Q_2 + \bar{A}_1 & C_2 & \bar{A}_2 \\ A_2 & C_2 & A_1 & C_1 \\ C_2 & \bar{A}_2 & C_1 & \bar{A}_1 \end{vmatrix} = 0. \quad (3.A.1)$$

The definitions that have been used are

$$Q_1 = \frac{1-z}{2(m+\bar{m})} \ln \frac{1+m+\bar{m}}{1-m-\bar{m}} \quad (3.A.2)$$

$$Q_2 = \frac{1-z}{2(m-\bar{m})} \ln \frac{1+m-\bar{m}}{1-m+\bar{m}} \quad (3.A.3)$$

$$A_1 = \frac{z}{2(1+\xi^2)} (\xi^2(\ell_{12} + \ell_{34}) + \ell_{13} + \ell_{24}) \quad (3.A.4)$$

$$\bar{A}_1 = \frac{z}{2(1+\xi^2)} (\ell_{12} + \ell_{34} + \xi^2(\ell_{13} + \ell_{24})) \quad (3.A.5)$$

$$A_2 = \frac{z}{2(1+\xi^2)} (\xi^2(\ell_{12} - \ell_{34}) + \ell_{13} - \ell_{24}) \quad (3.A.6)$$

$$\bar{A}_2 = \frac{z}{2(1+\xi^2)} (\ell_{12} - \ell_{34} + \xi^2(\ell_{13} - \ell_{24})) \quad (3.A.7)$$

$$C_1 = \frac{z}{2(1+\xi^2)} \xi(\ell_{12} - \ell_{34} - \ell_{13} + \ell_{24}) \quad (3.A.8)$$

$$C_2 = \frac{z}{2(1+\xi^2)} \xi(\ell_{12} + \ell_{34} - \ell_{13} - \ell_{24}), \quad (3.A.9)$$

where ξ and ℓ_{ij} are defined in section 3.3. Solving (3.A.1) in combination with equations (3.4.3) to (3.4.6) leads to an analytic expression for the boundary between the antiferromagnetic Ising phase and the mixed phase.

References

- [1] C.N. Yang and T.D. Lee, Phys. Rev. **87** (1952) 410
- [2] M.E. Fisher, Rep. Prog. Phys. **30** (1967) 615
- [3] T. Matsubara and H. Matsuda, Prog. Th. Phys. **16** (1956) 569,
H. Matsuda and T. Matsubara, Prog. Th. Phys. **17** (1957) 19
- [4] R. Micnas, J. Ranninger, and S. Robaszkiewicz, Rev. Mod. Phys. **62** (1990) 113
- [5] S. Robaszkiewicz, R. Micnas, and K.A. Chao, Phys. Rev. B **23** (1981) 1447
- [6] M. Suzuki, in: *Advances on Phase Transitions and Disorder Phenomena*, Proceedings of the international meeting held in Amalfi, Italy, June 1986 (G. Busiello, L. De Cesare, F. Mancini, and M. Marinaro, eds.), World Scientific, Singapore, 1987,
M. Suzuki, J. Phys. Soc. Jpn. **55** (1986) 4205,
M. Suzuki, M. Katori, and X. Hu, J. Phys. Soc. Jpn. **56** (1987) 3092
- [7] I.O. Kulik and A.G. Pedan, Sov. J. Low Temp. Phys. **9** (1983) 127

- [8] T. Morita, *J. Math. Phys.* **13** (1972) 115
- [9] G. An, *J. Stat. Phys.* **52** (1988) 727
- [10] G.S. Rushbrooke, G.A. Baker, Jr., and P.J. Wood, in: *Phase Transitions and Critical Phenomena*, Vol. 3 (C. Domb and M.S. Green, eds.), Academic Press, London, 1974
- [11] D.D. Betts, in: *Phase Transitions and Critical Phenomena*, Vol. 3 (C. Domb and M.S. Green, eds.), Academic Press, London, 1974,
J. Rogiers, E.W. Grundke, and D.D. Betts, *Can. J. Phys.* **57** (1979) 1719
- [12] C. Domb, in: *Phase Transitions and Critical Phenomena*, Vol. 3 (C. Domb and M.S. Green, eds.), Academic Press, London, 1974
- [13] R. Kikuchi, *Ann. Phys. (N.Y.)* **4** (1958) 1
- [14] P.W. Kasteleyn and J. van Kranendonk, *Physica* **22** (1956) 317, 367, 387
- [15] P.W. Anderson, *Phys. Rev.* **80** (1950) 922
- [16] R.C. Brower, F. Kuttner, M. Nauenberg, and K. Subbarao, *Phys. Rev. Lett.* **38** (1977) 1231
- [17] H. Takano and M. Suzuki, *J. Stat. Phys.* **26** (1981) 635
C. Castellani, C. Di Castro, and J. Ranninger, *Nucl. Phys.* **B200** [FS4] (1982) 45

Chapter 4

The phase diagram of the XXZ model for slab and layered geometries[†]

4.1 Introduction

The behaviour of systems as a function of their spatial dimension is an important issue in statistical physics. Indeed, some properties, like critical exponents and the existence of a phase transition, depend almost exclusively on the spatial dimension and the symmetry of the model. Many of these quantities have been accurately calculated, e.g. with momentum-space renormalization techniques. In addition to these so-called universal properties, there are also quantities, such as the critical temperature, that *do* depend on the details of the geometry and the Hamiltonian of the model. In some cases real-space renormalization has been successful in calculating these properties. Also, various series expansion methods have achieved a high accuracy in examining some specific models. For quantum spin models, however, real-space renormalization runs into considerable difficulties, while series expansions cannot give a global picture of the whole phase diagram of more complicated models. This is why practically the only general method used to deal with such models is the mean-field approximation. Since this method gives only a crude approximation of the phase diagram, more sophisticated approaches are needed. In this paper we use a more refined method to calculate phase diagrams and to study the influence of the spatial dimension on the details of these diagrams.

In order to study the influence of the dimension on the behaviour of a system, one may consider geometries that can be made to cross over between different dimensions. We will examine two quantum spin models that can be changed from two- to three-dimensional by varying a parameter of the model. In the first model we consider how a collection of uncoupled two-dimensional layers changes into a fully isotropic three-dimensional system as the inter-layer coupling is turned on. Second, we turn to a model consisting of a slab of n such layers, which becomes three-dimensional as

[†]Apart from some modifications, this chapter will appear in *J. Phys.: Cond. Matt.*

its width approaches infinity. For both models, we will examine the changes in the phase diagram as these parameters are varied.

The specific spin model we will be studying is the spin- $\frac{1}{2}$ XXZ model. Its Hamiltonian is

$$\mathcal{H} = \sum_{\langle ij \rangle} -J_{ij}(\sigma_i^x \sigma_j^x + \sigma_i^y \sigma_j^y) - J_{z,ij} \sigma_i^z \sigma_j^z - \sum_{i=1}^N h \sigma_i^z. \quad (4.1.1)$$

The sum $\sum_{\langle ij \rangle}$ is over nearest neighbour spins only, and the σ_i^α are Pauli matrices. The spin coupling is anisotropic in spin space, i.e. $J_{ij} \neq J_{z,ij}$, and by choosing J_{ij} and $J_{z,ij}$ to be different for different pairs of spins i and j , it can also be made anisotropic in real space. In addition to the coupling there is a homogeneous magnetic field h in the z -direction. We will consider bipartite lattices only, so an antiferromagnetic phase can always be accommodated without having to take into account frustration. For such a lattice we can assume that J_{ij} is positive, i.e. ferromagnetic, since the model is invariant under a change of sign of J_{ij} , [1] (we do not consider cases where different J_{ij} or $J_{z,ij}$ have different signs).

The Hamiltonian (4.1.1) is of interest for two reasons. First, it is interesting in itself, having two competing interactions, J and J_z , and both a continuous symmetry, for rotations of the spins around the z -axis, and a discrete up-down symmetry if $h = 0$. It also comprises various special cases like the Ising, Heisenberg, and XY models. Second, it is the Hamiltonian one obtains when writing a simple lattice gas model of a fluid consisting of interacting hard core bosons in the pseudo-spin formulation [1, 2]. As such, it has been used to examine both superfluidity [2, 3, 4] and superconductivity [5, 6, 7, 8], the latter in the framework of theories that assume the existence of preformed, real-space pairs in high- T_c superconductors. Apart from the obvious interpretation of the spin model as a magnetic system in a layered or film geometry, one could then also make a connection with superconductors that consist of weakly coupled layers, or superfluid films of ^4He . This model is much too simplified, however, to give more than a qualitative picture of such systems.

The method we use to construct the phase diagram of the spin system is the cluster variation method using two-spin clusters. This method can be viewed as an extension of the mean-field approximation that also takes into account the correlations between neighbouring spins. It is the quantum version of Kikuchi's variational method for classical spins [9, 10, 11], and it is essentially a mean-field-like method, e.g. it reproduces the mean-field values of the critical exponents. For getting a global picture of the phase diagram it is a considerable improvement over the mean-field approximation, which is one of the few general methods applied to the Hamiltonian (4.1.1) so far. The cluster variation method has turned out to give quite good results for the phase diagrams of fully isotropic two- and three-dimensional quantum spin models [12, 13], despite some unphysical behaviour at low temperature.

In section 4.2 we will give a description of the cluster variation method, and then,

in sections 4.3 and 4.4, apply it to the two geometries mentioned above. The results are discussed in section 4.5.

4.2 General theory

In this section we briefly outline the cluster variation method that is described in more detail in [13]. The starting point of this method is the variational principle for the free energy \mathcal{F} as a functional of the density matrix ρ of a system,

$$\mathcal{F}[\rho] = \text{Tr}(\rho\mathcal{H}) + k_B T \text{Tr}(\rho \ln \rho). \quad (4.2.1)$$

The density matrix must satisfy $\text{Tr} \rho = 1$, and for the true density matrix ρ_0 that minimizes \mathcal{F} one finds for the free energy

$$F = \min_{\rho} \mathcal{F}[\rho] = \mathcal{F}[\rho_0] = E - TS. \quad (4.2.2)$$

An approximation can be made by expanding \mathcal{F} in cumulants, and only considering the reduced density matrices $\rho_C^{(n)}$ for a limited set of small clusters \mathcal{C} . The reduced density matrix for a cluster \mathcal{C} containing n spins is

$$\rho_C^{(n)} = \text{Tr}_{\text{spins} \notin \mathcal{C}} \rho, \quad (4.2.3)$$

where all spins not in \mathcal{C} are traced out. We will limit ourselves to clusters consisting of single spins and nearest neighbour pairs.

For a Hamiltonian like (4.1.1), that only contains on-site terms $h_i^{(1)}$ and nearest neighbour interactions $h_{ij}^{(2)}$, one can, in this approximation, express \mathcal{F} in terms of $\rho_i^{(1)}$ and $\rho_{ij}^{(2)}$ as follows

$$\begin{aligned} \mathcal{F} = & \sum_{i=1}^N \text{Tr}(\rho_i^{(1)} h_i^{(1)}) + \sum_{\langle ij \rangle} \text{Tr}(\rho_{ij}^{(2)} h_{ij}^{(2)}) \\ & - T \left\{ \sum_{i=1}^N S_i^{(1)} + \sum_{\langle ij \rangle} (S_{ij}^{(2)} - S_i^{(1)} - S_j^{(1)}) \right\}, \end{aligned} \quad (4.2.4)$$

where the so-called cluster entropies $S_i^{(1)}$ and $S_{ij}^{(2)}$ are defined as

$$S_i^{(1)} \equiv -k_B \text{Tr}(\rho_i^{(1)} \ln \rho_i^{(1)}), \quad (4.2.5)$$

$$S_{ij}^{(2)} \equiv -k_B \text{Tr}(\rho_{ij}^{(2)} \ln \rho_{ij}^{(2)}). \quad (4.2.6)$$

These quantities are the most convenient from a calculational point of view, since they involve only a single reduced density matrix. All equivalent clusters have the same cluster entropy, and the number of non-equivalent clusters is determined by the

geometry of the lattice and the phase that one wants to describe. In order to have the possibility to describe an antiferromagnetic phase we must at least distinguish between $S_{i_a}^{(1)}$ and $S_{i_b}^{(1)}$, where a and b are the two sublattices of the bipartite lattice. In a more complicated geometry there will be more types of one-spin clusters, and also several different types of nearest neighbour pairs, each with its own cluster entropy $S_{ij}^{(2)}$. This will be the case when we consider the anisotropic and layered geometries in sections 4.3 and 4.4.

What remains to be done is to find a suitable parametrization for the reduced density matrices. In dealing with a spin- $\frac{1}{2}$ system one can always express these matrices in terms of Pauli spin matrices:

$$\begin{aligned} \rho_i^{(1)} &= \frac{1}{2} \left(1 + \sum_{\alpha} c_i^{\alpha} \sigma_i^{\alpha} \right), & (\alpha = x, y, z), \\ \rho_{ij}^{(2)} &= \frac{1}{4} \left(1 + \sum_{\alpha} (c_i^{\alpha} \sigma_i^{\alpha} + c_j^{\alpha} \sigma_j^{\alpha}) + \sum_{\alpha, \beta} c_{ij}^{\alpha\beta} \sigma_i^{\alpha} \sigma_j^{\beta} \right), & (\alpha, \beta = x, y, z). \end{aligned} \quad (4.2.7)$$

The functional \mathcal{F} is now a function of the parameters c_i^{α} and $c_{ij}^{\alpha\beta}$. These parameters are just the averages of the spin operators, $c_i^{\alpha} = \text{Tr}(\rho_i^{(1)} \sigma_i^{\alpha}) = \langle \sigma_i^{\alpha} \rangle$, and likewise $c_{ij}^{\alpha\beta} = \langle \sigma_i^{\alpha} \sigma_j^{\beta} \rangle$. From the symmetry of the Hamiltonian and of the phases under consideration one can deduce two properties of these parameters. First, not all of them are independent, e.g. one can take $c_i^x = c_i^y$ and $c_{ij}^{xx} = c_{ij}^{yy}$ etc. because of the rotation symmetry around the z -axis in spin space of (4.1.1). Second, some of the parameters are characteristic of the ordered phases of the system, i.e. they are only non-zero when a symmetry in the Hamiltonian is spontaneously broken. The most important of these is the order parameter of the ordered phase. We will refer to these parameters characteristic of an ordered phase as "order" parameters. The parameters can be classified accordingly:

- In the disordered, high temperature phase only c_{ij}^{xx} and c_{ij}^{zz} and, provided that $h \neq 0$, the magnetization $m_i \equiv \frac{1}{2}(c_{i_a}^z + c_{i_b}^z)$ are non-zero. There is no spontaneous breaking of any of the symmetries of the Hamiltonian.
- For negative values of J_z the system can order antiferromagnetically in the z -direction. The order parameter of this antiferromagnetic Ising phase is the staggered magnetization $\bar{m}_i \equiv \frac{1}{2}(c_{i_a}^z - c_{i_b}^z)$.
- If the x - y rotation symmetry is spontaneously broken, the system has a non-zero magnetization in the x - y plane. The order parameter for this x - y ordered phase is c_i^x , while the other "order" parameters are c_{ij}^{xx} , c_{ij}^{yy} , and c_{ij}^{xy} .
- In the case that $h = 0$ there is a phase where the spins order spontaneously in the z -direction. The order parameter for this ferromagnetically ordered Ising phase

is m_i . In the following we will generally assume that $h \neq 0$, and occasionally make a remark concerning the case $h = 0$.

We can express the reduced density matrices in these parameters as follows (the bases $\{|+\rangle, |-\rangle\}$ and $\{|+\rangle, |+\rangle, |-\rangle, |-\rangle\}$ have been used):

$$\rho_i^{(1)} = \frac{1}{2} \begin{pmatrix} 1 + c_i^z & (1-i)c_i^z \\ (1+i)c_i^z & 1 - c_i^z \end{pmatrix},$$

$$\rho_{ij}^{(2)} = \frac{1}{4} \begin{pmatrix} 1 + c_i^z + c_j^z + c^{xz} & (1-i)(c_j^z + c^{xz}) & (1-i)(c_i^z + c^{xz}) & -2ic^{xz} \\ (1+i)(c_j^z + c^{xz}) & 1 + c_i^z - c_j^z - c^{xz} & 2c^{xz} & (1-i)(c_i^z - c^{xz}) \\ (1+i)(c_i^z + c^{xz}) & 2c^{xz} & 1 - c_i^z + c_j^z - c^{xz} & (1-i)(c_j^z - c^{xz}) \\ 2ic^{xz} & (1+i)(c_i^z - c^{xz}) & (1+i)(c_j^z - c^{xz}) & 1 - c_i^z - c_j^z + c^{xz} \end{pmatrix}, \quad (4.2.8)$$

where we have, for clarity, omitted the label ij for the parameters $c_{ij}^{\alpha\beta}$ in the expression for $\rho_{ij}^{(2)}$. While it is easy to calculate the energy part in (4.2.4) with these expressions, for the entropy part we need to evaluate traces like

$$\text{Tr}(\rho \ln \rho) = \sum_k \lambda_k \ln \lambda_k, \quad (4.2.9)$$

where λ_k are the eigenvalues of the matrix ρ . It was shown in [13] that, if one is only interested in locating the phase boundaries, it suffices to calculate the eigenvalues perturbatively up to second order in the x - y "order" parameters c_i^z , c_{ij}^z , and c_{ij}^{xz} . For a continuous transition one can then find the boundaries between the ordered phases and the disordered high temperature phase, since these parameters are small near the phase boundaries. The first order term λ_k^1 turns out to be zero, and one finds for the eigenvalues

$$\lambda_k = \lambda_k^0 + \lambda_k^2 + \mathcal{O}(c^{z4}), \quad (4.2.10)$$

and hence for the trace (4.2.9)

$$\text{Tr}(\rho \ln \rho) = \sum_k \lambda_k \ln \lambda_k = \sum_k (\lambda_k^0 + \lambda_k^2) \ln \lambda_k^0 + \mathcal{O}(c^{z4}). \quad (4.2.11)$$

The eigenvalues μ one finds in this way for $\rho_i^{(1)}$ are

$$\begin{aligned} \mu_{i1}^0 &= \frac{1}{2}(1 + c_i^z), & \mu_{i2}^0 &= \frac{1}{2}(1 - c_i^z), \\ \mu_{i1}^2 &= \frac{c_i^{z2}}{2c_i^z}, & \mu_{i2}^2 &= -\frac{c_i^{z2}}{2c_i^z}. \end{aligned} \quad (4.2.12)$$

To zeroth order the eigenvalues λ_{ij} of $\rho_{ij}^{(2)}$ are (again dropping the label ij)

$$\begin{aligned}\lambda_1^0 &= \frac{1}{4} (1 + c_i^z + c_j^z + c^{zz}), \\ \lambda_2^0 &= \frac{1}{4} \left(1 + ((c_i^z - c_j^z)^2 + 4c^{zz2})^{1/2} - c^{zz} \right), \\ \lambda_3^0 &= \frac{1}{4} \left(1 - ((c_i^z - c_j^z)^2 + 4c^{zz2})^{1/2} - c^{zz} \right), \\ \lambda_4^0 &= \frac{1}{4} (1 - c_i^z - c_j^z + c^{zz}).\end{aligned}\quad (4.2.13)$$

The second order terms are

$$\lambda_k^2 = \frac{1}{8(1 + \xi^2)} \left\{ \frac{P_{km}}{\lambda_k^0 - \lambda_m^0} + \frac{P_{kn}}{\lambda_k^0 - \lambda_n^0} \right\}, \quad (4.2.14)$$

with $m = 2, n = 3$ for $k = 1, 4$ and $m = 1, n = 4$ for $k = 2, 3$, and where ξ is defined by

$$\xi \equiv \frac{c_i^z - c_j^z}{2c^{zz}} \left\{ \left(1 + \frac{4c^{zz2}}{(c_i^z - c_j^z)^2} \right)^{1/2} - 1 \right\}. \quad (4.2.15)$$

The P_{km} are given by

$$\begin{aligned}P_{12} &= P_{21} = (c_j^z + c^{zz} + \xi(c_i^z + c^{zz}))^2, \\ P_{13} &= P_{31} = (c_i^z + c^{zz} - \xi(c_j^z + c^{zz}))^2, \\ P_{24} &= P_{42} = (c_i^z - c^{zz} + \xi(c_j^z - c^{zz}))^2, \\ P_{34} &= P_{43} = (c_j^z - c^{zz} - \xi(c_i^z - c^{zz}))^2.\end{aligned}\quad (4.2.16)$$

On substituting all this into expression (4.2.4) for \mathcal{F} one finds for the free energy functional per spin Φ

$$\begin{aligned}\Phi \equiv \frac{\mathcal{F}}{Nk_B T} &= -\frac{1}{N} \left\{ \sum_{(ij)} 2K_{ij} c_{ij}^{zz} + K_{z ij} c_{ij}^{zz} + \sum_{i=1}^N H c_i^z \right\} \\ &+ \frac{1}{N} \left\{ \sum_{i=1}^N \sum_{k=1}^2 (\mu_{ik}^0 + \mu_{ik}^2) \ln \mu_{ik}^0 \right. \\ &+ \sum_{(ij)} \sum_{k=1}^4 (\lambda_{ij k}^0 + \lambda_{ij k}^2) \ln \lambda_{ij k}^0 \\ &\left. - \sum_{(ij)} \sum_{k=1}^2 (\mu_{ik}^0 + \mu_{ik}^2) \ln \mu_{ik}^0 + (\mu_{jk}^0 + \mu_{jk}^2) \ln \mu_{jk}^0 \right\},\end{aligned}\quad (4.2.17)$$

where

$$K_{ij} \equiv \frac{J_{ij}}{k_B T}, \quad K_{zij} \equiv \frac{J_{zij}}{k_B T}, \quad H \equiv \frac{h}{k_B T}. \quad (4.2.18)$$

After also expanding this expression to second order in the other "order" parameters (like \bar{m}_i), it can be separated into two terms. The first one, Φ_0 , only contains the parameters associated with the disordered phase, c_{ij}^{xz} , c_{ij}^{yz} , and m_i , while the other one, Φ_2 , is bilinear in the various "order" parameters. (If one wants to consider the case $h = 0$, one should expand Φ to second order in m_i , too, and include m_i in the set of "order" parameters.) Φ can now be written

$$\begin{aligned} \Phi &= \Phi_0 + \Phi_2 + \dots \\ &= \Phi_0 + c^T \cdot M \cdot c + \dots, \end{aligned} \quad (4.2.19)$$

where c is a vector containing all "order" parameters, and M is the symmetric matrix

$$M_{ij} = \left. \frac{\partial^2 \Phi}{\partial c_i \partial c_j} \right|_{c=0}. \quad (4.2.20)$$

The matrix M itself only depends on the parameters of the disordered phase, c_{ij}^{xz} , c_{ij}^{yz} , and m_i . Since Φ_2 does not contain terms that are a product of "order" parameters for different phases, the matrix M is block diagonal. It contains a block M^{AI} corresponding to the "order" parameters of the antiferromagnetic Ising phase, a block M^{XY} for those of the x - y ordered phase, and in the case $h = 0$ a block M^{FI} for the ferromagnetic Ising phase.

Now the minimization of Φ in the disordered phase boils down to minimizing Φ_0 , since the minimization with respect to c gives the equation $M \cdot c = 0$, which in this phase has the trivial solution $c = 0$, i.e. all "order" parameters are zero. In an ordered phase, on the other hand, there is also a solution for the minimization equations for Φ with some elements of c non-zero. The two solutions bifurcate for $\det M = 0$, so this is the equation giving the phase boundary. Since M is block diagonal the three different phase boundaries follow from

$$\det M^P = 0, \quad (4.2.21)$$

with $P = AI, XY, FI$ for the antiferromagnetic Ising phase, the x - y ordered phase, and the ferromagnetic Ising phase, respectively. The procedure for finding the phase boundaries is then to first solve the minimization equations for Φ_0 for the disordered phase only, substitute the result into M , and then to solve (4.2.21). In some cases, e.g. when the field h is zero, this can be done analytically, but if necessary the whole minimization can be done numerically.

4.3 The spatially anisotropic geometry

To apply the method described in the previous section to a specific geometry, one only needs to identify the different types of clusters, and count how often they occur in the

lattice. As a first example we will consider a cubic lattice with a spatially anisotropic interaction. The lattice consists of a collection of parallel quadratic planes, and the coupling between spins that lie in the same plane is different from the coupling between spins in adjacent planes. We will take the coupling within the planes to be larger than that between planes, so one has a stack of (more or less) weakly coupled layers. By varying the ratio of the inter-layer and intra-layer couplings from zero to one, the system changes from a collection of uncoupled, two-dimensional quadratic lattices to an isotropic three-dimensional cubic lattice.

4.3.1 The calculation of M^p

For this geometry the Hamiltonian (4.1.1) reduces to

$$\mathcal{H} = \sum_{\langle ij \rangle_{\parallel}} -J_{\parallel}(\sigma_i^x \sigma_j^x + \sigma_i^y \sigma_j^y) - J_{z\parallel} \sigma_i^z \sigma_j^z + \sum_{\langle ij \rangle_{\perp}} -J_{\perp}(\sigma_i^x \sigma_j^x + \sigma_i^y \sigma_j^y) - J_{z\perp} \sigma_i^z \sigma_j^z - \sum_{i=1}^N h \sigma_i^z. \quad (4.3.1)$$

The summation $\sum_{\langle ij \rangle_{\parallel}}$ extends over all nearest neighbour pairs of spins inside the layers, while the sum $\sum_{\langle ij \rangle_{\perp}}$ runs over nearest neighbour pairs that lie in adjacent layers. The couplings J_{\parallel} and $J_{z\parallel}$, and J_{\perp} and $J_{z\perp}$ are the intra-layer and inter-layer couplings, respectively.

Apart from the distinction between the sublattices a and b , all sites of the lattice are equivalent. There are, therefore, two one-spin reduced density matrices, $\rho_a^{(1)}$ and $\rho_b^{(1)}$, and two corresponding cluster entropies, $S_a^{(1)}$ and $S_b^{(1)}$. There are also two different types of two-spin clusters, since in this geometry a cluster of two spins in the same layer is not equivalent to one of two spins in adjacent layers. Thus one has two two-spin reduced density matrices, $\rho_{\parallel}^{(2)}$ and $\rho_{\perp}^{(2)}$, and two cluster entropies, $S_{\parallel}^{(2)}$ and $S_{\perp}^{(2)}$. Consequently, one finds for the energy terms in (4.2.4)

$$\begin{aligned} \text{Tr}(\rho \mathcal{H}) &= \sum_{i=1}^N \text{Tr}(\rho_i^{(1)} h_i^{(1)}) + \sum_{\langle ij \rangle_{\parallel}} \text{Tr}(\rho_{\parallel}^{(2)} h_{ij}^{(2)}) + \sum_{\langle ij \rangle_{\perp}} \text{Tr}(\rho_{\perp}^{(2)} h_{ij}^{(2)}) \\ &= -N (4J_{\parallel} c_{\parallel}^{xz} + 2J_{z\parallel} c_{\parallel}^{zz} + 2J_{\perp} c_{\perp}^{xz} + J_{z\perp} c_{\perp}^{zz} + mh), \end{aligned} \quad (4.3.2)$$

since out of the 6 neighbours of a particular spin 4 lie in the same layer, and 2 lie in adjacent layers. For the entropy one similarly finds

$$\begin{aligned} k_B \text{Tr}(\rho \ln \rho) &= \left\{ 5 \sum_{i=1}^N S_i^{(1)} - \sum_{\langle ij \rangle_{\parallel}} S_{\parallel}^{(2)} - \sum_{\langle ij \rangle_{\perp}} S_{\perp}^{(2)} \right\} \\ &= k_B N \left\{ -\frac{5}{2} \sum_{q=a,b} \text{Tr}(\rho_q^{(1)} \ln \rho_q^{(1)}) + 2 \text{Tr}(\rho_{\parallel}^{(2)} \ln \rho_{\parallel}^{(2)}) + \text{Tr}(\rho_{\perp}^{(2)} \ln \rho_{\perp}^{(2)}) \right\} \end{aligned} \quad (4.3.3)$$

The disordered phase is described by five parameters, viz. m , c_{\parallel}^{xz} , c_{\parallel}^{yz} , c_{\perp}^{xz} , and c_{\perp}^{yz} . The values of these parameters can be found by minimizing Φ_0 , which in this case is given by

$$\Phi_0 = -(4K_{\parallel}c_{\parallel}^{xz} + 2K_{z\parallel}c_{\parallel}^{yz} + 2K_{\perp}c_{\perp}^{xz} + K_{z\perp}c_{\perp}^{yz} + mH) - 5\mathcal{P}^{(1)} + 2\mathcal{P}_{\parallel}^{(2)} + \mathcal{P}_{\perp}^{(2)}. \quad (4.3.4)$$

The contributions from the three terms in (4.3.3) are obtained by setting the "order" parameters equal to zero in the eigenvalues of the density matrices. This gives

$$\begin{aligned} \mathcal{P}^{(1)} &= \frac{1}{2} \left(\ln(1 - m^2) + m \ln \frac{1+m}{1-m} \right) - \ln 2, \\ \mathcal{P}_{\zeta}^{(2)} &= \sum_{k=1}^4 \lambda_{\zeta k}^0 \ln \lambda_{\zeta k}^0, \quad (\zeta = \parallel, \perp). \end{aligned} \quad (4.3.5)$$

The eigenvalues $\lambda_{\zeta k}^0$ in the disordered phase are simply the expressions (4.2.13) with $c_i^z = c_i^y = m$.

Performing the minimization with respect to c_{ζ}^{α} , we find that the equations for $\zeta = \parallel$ and $\zeta = \perp$ decouple, and that they are the same apart from an overall factor,

$$\begin{aligned} \frac{\partial}{\partial c_{\zeta}^{xz}} \Phi_0 &\propto 2K_{\zeta} - \frac{\partial}{\partial c_{\zeta}^{xz}} \mathcal{P}_{\zeta}^{(2)} = 2K_{\zeta} - \frac{1}{2} \ln \frac{\lambda_{\zeta 2}^0}{\lambda_{\zeta 3}^0} = 0, \\ \frac{\partial}{\partial c_{\zeta}^{yz}} \Phi_0 &\propto K_{z\zeta} - \frac{\partial}{\partial c_{\zeta}^{yz}} \mathcal{P}_{\zeta}^{(2)} = K_{z\zeta} - \frac{1}{4} \ln \frac{\lambda_{\zeta 1}^0 \lambda_{\zeta 4}^0}{\lambda_{\zeta 2}^0 \lambda_{\zeta 3}^0} = 0. \end{aligned} \quad (4.3.6)$$

Equations (4.3.6) can be solved, and the result is the same as that for an infinite isotropic lattice [13],

$$\begin{aligned} c_{\zeta}^{xz} &= \frac{\sigma_{\zeta} + \theta_{\zeta} - 2(\sigma_{\zeta}\theta_{\zeta} + m^2(\theta_{\zeta}^2 - \sigma_{\zeta}\theta_{\zeta}))^{1/2}}{\sigma_{\zeta} - \theta_{\zeta}}, \\ c_{\zeta}^{yz} &= \frac{1}{2}(1 - c_{\zeta}^{xz}) \tanh(2K_{\zeta}), \end{aligned} \quad (4.3.7)$$

where

$$\sigma_{\zeta} \equiv e^{4K_{z\zeta}}, \quad \theta_{\zeta} \equiv \cosh^2(2K_{\zeta}). \quad (4.3.8)$$

The result of minimizing in m is

$$\begin{aligned} \frac{\partial}{\partial m} \Phi_0 &= -H + \frac{\partial}{\partial m} \left(-5\mathcal{P}^{(1)} + 2\mathcal{P}_{\parallel}^{(2)} + \mathcal{P}_{\perp}^{(2)} \right) \\ &= -H - \frac{5}{2} \ln \frac{1+m}{1-m} + \ln \frac{1+2m+c_{\parallel}^{xz}}{1-2m+c_{\parallel}^{xz}} + \frac{1}{2} \ln \frac{1+2m+c_{\perp}^{xz}}{1-2m+c_{\perp}^{xz}} = 0 \end{aligned} \quad (4.3.9)$$

This equation should be solved, together with (4.3.7), to give m as a function of H , or, if m is considered as an externally imposed parameter, it gives the field H required to produce that value of m .

The second order term Φ_2 is

$$\Phi_2 = \mathbf{c}^T \cdot \mathbf{M} \cdot \mathbf{c}, \quad (4.3.10)$$

where the vector $\mathbf{c}^T = (\bar{m}, c^x, c_{\parallel}^{xz}, c_{\perp}^{xz})$ contains the "order" parameters. The matrix \mathbf{M} is a block diagonal matrix consisting of a 1 by 1 block \mathbf{M}^{A1} , giving the coefficient of the term quadratic in \bar{m} , and a 3 by 3 block \mathbf{M}^{XY} coupling the other three "order" parameters, $(c^x, c_{\parallel}^{xz}, c_{\perp}^{xz})$,

$$\mathbf{M}^{A1} = -\frac{5}{1-m^2} + \frac{1}{c_{\parallel}^{xz}} \ln \frac{\lambda_{\parallel 2}^0}{\lambda_{\parallel 3}^0} + \frac{1}{2c_{\perp}^{xz}} \ln \frac{\lambda_{\perp 2}^0}{\lambda_{\perp 3}^0}, \quad (4.3.11)$$

and

$$\begin{aligned} M_{1,1}^{XY} &= -\frac{5}{m} \ln \frac{1+m}{1-m} + 4(\ell_{12}^{\parallel} + \ell_{24}^{\parallel}) + 2(\ell_{12}^{\perp} + \ell_{24}^{\perp}), \\ M_{1,2}^{XY} &= M_{2,1}^{XY} = 4(\ell_{12}^{\parallel} - \ell_{24}^{\parallel}), \\ M_{1,3}^{XY} &= M_{3,1}^{XY} = 2(\ell_{12}^{\perp} - \ell_{24}^{\perp}), \\ M_{2,2}^{XY} &= 4(\ell_{12}^{\parallel} + \ell_{24}^{\parallel}), \\ M_{2,3}^{XY} &= M_{3,2}^{XY} = 0, \\ M_{3,3}^{XY} &= 2(\ell_{12}^{\perp} + \ell_{24}^{\perp}), \end{aligned} \quad (4.3.12)$$

where

$$\ell_{km}^{\zeta} \equiv \frac{\ln(\lambda_{\zeta k}^0 / \lambda_{\zeta m}^0)}{4(\lambda_{\zeta k}^0 - \lambda_{\zeta m}^0)}, \quad (\zeta = \parallel, \perp). \quad (4.3.13)$$

If one wants to consider the case $h = 0$, m must be set equal to zero in Φ_0 , and included in the vector \mathbf{c} . \mathbf{M} will then also contain a 1 by 1 block \mathbf{M}^{F1} giving the coefficient of m^2 , which is equal to

$$\mathbf{M}^{F1} = -5 + \frac{4}{1+c_{\parallel}^{xz}} + \frac{2}{1+c_{\perp}^{xz}}. \quad (4.3.14)$$

4.3.2 Results

The phase diagram we obtain for this geometry is shown in figure 4.1 for different values of the spatial anisotropy η , and the magnetic field H equal to zero. We will always take the anisotropy in spin space equal for the intra-layer and inter-layer couplings, so that for the spatial anisotropy we have $\eta = K_{\perp}/K_{\parallel} = K_{z\perp}/K_{z\parallel}$. The two-dimensional case is recovered for $\eta = 0$, and the three-dimensional one for

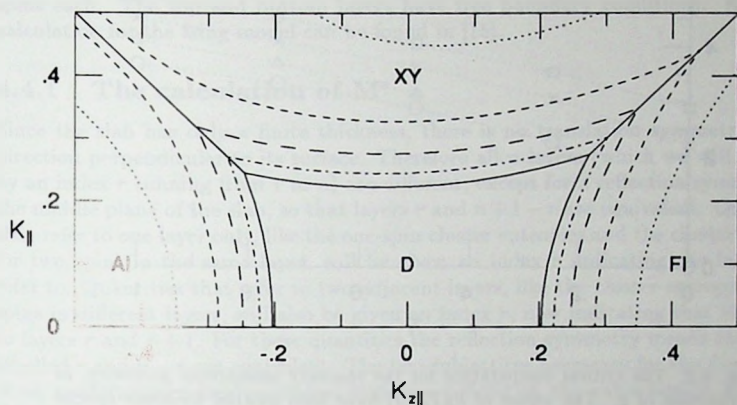


Fig. 4.1. The phase diagram for the spatially anisotropic geometry. The phase boundaries have been drawn for $\eta = 0$ (dotted), $1/4$ (short dashes), $1/2$ (long dashes), $3/4$ (dot-dashed), and 1 (solid). The magnetic field H is zero.

$\eta = 1$. The other three values, $\eta = 1/4, 1/2, 3/4$, interpolate between these two. The structure of the phase diagrams is roughly as follows: at high temperatures (around $K_{\parallel} = K_{z\parallel} = 0$) the system is in the disordered phase (D). The ordered phases one finds at lower temperature are the ferromagnetic Ising phase (FI) for $K_{z\parallel} > K_{\parallel} > 0$, the antiferromagnetic Ising phase (AI) for $-K_{z\parallel} > K_{\parallel} > 0$, and the x - y ordered phase (XY) for $K_{\parallel} > |K_{z\parallel}|$. The boundaries between these three phases and the disordered phase follow from the equations $\det M^F = 0$. For $H = 0$ the Ising phases are separated from the XY phase by the lines $K_{\parallel} = K_{z\parallel}$ and $K_{\parallel} = -K_{z\parallel}$.

As η is increased from zero to one, the disordered region (D) shrinks, the phase boundaries moving towards lower values of K (higher temperatures). The general shape of the disordered region changes little; for the Ising, XY, antiferromagnetic and ferromagnetic Heisenberg models one has $K_c^I < K_c^{XY} < K_c^{AH} < K_c^{FH}$ for most values of η . Two qualitative changes take place. First, the critical coupling of the ferromagnetic Heisenberg model, which is infinite in two dimensions, becomes finite as soon as the inter-layer coupling is turned on. This is consistent with the fact that the lower critical dimension of this model is 2. Second, the antiferromagnetic Heisenberg model does not exhibit a phase transition for $\eta \lesssim 1/4$. This is related to the fact that the cluster variation method, and similar approximations, predict a spurious phase transition at low temperatures [12, 13, 14]. As the temperature is lowered, both the AI and XY order disappear, and the system remains disordered down to $T = 0$. For low dimensions, and in this case for small η , this artifact of the approximation

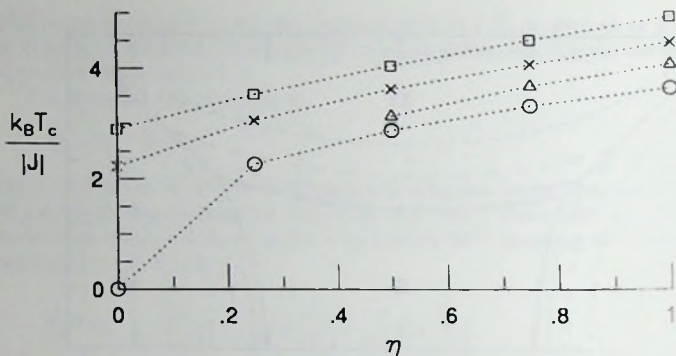


Fig. 4.2. The critical temperature for the spatially anisotropic geometry, as a function of η . The values of $k_B T_c / |J|$ have been plotted for some special cases of the XXZ Hamiltonian, viz. Ising (squares), XY (crosses), antiferromagnetic Heisenberg (triangles), and ferromagnetic Heisenberg (circles) interactions. The lines have only been drawn to guide the eye.

interferes with the phase transition at higher temperature. So, unfortunately, no conclusions can be drawn about the behaviour of the antiferromagnetic Heisenberg model near two dimensions, which is of great interest in connection with theories of high- T_c superconductors. For $\eta \gtrsim 1/2$, this unphysical transition takes place at such a low temperature that it is clearly separated from the physical ones, and the phase diagram is barely influenced by it. In fact, for the three-dimensional isotropic case ($\eta = 1$), it turns out that the accuracy is quite good when compared to high temperature series expansions.

In order to show the change of T_c from its two-dimensional value to that for three dimensions, figure 4.2 shows a plot of $k_B T_c / |J| = 1/|K|$ versus the spatial anisotropy η . The values given are for some special cases of the Hamiltonian (4.3.1), namely the Ising, XY, antiferromagnetic and ferromagnetic Heisenberg models.

4.4 The slab geometry

Another geometry that shows a cross-over from two to three dimensions is that of a slab consisting of a finite number, n , of simple quadratic layers. We will take the coupling constants equal in all directions, and by letting n run from 1 to ∞ the system changes from a two-dimensional simple quadratic lattice to a three-dimensional cubic lattice. The Hamiltonian is basically given by (4.1.1), with $J_{ij} = J$, $J_{zij} = J_z$, a homogeneous magnetic field h , and the sum running over n layers containing N/n

spins each. The top and bottom layers have free boundary conditions. A similar calculation for the Ising model can be found in [15].

4.4.1 The calculation of M^z

Since the slab has only a finite thickness, there is no translation symmetry in the direction perpendicular to its surface. Therefore all n layers (which we will indicate by an index r running from 1 to n) are different, except for a reflection symmetry in the middle plane of the slab, so that layers r and $n+1-r$ are equivalent. Quantities that refer to one layer only, like the one-spin cluster entropies and the cluster entropy for two spins in the same layer, will be given an index r indicating the layer they refer to. Quantities that refer to two adjacent layers, like the cluster entropy for two spins in different layers, will also be given an index r , now indicating that they refer to layers r and $r+1$. For these quantities the reflection symmetry means that those labelled r and $n-r$ are equivalent. The two sublattices necessary for the description of an antiferromagnetically ordered state are defined on the cubic lattice, so that a site on sublattice a in layer r is adjacent to sites on sublattice b in layers $r-1$, $r+1$, and r .

For each layer r we consequently have two one-spin cluster entropies, $S_{r_a}^{(1)}$ and $S_{r_b}^{(1)}$, and one cluster entropy for two spins within the layer, $S_{r_{\parallel}}^{(2)}$. There are two cluster entropies for spins in different layers, $S_{r_{\perp a}}^{(2)}$ where the spin in layer r is on the a sublattice and the one in layer $r+1$ on the b sublattice, and $S_{r_{\perp b}}^{(2)}$, where this is the other way round.

For the free energy functional Φ this leads to the expression

$$\begin{aligned} n\Phi = & \sum_{r=1}^n \left[-4(Kc_{r_{\parallel}}^{xx} + \frac{K_z}{2}c_{r_{\parallel}}^{zz}) - Hm_r + \frac{1}{k_B} \left\{ \frac{5}{2}(S_{r_a}^{(1)} + S_{r_b}^{(1)}) - 2S_{r_{\parallel}}^{(2)} \right\} \right] \\ & + \sum_{r=1}^{n-1} \sum_{q=a,b} \left\{ -(Kc_{r_{\perp q}}^{xx} + \frac{K_z}{2}c_{r_{\perp q}}^{zz}) - \frac{1}{2k_B} S_{r_{\perp q}}^{(2)} \right\} \\ & - \frac{1}{2k_B} (S_{1a}^{(1)} + S_{1b}^{(1)} + S_{na}^{(1)} + S_{nb}^{(1)}). \end{aligned} \quad (4.4.1)$$

The last term is a correction due to the fact that the top and bottom layers have only one neighbouring layer. In the disordered phase the non-zero parameters are m_r , $c_{r_{\parallel}}^{xx}$, and $c_{r_{\parallel}}^{zz}$ for every layer, and $c_{r_{\perp a}}^{xx}$ and $c_{r_{\perp a}}^{zz}$ for every pair of adjacent layers ($c_{r_{\perp a}}^{\alpha\alpha} = (c_{r_{\perp a}a}^{\alpha\alpha} + c_{r_{\perp a}b}^{\alpha\alpha})/2$). Hence we find for Φ_0

$$\begin{aligned} n\Phi_0 = & \sum_{r=1}^n \left\{ -4(Kc_{r_{\parallel}}^{xx} + \frac{K_z}{2}c_{r_{\parallel}}^{zz}) - Hm_r - 5\mathcal{P}_r^{(1)} + 2\mathcal{P}_{r_{\parallel}}^{(2)} \right\} \\ & + \sum_{r=1}^{n-1} \left\{ -2(Kc_{r_{\perp a}}^{xx} + \frac{K_z}{2}c_{r_{\perp a}}^{zz}) + \mathcal{P}_{r_{\perp a}}^{(2)} \right\} + \mathcal{P}_1^{(1)} + \mathcal{P}_n^{(1)}. \end{aligned} \quad (4.4.2)$$

where

$$\begin{aligned} \mathcal{P}_r^{(1)} &= \frac{1}{2} \left(\ln(1 - m_r^2) + m_r \ln \frac{1 + m_r}{1 - m_r} \right) - \ln 2, \\ \mathcal{P}_{r\zeta}^{(2)} &= \sum_{k=1}^4 \lambda_{r\zeta k}^0 \ln \lambda_{r\zeta k}^0, \quad (\zeta = \parallel, \perp). \end{aligned} \quad (4.4.3)$$

In the disordered phase, the eigenvalues $\lambda_{r\parallel k}^0$, where both spins in the cluster are in layer r , are obtained from (4.2.13) by setting $c_i^z = c_j^z = m_r$. For two spins in adjacent layers, r and $r+1$, we get $\lambda_{r\perp k}^0$ from (4.2.13) by setting $c_i^z = m_r$ and $c_j^z = m_{r+1}$. The presence of the magnetization profile m_r prevents us from treating the disordered phase analytically, so the minimization in the presence of a field H has to be done numerically. If H is zero, however, and consequently there is no magnetization, an analytical treatment is possible. This will be done in the following section.

The second order term Φ_2 is again of the form $\Phi_2 = \mathbf{c}^T \cdot \mathbf{M} \cdot \mathbf{c}$, where now $\mathbf{c}^T = (\bar{m}_r, \delta_r^{xx}, \delta_r^{zz}, c_r^x, c_{r\parallel}^{xx}, c_{r\perp}^{xx}, c_{r\parallel}^{xz}, c_{r\perp}^{xz})$ contains a large number of "order" parameters. For the antiferromagnetic Ising phase there is the staggered magnetization $\bar{m}_r = (c_{ra}^z - c_{rb}^z)/2$ for each layer. In addition, the quantities $\delta_r^{\alpha\alpha} = (c_{r\perp a}^{\alpha\alpha} - c_{r\perp b}^{\alpha\alpha})/2$ are also non-zero when the two sublattices a and b are different, which gives rise to these new "order" parameters. For the x - y ordered phase \mathbf{c} contains the magnetization in the x - y plane, c_r^x , the intra-layer correlation $c_{r\parallel}^{xx}$, and the two inter-layer correlations $c_{r\perp}^{xz}$ and $c_{r\perp}^{zz}$. For the case $h = 0$ the parameters m_r must be set equal to zero in Φ_0 , and included in \mathbf{c} as the "order" parameters for the ferromagnetic Ising phase. The structure of the matrices \mathbf{M}^p is given in appendix 4.A.

4.4.2 The case $H = 0$

In general the determination of the phase boundaries for the slab geometry must be done numerically, but if $H = 0$ one can proceed analytically, which we will first do for the x - y phase boundary. In this case the description of the disordered phase simplifies due to the fact that there is no magnetization profile m_r . For $H = 0$ and $m_r = 0$, (4.4.2) becomes

$$n\Phi_0 = \sum_{r=1}^n f_r^{\parallel} + \sum_{r=1}^{n-1} f_r^{\perp} - 2 \ln 2, \quad (4.4.4)$$

with

$$\begin{aligned} f_r^{\parallel}(c_{r\parallel}^{xx}, c_{r\parallel}^{zz}) &= -4(K c_{r\parallel}^{xx} + \frac{K_z}{2} c_{r\parallel}^{zz}) - 5 \ln 2 + 2\mathcal{P}_{r\parallel}^{(2)}, \\ f_r^{\perp}(c_{r\perp}^{xx}, c_{r\perp}^{zz}) &= -2(K c_{r\perp}^{xx} + \frac{K_z}{2} c_{r\perp}^{zz}) + \mathcal{P}_{r\perp}^{(2)}. \end{aligned} \quad (4.4.5)$$

Now minimizing Φ_0 with respect to a parameter $c_{r\zeta}^{\alpha\alpha}$ of the disordered phase gives

$$\frac{\partial}{\partial c_{r\zeta}^{\alpha\alpha}} n\Phi_0 = \frac{\partial}{\partial c_{r\zeta}^{\alpha\alpha}} f_r^\zeta = 0, \quad (\alpha = x, z), \quad (4.4.6)$$

because there is only one term in (4.4.4) containing the parameter $c_{r\zeta}^{\alpha\alpha}$. Moreover, apart from an overall factor of 2, the dependence of f_r^ζ on $c_{r\zeta}^{\alpha\alpha}$ is the same for any r and ζ . So, as in (4.3.6), we find for all r and ζ

$$\begin{aligned} 2K - \frac{\partial}{\partial c_{r\zeta}^{\alpha\alpha}} \mathcal{P}_{r\zeta}^{(2)} &= 2K - \frac{1}{2} \ln \frac{\lambda_{r\zeta 2}^0}{\lambda_{r\zeta 3}^0} = 0, \\ K_x - \frac{\partial}{\partial c_{r\zeta}^{\alpha\alpha}} \mathcal{P}_{r\zeta}^{(3)} &= K_x - \frac{1}{4} \ln \frac{(\lambda_{r\zeta 1}^0)^2}{\lambda_{r\zeta 2}^0 \lambda_{r\zeta 3}^0} = 0. \end{aligned} \quad (4.4.7)$$

The expressions (4.4.7) only depend, through (4.4.3) and (4.2.13), on $c_{r\zeta}^{\alpha\alpha}$ and $c_{r\zeta}^{\beta\beta}$. The equations (4.4.7) that determine the correlations $c_{r\zeta}^{\alpha\alpha}$, can be solved independently of r and ζ . The solutions one finds are again just the same as in the case of an infinite lattice, namely

$$c_{r\zeta}^{zz} \equiv c^{zz} = \frac{e^{2K_z} - \cosh 2K}{e^{2K_z} + \cosh 2K}, \quad (4.4.8)$$

$$c_{r\zeta}^{xx} \equiv c^{xx} = \frac{\sinh 2K}{e^{2K_x} + \cosh 2K}. \quad (4.4.9)$$

To find the phase boundary, we calculate the second order term Φ_2 of the free energy functional,

$$n\Phi_2 = \sum_{r=1}^n -5Q_r^{(1)} + 2Q_{r\parallel}^{(2)} + \sum_{r=1}^{n-1} Q_{r\perp}^{(2)} + Q_1^{(1)} + Q_n^{(1)}, \quad (4.4.10)$$

with

$$\begin{aligned} Q_r^{(1)} &= c_r^{z^2}, \\ Q_{r\zeta}^{(2)} &= \sum_{k=1}^4 \lambda_{r\zeta k}^2 \ln \lambda_{r\zeta k}^0 = \begin{cases} 4uc_r^{z^2} & (\zeta = \parallel) \\ u(c_r^x + c_{r+1}^x)^2 + v(c_r^x - c_{r+1}^x)^2 & (\zeta = \perp), \end{cases} \end{aligned} \quad (4.4.11)$$

and, using (4.4.7),

$$\begin{aligned} u &= \frac{K_z - K}{2(c^{zz} - c^{xx})}, \\ v &= \frac{K_z + K}{2(c^{zz} + c^{xx})}. \end{aligned} \quad (4.4.12)$$

Minimizing Φ_2 we find the system of equations $\frac{\partial}{\partial c_r^{\alpha\alpha}} n\Phi_2 = 0$, which turns out to be

$$\begin{aligned} b_1 c_1^x + a c_2^x &= 0, \\ a c_{r-1}^x + b c_r^x + a c_{r+1}^x &= 0 \quad (1 < r < n), \\ a c_{n-1}^x + b_1 c_n^x &= 0, \end{aligned} \quad (4.4.13)$$

with

$$\begin{aligned}
 a &= \frac{K_x - K}{c^{zx} - c^{xx}} - \frac{K_x + K}{c^{zx} + c^{xx}}, \\
 b &= 10 \frac{K_x - K}{c^{zx} - c^{xx}} + 2 \frac{K_x + K}{c^{zx} + c^{xx}} - 10, \\
 b_1 &= 9 \frac{K_x - K}{c^{zx} - c^{xx}} + \frac{K_x + K}{c^{zx} + c^{xx}} - 8.
 \end{aligned} \tag{4.4.14}$$

The system (4.4.13) admits solutions of the form $c_r^x = \alpha y^r$. From the equation for $1 < r < n$ we find

$$a(y^{r-1} + y^{r+1}) + by^r = 0, \tag{4.4.15}$$

or

$$y_{\pm} = \frac{-b \pm \sqrt{b^2 - 4a^2}}{2a}, \tag{4.4.16}$$

and

$$c_r^x = \alpha y_+^r + \beta y_-^r. \tag{4.4.17}$$

Substituting (4.4.17) into the equations for the boundary layers then gives

$$\begin{aligned}
 (b_1 y_+ + a y_+^2) \alpha + (b_1 y_- + a y_-^2) \beta &= 0, \\
 (b_1 y_+^n + a y_+^{n-1}) \alpha + (b_1 y_-^n + a y_-^{n-1}) \beta &= 0.
 \end{aligned} \tag{4.4.18}$$

The trivial solution $\alpha = \beta = 0$ gives the disordered phase, where the magnetization is zero; at the point where the determinant of the coefficients vanishes, the solution bifurcates, and this signals the transition into the x - y ordered phase.

It follows from (4.4.15) that $y_+ y_- = 1$, and for $b^2 > 4a^2$, y_{\pm} are real. For $b^2 < 4a^2$ they are complex conjugates, so $y_+ = e^{-i\phi}$, $y_- = e^{i\phi}$. For high temperatures one finds that $b^2 > 4a^2$, giving real y_{\pm} . Lowering T , one comes to a point where $b^2 = 4a^2$, and $y_+ = y_- = 1$. This happens at $T_c(\infty)$, the critical temperature for the infinite cubic lattice. Due to translation invariance, the spontaneous magnetization of this system is homogeneous. The equation $b = -2a$ is equivalent to

$$6(K_x - K) \frac{e^{2K_x} + \cosh 2K}{e^{2K_x} - e^{2K}} = 5, \tag{4.4.19}$$

which is indeed the equation for the phase boundary of a system with coordination number $z = 6$ as found previously [13]. At $T_c(\infty)$ a layer of finite width is still disordered, since the bifurcation of the solution of (4.4.18) has not yet taken place.

Below $T_c(\infty)$, we have $y_+ = e^{-i\phi}$ and $y_- = e^{i\phi}$, so $c_r^x = \alpha e^{-ir\phi} + \beta e^{ir\phi}$, with $\tan \phi = \sqrt{4a^2/b^2 - 1}$. The determinant of (4.4.18) then gives

$$(b_1 + a e^{-i\phi})^2 = e^{-2(n-1)i\phi} (b_1 + a e^{i\phi})^2. \tag{4.4.20}$$

The solution with $\phi = 0$ corresponds to the bulk transition temperature $T_c(\infty)$, and does not indicate a phase transition in the finite slab. This transition corresponds to the first non-zero value of ϕ satisfying (4.4.20), which is a solution of

$$b_1 + ae^{-i\phi} = -e^{-(n-1)i\phi}(b_1 + ae^{i\phi}). \quad (4.4.21)$$

Hence we find that the solution of (4.4.21) corresponding to the smallest non-zero value for ϕ gives the critical temperature $T_c(n)$ of an n -layer slab. In the limit of large n , the value of ϕ at $T_c(n)$ approaches its value for the infinite lattice, $\phi = 0$ at $T_c(\infty)$. By expanding (4.4.21) for small ϕ and large n we find that ϕ goes to zero as $\phi \approx \pi/(n+q)$, with q given by $q = -(3a + b_1)/(a + b_1)$ calculated at $T_c(\infty)$. It can be shown that $q > 0$ for all K and K_2 .

In addition to the critical temperature, we also find the shape of the order parameter profile c_r^z at the onset of the ordered phase. The normalization is determined by the higher-order terms of Φ , but since at $T_c(n)$ the amplitude is zero anyway, the shape of the profile is the only quantity of interest. We first observe that, in order to have a real valued magnetization, we must have $\beta = \alpha^*$, so

$$c_r^z = |\alpha|(e^{-i(r\phi + \phi_0)} + e^{i(r\phi + \phi_0)}) = 2|\alpha|\cos(r\phi + \phi_0). \quad (4.4.22)$$

The angle ϕ_0 can easily be found from the symmetry requirement that $c_r^z = c_{n+1-r}^z$, which gives $\phi_0 \equiv \theta - \pi/2 = -(n+1)\phi/2$, and

$$c_r^z = 2|\alpha|\sin(r\phi + \theta). \quad (4.4.23)$$

Exactly the same treatment can be applied to the ferromagnetic and antiferromagnetic Ising phases; the only difference lies in the expressions for a , b , and b_1 . For the ferromagnetic Ising phase they are

$$\begin{aligned} a &= \frac{1}{1 + c^{xz}} - \frac{K}{c^{xz}}, \\ b &= \frac{10}{1 + c^{xz}} + 2\frac{K}{c^{xz}} - 10, \\ b_1 &= \frac{9}{1 + c^{xz}} + \frac{K}{c^{xz}} - 8, \end{aligned} \quad (4.4.24)$$

and for the antiferromagnetic Ising phase

$$\begin{aligned} a &= \frac{K}{c^{xz}} - \frac{1}{1 + c^{xz}}, \\ b &= 10\frac{K}{c^{xz}} + \frac{2}{1 + c^{xz}} - 10, \\ b_1 &= 9\frac{K}{c^{xz}} + \frac{1}{1 + c^{xz}} - 8. \end{aligned} \quad (4.4.25)$$

Using (4.4.21) combined with (4.4.15), (4.4.24), and (4.4.25) we can construct the phase diagram for $H = 0$.

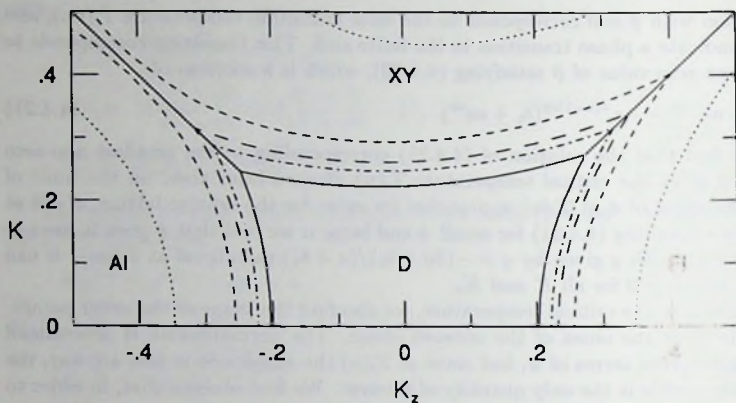


Fig. 4.3. The phase diagram for the slab geometry. Phase boundaries are given for $n = 1$ (dotted), 2 (short dashes), 3 (long dashes), 4 (dot-dashed), and ∞ (solid). The magnetic field H is zero.

4.4.3 Results

The phase diagram we find for the slab geometry is shown in figure 4.3 for $n = 1, 2, 3, 4$, and ∞ and $H = 0$. For the two- and three-dimensional cases $n = 1$ and $n = \infty$ they are of course equal to the results for the infinite lattices with coordination number $z = 4$ and 6 , respectively, while the double layer corresponds to the case $z = 5$. The basic features of the phase diagram are the same as in section 4.3, with in this case the unphysical gap around $K_{z\parallel} = -K_{\parallel}$ disappearing for $n > 2$. Figure 4.4 again displays the behaviour of T_c when going from two to three dimensions.

For this geometry we also calculated the order parameter profile in the layer. In particular for the x - y ordered phase this is of interest, since the order parameter \vec{c}_i^x (indicating off-diagonal long range order) corresponds, in the pseudo-spin formulation of the quantum lattice gas [1], to the superfluid condensate wave function. It was shown in the previous section that the shape of the order parameter profile at T_c is given by $\vec{c}_i^x \propto \sin(r\phi + \theta)$. In figure 4.5 we show the profile for the XY model in a slab of $n = 30$ layers. The critical coupling for this thickness is $K_c = 0.2243$, which corresponds to $\phi = 0.09873$, and $\theta = 0.04045$. As a comparison we have also drawn the result of numerically minimizing the full free energy functional Φ at a coupling slightly below T_c , $K = 0.2244$. The plots have been scaled so as to coincide at their maxima. Obviously the approximations made in section 4.4.2 hold in a small temperature range below T_c . For temperatures farther below T_c , the magnetization \vec{c}_i^x starts to saturate in the interior of the slab, and since this behaviour is governed

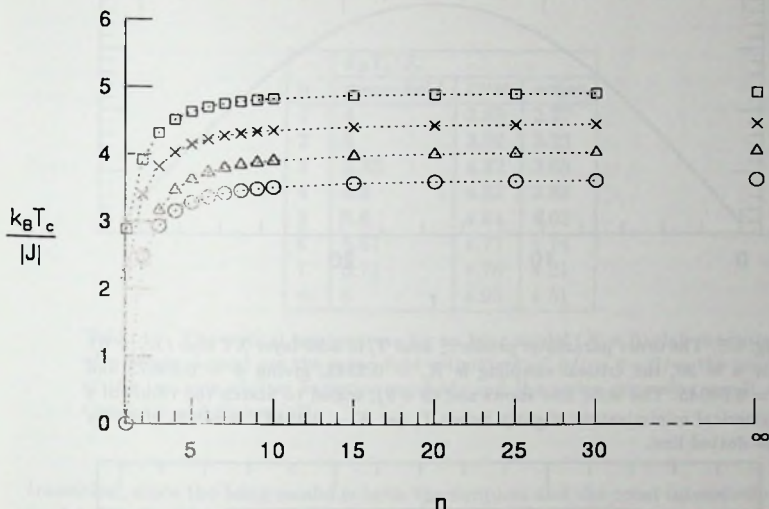


Fig. 4.4. The critical temperature for the slab geometry for various values of n . The values of $k_B T_c / |J|$ have been plotted for some special cases of the XXZ Hamiltonian, viz. Ising (squares), XY (crosses), antiferromagnetic Heisenberg (triangles), and ferromagnetic Heisenberg (circles) interactions. The lines are a guide for the eye.

by the higher order terms in Φ the order parameter profile is no longer sinusoidal.

Some conclusions we can draw from the behaviour of c_i^z near T_c are, first, that all order parameters become non-zero simultaneously at the same temperature, so there is no separate surface transition. Second, the order parameter drops almost to zero at the slab boundary; in fact the profile goes through zero at $r_0 = (n+1)/2 - \pi/2\phi$, which is right outside the slab. In the limit $n \rightarrow \infty$ we find that $r_0 = (1-q)/2 < 1/2$. This supports a proposition that was made recently [16], that the use of Dirichlet boundary conditions in finite size scaling theory would be fairly realistic.

Farther away from T_c , we observe that there are two effects that suppress the value of the order parameter in a layer with respect to its value in a three-dimensional lattice. For any temperature, its value will be lower in the outer layers, because of the proximity of the free boundary layer. Second, for temperatures just below T_c , the order parameter will be smaller than its three-dimensional value over the whole width of the slab, because T_c for the three-dimensional system is higher. For low enough temperatures, the magnetization takes on its three-dimensional value in the inner layers of the slab. The order parameter profile for a 30-layer slab is plotted in

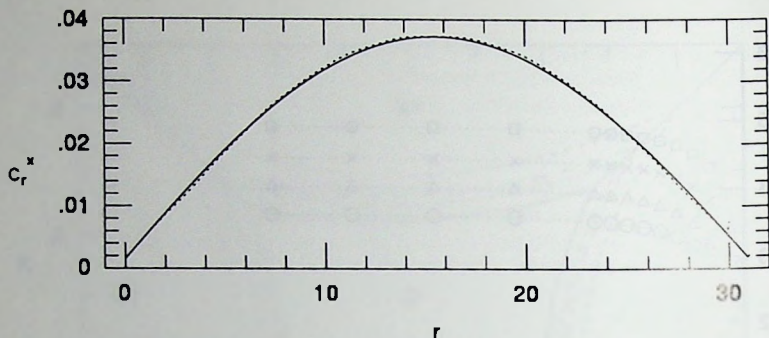


Fig. 4.5. The order parameter profile c_r^x near T_c in a 30-layer XY slab ($K_z = 0$). For $n = 30$, the critical coupling is $K_c = 0.2243$, giving $\phi = 0.09873$ and $\theta = 0.04045$. The solid line shows $\sin(r\phi + \theta)$, scaled to match the result of a numerical minimization slightly below T_c (at $K = 0.2244$), which is given by the dotted line.

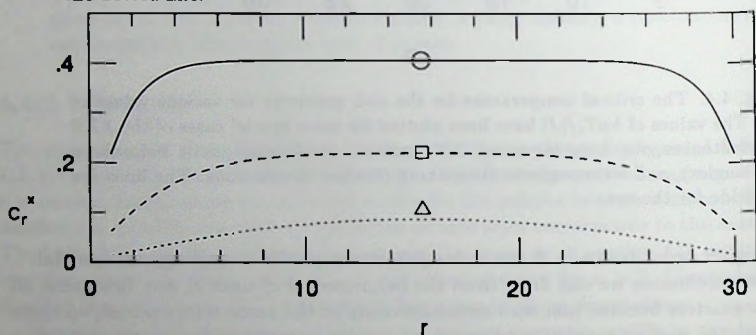


Fig. 4.6. The order parameter profile c_r^x in a 30-layer XY slab for $K = 0.225$ (dotted), $K = 0.23$ (short dashes), and $K = 0.25$ (solid). The critical coupling for $n = 30$ is $K_c = 0.2243$. Also plotted are the values of c_r^x in a three-dimensional lattice at the same coupling strengths (open symbols).

figure 4.6 for various values of K for the XY model ($K_z = 0$).

4.5 Discussion

To examine the merits of the cluster variation method applied to these spin models, we will compare its results with those of other approaches. We first examine the Ising

n	$k_B T_c / J_z$		
	mean-field	CVM	series
1	4	2.89	2.27
2	5	3.92	3.23
3	5.33	4.32	3.65
4	5.5	4.52	3.88
5	5.6	4.64	4.03
6	5.67	4.71	4.14
7	5.71	4.76	4.21
∞	6	4.93	4.51

Table 4.1. The critical temperature for an Ising model ($K = 0$) slab consisting of n layers. Listed are the mean-field estimate $k_B T_c / J_z = 6 - 2/n$, the result of the two-spin cluster variation method, and the series expansion result of Capehart and Fisher [17].

transition, since the Ising model is both the simplest and the most intensively studied model described by a Hamiltonian of the form (4.1.1). The Ising model is known to have ordered phases with a non-zero magnetization in two and three dimensions, and in both dimensions the cluster variation estimate of T_c is considerably better than that of the mean-field approximation. Hence one would expect its result to be an improvement for the slab geometry, too. This is indeed the case, as is shown in table 4.1, where we compare the results of these two approximations with those of series expansion techniques [17] for the pure Ising case $K = 0$. Similarly, for the spatially anisotropic geometry one would expect the cluster variation result to be an improvement over the mean-field estimate $k_B T_c / J_{\parallel z} = 4 + 2\eta$. Thus the Ising transition seems to confirm the pattern one usually finds for classical models: the two-spin cluster variation method overestimates T_c , but much less than the mean-field approximation. In turn, the cluster variation result can be expected to improve when one uses larger clusters. Also, as long as the Hamiltonian is Ising-like ($K_x > K \geq 0$), there is no unphysical transition back to the disordered state at low temperature.

The situation for the x - y transition is more complicated. For the slab geometry one expects a transition to a phase that does not have a magnetization, since it is known that such a phase cannot exist at $T \neq 0$ in a finite slab [18, 19]. This phase might have topological order à la Kosterlitz-Thouless [20]. For thick slabs the transition should cross over to a three-dimensional x - y transition. For the anisotropic geometry, on the other hand, a three-dimensional x - y transition is expected, only crossing over to a two-dimensional transition in the limit of uncoupled layers. The cluster variation method is not capable of producing a topological phase transition in these situations, and yields, as a refined mean-field method, transitions to an x -

	simple quadratic			simple cubic		
	mean-field	CVM	series	mean-field	CVM	series
I	0.25	0.347	0.441	0.167	0.203	0.222
XY	0.25	0.451	0.635	0.167	0.224	0.248
AH	0.25	-	-	0.167	0.246	0.260
FH	0.25	∞	∞	0.167	0.275	0.298

Table 4.2. The results of the cluster variation method compared with those of the mean field approximation and of series expansion techniques [20]. Shown are the critical couplings for the Ising, XY, antiferromagnetic Heisenberg and ferromagnetic Heisenberg models, on a simple quadratic ($z = 4$) and a simple cubic ($z = 6$) lattice.

phase with a non-zero magnetization. Only the location of the critical temperature can be meaningfully extracted from the cluster variation method. As it agrees reasonably for the pure XY model ($K_z = 0$), we may expect that in the general case $K_z \neq 0$ it also gives a good description of the phase boundary. The fact that the behaviour of T_c as a function of n is qualitatively similar to that for the Ising model is confirmed by renormalization group studies [21].

The situation near the Heisenberg model ($K_z = \pm K$) is particularly delicate. In the slab geometry, being basically two-dimensional, the transition point should diverge to $K_c = \infty$ for all slabs of a finite thickness. In the anisotropic geometry K_c stays finite for all anisotropies except for the case of uncoupled layers. To a certain extent the cluster variation method shows this picture for the ferromagnetic Heisenberg model. It gives a transition temperature $T = 0$ for the two-dimensional case, but finite transition temperatures in all other cases. It gives an increase of K_c for finite layers near the Heisenberg model, but fails to produce the divergence of K_c (or $T_c = 0$).

For the antiferromagnetic Heisenberg model the picture is similar but blurred by the interference of the spurious disordered phase at $T = 0$. The fact that for layer thicknesses below $n = 3$ the transition temperature drops to zero cannot be seen as a virtue of the cluster variation method, since it gives a similar behaviour for sufficiently anisotropic geometries. Incorporation of long wavelength fluctuations is an essential ingredient to improve the phase diagram at points where higher symmetries of the model drive the phase transition to $T = 0$.

A further comparison with series expansion results [22] is shown in table 4.2 for the two- and three-dimensional infinite lattice. In all cases the cluster variation method gives a considerable improvement over the mean-field result. Also, whereas the mean-field approximation gives the same value of K_c for all models listed in table 4.2, the cluster variation method has $K_c^I < K_c^{XY} < K_c^{AH} < K_c^{FH}$, in accordance with the

series results. We may conclude that while the cluster variation method does not always give a good description of the phase transition, its estimate for the critical temperature is in general quite good. Especially in cases where it is not feasible to examine the whole phase diagram by more sophisticated methods, it is a useful tool.

Appendix

In this appendix we give the structure of the matrices M^p for the slab geometry described in section 4.4. Due to the reflection symmetry there are w different layers in an n -layer slab, with $w = n/2$ for even n , and $w = (n+1)/2$ for odd n . Quantities that pertain only to one layer will, therefore, give rise to w independent "order" parameters, while the exact number of "order" parameters for quantities that concern two layers depends on n being odd or even, and also on the effect of the reflection symmetry on these "order" parameters. The matrices M^p are always symmetric, $M_{ij}^p = M_{ji}^p$. The elements that are not given below, and that cannot be obtained from the elements given below by using this symmetry are all zero. As was already pointed out in section 4.4, for $n = 1$ and 2 the results are equivalent to those for an infinite lattice with coordination number $z = 4$ and 5 respectively. Hence we will assume here that n is larger than 3.

For the antiferromagnetic Ising phase the situation is as follows. The staggered magnetization, \bar{m}_r for each layer, gives rise to w different "order" parameters. The quantities δ_r^{xx} and δ_r^{zz} give an additional $w - 1$ parameters. There is no $\delta_w^{\alpha\alpha}$, since for even n the layers w and $w + 1$ are equivalent because of the reflection symmetry, and hence $\delta_w^{\alpha\alpha} = 0$, and for odd n , $\delta_w^{\alpha\alpha} = \delta_{w-1}^{\alpha\alpha}$. So in total the vector c contains $3w - 2$ parameters connected with the antiferromagnetic Ising phase; these elements of c will be ordered as follows:

$$\begin{aligned} c_{3r-2} &= \bar{m}_r & (r = 1, \dots, w) \\ c_{3r-1} &= \delta_r^{xx} & (r = 1, \dots, w-1) \\ c_{3r} &= \delta_r^{zz} & (r = 1, \dots, w-1). \end{aligned} \quad (4.A.1)$$

In this notation the elements of M^{A1} are, for $r < w$:

$$\begin{aligned} M_{1,1}^{A1} &= \frac{-8}{1-m_1^2} + \frac{2}{c_{1||}^{xx}} \ln \frac{\lambda_{1||2}^0}{\lambda_{1||3}^0} + \frac{1}{2} \left\{ \alpha_1^+ + \frac{\Delta_1^2}{\omega_1^2} \beta_1^+ \right\} + \frac{1}{4\omega_1} \left(1 - \frac{\Delta_1^2}{\omega_1^2} \right) \gamma_1 \\ M_{3r-2,3r-2}^{A1} &= \frac{-10}{1-m_r^2} + \frac{2}{c_{r||}^{xx}} \ln \frac{\lambda_{r||2}^0}{\lambda_{r||3}^0} + \frac{1}{2} \left\{ \alpha_r^+ + \frac{\Delta_r^2}{\omega_r^2} \beta_r^+ \right\} + \frac{1}{4\omega_r} \left(1 - \frac{\Delta_r^2}{\omega_r^2} \right) \gamma_r \\ &\quad + \frac{1}{2} \left\{ \alpha_{r-1}^+ + \frac{\Delta_{r-1}^2}{\omega_{r-1}^2} \beta_{r-1}^+ \right\} + \frac{1}{4\omega_{r-1}} \left(1 - \frac{\Delta_{r-1}^2}{\omega_{r-1}^2} \right) \gamma_{r-1} \quad (r \neq 1) \\ M_{3r-2,3r-1}^{A1} &= \frac{\Delta_r c_{r\perp}^{xx}}{\omega_r^2} \beta_r^+ - \frac{\Delta_r c_{r\perp}^{xx}}{2\omega_r^3} \gamma_r \end{aligned}$$

$$\begin{aligned}
M_{3r-2,3r}^{A1} &= \frac{1}{2} \left\{ \alpha_r^- - \frac{\Delta_r}{\omega_r} \beta_r^- \right\} & (4.A.2) \\
M_{3r-2,3r+1}^{A1} &= -\frac{1}{2} \left\{ \alpha_r^+ - \frac{\Delta_r^2}{\omega_r^2} \beta_r^+ \right\} + \frac{1}{4\omega_r} \left(1 - \frac{\Delta_r^2}{\omega_r^2} \right) \gamma_r \\
M_{3r-1,3r-1}^{A1} &= \frac{c_{r1}^{xx2}}{\omega_r^2} \beta_r^+ + \frac{1}{\omega_r} \left(1 - \frac{c_{r1}^{xx2}}{\omega_r^2} \right) \gamma_r \\
M_{3r-1,3r}^{A1} &= -\frac{c_{r1}^{xx}}{\omega_r} \beta_r^- \\
M_{3r-1,3r+1}^{A1} &= M_{3r-2,3r-1}^{A1} \\
M_{3r,3r}^{A1} &= \frac{1}{2} \left\{ \alpha_r^+ + \beta_r^+ \right\} \\
M_{3r,3r+1}^{A1} &= -\frac{1}{2} \left\{ \alpha_r^- + \frac{\Delta_r}{\omega_r} \beta_r^- \right\}.
\end{aligned}$$

From the last layer there is, for even n , a contribution

$$\begin{aligned}
M_{3w-2,3w-2}^{A1} &= \frac{-10}{1-m_w^2} + \frac{2}{c_{w\parallel}^{xx}} \ln \frac{\lambda_{w\parallel 2}^0}{\lambda_{w\parallel 3}^0} + \frac{1}{2c_{w1}^{xx}} \ln \frac{\lambda_{w1 2}^0}{\lambda_{w1 3}^0} & (4.A.3a) \\
&+ \frac{1}{2} \left\{ \alpha_{w-1}^+ + \frac{\Delta_{w-1}^2}{\omega_{w-1}^2} \beta_{w-1}^+ \right\} + \frac{1}{4\omega_{w-1}} \left(1 - \frac{\Delta_{w-1}^2}{\omega_{w-1}^2} \right) \gamma_{w-1},
\end{aligned}$$

and for odd n

$$\begin{aligned}
M_{3w-2,3w-2}^{A1} &= \frac{-5}{1-m_w^2} + \frac{1}{c_{w\parallel}^{xx}} \ln \frac{\lambda_{w\parallel 2}^0}{\lambda_{w\parallel 3}^0} & (4.A.3b) \\
&+ \frac{1}{2} \left\{ \alpha_{w-1}^+ + \frac{\Delta_{w-1}^2}{\omega_{w-1}^2} \beta_{w-1}^+ \right\} + \frac{1}{4\omega_{w-1}} \left(1 - \frac{\Delta_{w-1}^2}{\omega_{w-1}^2} \right) \gamma_{w-1}.
\end{aligned}$$

The following definitions have been used

$$\begin{aligned}
\alpha_r^\pm &= \frac{1}{4\lambda_{r1}^0} \pm \frac{1}{4\lambda_{r14}^0} \\
\beta_r^\pm &= \frac{1}{4\lambda_{r12}^0} \pm \frac{1}{4\lambda_{r13}^0} \\
\gamma_r &= \ln \frac{\lambda_{r1 2}^0}{\lambda_{r1 3}^0} & (4.A.4) \\
\Delta_r &= \frac{1}{2}(m_r - m_{r+1}) \\
\omega_r &= \sqrt{\Delta_r^2 + c_{r1}^{xx2}}.
\end{aligned}$$

In the x - y ordered phase there are w parameters $c_{r\parallel}^{xx}$ and c_{r1}^{xx} and $w-1$ different parameters c_{r1}^{xx} and c_{r1}^{xx} . Finally, if n is even, there is one additional parameter $c_{w1}^{xx} =$

$c_{w,1}^{xx}$ because of the reflection symmetry. So in total c contains $4w - 2$ parameters for odd n , $4w - 1$ for even n , ordered as follows:

$$\begin{aligned}
 c_{4r-3} &= c_r^{xx} & (r = 1, \dots, w) \\
 c_{4r-2} &= c_{r||}^{xx} & (r = 1, \dots, w) \\
 c_{4r-1} &= c_{r\perp}^{xx} & (r = 1, \dots, w-1) \\
 c_{4r} &= c_{r\perp}^{xx} & (r = 1, \dots, w-1) \\
 c_{4w-1} &= c_{w,1}^{xx} & (\text{for } n \text{ even}).
 \end{aligned} \tag{4.A.5}$$

For the matrix M^{xy} find, for $r < w$

$$\begin{aligned}
 M_{1,1}^{xy} &= -\frac{8}{m_1} \ln \frac{1+m_1}{1-m_1} + 8 \left\{ \ell_{12}^{||} + \ell_{24}^{||} \right\} \\
 &\quad + \frac{2}{1+\xi_1^2} \left\{ \xi_1^2 (\ell_{12}^{\perp} + \ell_{34}^{\perp}) + \ell_{13}^{\perp} + \ell_{34}^{\perp} \right\} \\
 M_{4r-3,4r-3}^{xy} &= -\frac{10}{m_r} \ln \frac{1+m_r}{1-m_r} + 8 \left\{ \ell_{12}^{||} + \ell_{24}^{||} \right\} \\
 &\quad + \frac{2}{1+\xi_r^2} \left\{ \xi_r^2 (\ell_{12}^{\perp} + \ell_{34}^{\perp}) + \ell_{13}^{\perp} + \ell_{24}^{\perp} \right\} \\
 &\quad + \frac{2}{1+\xi_{r-1}^2} \left\{ \xi_{r-1}^2 (\ell_{13}^{r-1} + \ell_{24}^{r-1}) + \ell_{12}^{r-1} + \ell_{34}^{r-1} \right\} \quad (r \neq 1) \\
 M_{4r-3,4r-2}^{xy} &= 8 \left\{ \ell_{12}^{||} - \ell_{24}^{||} \right\} \\
 M_{4r-3,4r-1}^{xy} &= \frac{2}{1+\xi_r^2} \left\{ \xi_r^2 (\ell_{12}^{\perp} - \ell_{34}^{\perp}) + \ell_{13}^{\perp} - \ell_{24}^{\perp} \right\} \\
 M_{4r-3,4r}^{xy} &= \frac{2\xi_r}{1+\xi_r^2} \left\{ \ell_{12}^{\perp} + \ell_{34}^{\perp} - \ell_{13}^{\perp} - \ell_{24}^{\perp} \right\} \\
 M_{4r-3,4r+1}^{xy} &= \frac{2\xi_r}{1+\xi_r^2} \left\{ \ell_{12}^{\perp} - \ell_{34}^{\perp} - \ell_{13}^{\perp} + \ell_{24}^{\perp} \right\} \\
 M_{4r-2,4r-2}^{xy} &= 8 \left\{ \ell_{12}^{||} + \ell_{24}^{||} \right\} \\
 M_{4r-1,4r-1}^{xy} &= \frac{2}{1+\xi_r^2} \left\{ \xi_r^2 (\ell_{12}^{\perp} + \ell_{34}^{\perp}) + \ell_{13}^{\perp} + \ell_{24}^{\perp} \right\} \\
 M_{4r-1,4r}^{xy} &= \frac{2\xi_r}{1+\xi_r^2} \left\{ \ell_{12}^{\perp} - \ell_{34}^{\perp} - \ell_{13}^{\perp} + \ell_{24}^{\perp} \right\} \\
 M_{4r-1,4r+1}^{xy} &= \frac{2\xi_r}{1+\xi_r^2} \left\{ \ell_{12}^{\perp} + \ell_{34}^{\perp} - \ell_{13}^{\perp} - \ell_{24}^{\perp} \right\} \\
 M_{4r,4r}^{xy} &= \frac{2}{1+\xi_r^2} \left\{ \xi_r^2 (\ell_{13}^{\perp} + \ell_{24}^{\perp}) + \ell_{12}^{\perp} + \ell_{34}^{\perp} \right\} \\
 M_{4r,4r+1}^{xy} &= \frac{2}{1+\xi_r^2} \left\{ \xi_r^2 (\ell_{13}^{\perp} - \ell_{24}^{\perp}) + \ell_{12}^{\perp} - \ell_{34}^{\perp} \right\}.
 \end{aligned} \tag{4.A.6}$$

The last few elements are, for even n

$$\begin{aligned}
 M_{4w-3,4w-3}^{xy} &= -\frac{10}{m_w} \ln \frac{1+m_w}{1-m_w} + 8 \left\{ \ell_{12}^{w\parallel} + \ell_{24}^{w\parallel} \right\} + 2 \left\{ \ell_{12}^{w\perp} + \ell_{24}^{w\perp} \right\} \\
 &\quad + \frac{2}{1+\xi_{w-1}^2} \left\{ \xi_{w-1}^2 (\ell_{13}^{w-1\perp} + \ell_{24}^{w-1\perp}) + \ell_{12}^{w-1\perp} + \ell_{34}^{w-1\perp} \right\} \\
 M_{4w-3,4w-2}^{xy} &= 8 \left\{ \ell_{12}^{w\parallel} - \ell_{24}^{w\parallel} \right\} \\
 M_{4w-3,4w-1}^{xy} &= 2 \left\{ \ell_{12}^{w\perp} - \ell_{24}^{w\perp} \right\} \\
 M_{4w-2,4w-2}^{xy} &= 8 \left\{ \ell_{12}^{w\parallel} + \ell_{24}^{w\parallel} \right\} \\
 M_{4w-1,4w-1}^{xy} &= 2 \left\{ \ell_{12}^{w\perp} + \ell_{24}^{w\perp} \right\},
 \end{aligned} \tag{4.A.7a}$$

and for odd n

$$\begin{aligned}
 M_{4w-3,4w-3}^{xy} &= -\frac{5}{m_w} \ln \frac{1+m_w}{1-m_w} + 4 \left\{ \ell_{12}^{w\parallel} + \ell_{24}^{w\parallel} \right\} \\
 &\quad + \frac{2}{1+\xi_{w-1}^2} \left\{ \xi_{w-1}^2 (\ell_{13}^{w-1\perp} + \ell_{24}^{w-1\perp}) + \ell_{12}^{w-1\perp} + \ell_{34}^{w-1\perp} \right\} \\
 M_{4w-3,4w-2}^{xy} &= 4 \left\{ \ell_{12}^{w\parallel} - \ell_{24}^{w\parallel} \right\} \\
 M_{4w-2,4w-2}^{xy} &= 4 \left\{ \ell_{12}^{w\parallel} + \ell_{24}^{w\parallel} \right\}.
 \end{aligned} \tag{4.A.7b}$$

We have used the definitions

$$\begin{aligned}
 \xi_r &= \left(\frac{(c_r^z - c_{r+1}^z)^2}{4c_{r\perp}^{xz}} + 1 \right)^{1/2} - \frac{(c_r^z - c_{r+1}^z)}{2c_{r\perp}^{xz}} \\
 \ell_{km}^{r\zeta} &= \frac{\ln(\lambda_{r\zeta k}^0 / \lambda_{r\zeta m}^0)}{4(\lambda_{r\zeta k}^0 - \lambda_{r\zeta m}^0)} \quad (\zeta = \parallel, \perp).
 \end{aligned} \tag{4.A.8}$$

Finally, if $h = 0$, there are w parameters m_r for the ferromagnetic Ising phase, giving a vector c :

$$c_r = m_r \quad (r = 1, \dots, w), \tag{4.A.9}$$

and a matrix M^{PI} (for $r < w$):

$$\begin{aligned}
 M_{1,1}^{PI} &= -8 + \frac{8}{1+c_{1\parallel}^{xz}} + \frac{1}{1+c_{1\perp}^{xz}} + \frac{1}{4c_{1\perp}^{xz}} \ln \frac{\lambda_{1\perp 2}^0}{\lambda_{1\perp 3}^0} \\
 M_{r,r}^{PI} &= -10 + \frac{8}{1+c_{r\parallel}^{xz}} + \frac{1}{1+c_{r\perp}^{xz}} + \frac{1}{4c_{r\perp}^{xz}} \ln \frac{\lambda_{r\perp 2}^0}{\lambda_{r\perp 3}^0} \\
 &\quad + \frac{1}{1+c_{r-1\perp}^{xz}} + \frac{1}{4c_{r-1\perp}^{xz}} \ln \frac{\lambda_{r-1\perp 2}^0}{\lambda_{r-1\perp 3}^0} \quad (r \neq 1) \\
 M_{r,r+1}^{PI} &= \frac{1}{1+c_{r\perp}^{xz}} - \frac{1}{4c_{r\perp}^{xz}} \ln \frac{\lambda_{r\perp 2}^0}{\lambda_{r\perp 3}^0},
 \end{aligned} \tag{4.A.10}$$

while for $r = w$ and n even we find

$$M_{w,w}^{F1} = -10 + \frac{8}{1 + c_{w||}^{zz}} + \frac{2}{1 + c_{w\perp}^{zz}} + \frac{1}{1 + c_{w-1\perp}^{zz}} + \frac{1}{4c_{w-1\perp}^{zz}} \ln \frac{\lambda_{w-1\perp 2}^0}{\lambda_{w-1\perp 3}^0}, \quad (4.A.11a)$$

and for n odd

$$M_{w,w}^{F1} = -5 + \frac{4}{1 + c_{w||}^{zz}} + \frac{1}{1 + c_{w-1\perp}^{zz}} + \frac{1}{4c_{w-1\perp}^{zz}} \ln \frac{\lambda_{w-1\perp 2}^0}{\lambda_{w-1\perp 3}^0}. \quad (4.A.11b)$$

References

- [1] M.E. Fisher, *Rev. Prog. Phys.* **30** (1967) 615
- [2] T. Matsubara and H. Matsuda, *Prog. Theor. Phys.* **16** (1956) 569;
H. Matsuda and T. Matsubara, *Prog. Theor. Phys.* **17** (1957) 19
- [3] H. Matsuda and T. Tsuneto, *Prog. Theor. Phys. Suppl.* **46** (1970) 411
- [4] K.-S. Liu and M.E. Fisher, *J. Low Temp. Phys.* **10** (1973) 655
- [5] S. Robaszkiewicz, R. Micnas, and K.A. Chao, *Phys. Rev. B* **23** (1981) 1447
- [6] R. Micnas, J. Ranninger, and S. Robaszkiewicz, *Rev. Mod. Phys.* **62** (1990) 113
- [7] L.J. de Jongh, *Physica C* **161** (1989) 631
- [8] E. Manousakis, *Rev. Mod. Phys.* **63** (1991) 1
- [9] R. Kikuchi, *Phys. Rev.* **81** (1951) 988
- [10] T. Morita, *J. Math. Phys.* **13** (1972) 115
- [11] G. An, *J. Stat. Phys.* **52** (1988) 727
- [12] S. Katsura and K. Shimada, *phys. stat. sol. (b)* **102** (1980) 163
- [13] D.J. Bukman, G. An, and J.M.J. van Leeuwen, *Phys. Rev. B* **43** (1991) 13352
- [14] M. Schick and R.L. Siddon, *Phys. Rev. A* **8** (1973) 339
- [15] A. Maritan, G. Langie, and J.O. Indekeu, *Physica A* **170** (1991) 326
- [16] W. Huhn and V. Dohm, *Phys. Rev. Lett.* **61** (1988) 1368;
R. Schmolke, A. Wacker, V. Dohm, D. Franck, *Physica B* **165-166** (1990) 575
- [17] T.W. Capehart and M.E. Fisher, *Phys. Rev. B* **13** (1976) 5021
- [18] N.D. Mermin and H. Wagner, *Phys. Rev. Lett.* **17** (1966) 1133

- [19] D. Jasnow and M.E. Fisher, Phys. Rev. **B 3** (1971) 895;
M.E. Fisher and D. Jasnow, Phys. Rev. **B 3** (1971) 907
- [20] J.M. Kosterlitz and D.J. Thouless, J. Phys. **C 6** (1973) 1181
- [21] N. Parga and J.E. van Himbergen, Ann. Phys. **134** (1981) 286
- [22] G.S. Rushbrooke, G.A. Baker, Jr., and P.J. Wood, in: *Phase Transitions and Critical Phenomena*, Vol. 3 (C. Domb and M.S. Green, eds.), Academic Press, London, 1974; D.D. Betts, *ibid.* Vol. 3; C. Domb, *ibid.* Vol. 3;
J. Rogiers, E.W. Grundke, and D.D. Betts, Can. J. Phys. **57** (1979) 1719

Chapter 5

Mean field renormalization group for the spin- $\frac{1}{2}$ XXZ model[†]

5.1 Introduction

The mean field renormalization group (MFRG) method introduced by Indekeu et al. [1, 2] has turned out to be a rather successful method for computing phase diagrams and critical properties of statistical models. The strength of this method lies in the fact that it gives quite good results (at least for the critical temperatures) at a relatively low computational cost. As a result it has been applied to a variety of classical and quantum spin systems. The relative simplicity of the method makes it possible to examine reasonably complicated models for a variety of lattice structures in two and three dimensions. In this paper we apply the MFRG method to the spin- $\frac{1}{2}$ XXZ model, and draw some conclusions about its value in this case.

The XXZ model is described by the reduced Hamiltonian

$$-\beta\mathcal{H} = \sum_{\langle ij \rangle} K(\sigma_i^x \sigma_j^x + \sigma_i^y \sigma_j^y) + K_z \sigma_i^z \sigma_j^z. \quad (5.1.1)$$

The sum $\sum_{\langle ij \rangle}$ is over nearest neighbour spins, and the σ_i^α are Pauli matrices. If the z coupling K_z is positive (ferromagnetic), and larger than the x - y coupling K , the system has an Ising-like ferromagnetically ordered phase (FI), with a non-zero magnetization along the z -axis. If the x - y coupling dominates, there is an ordered phase with a magnetization in the x - y plane (XY). If K_z is negative (antiferromagnetic) an Ising-like phase with a non-zero staggered magnetization forms for bipartite lattices (AI). (For such lattices there is a symmetry between K and $-K$, and hence between the ferromagnetic and antiferromagnetic XY phases. We will always take K positive in this case.) A lattice that is not bipartite cannot accommodate such a phase due to the frustration of the lattice. We will not consider the phases that form under such circumstances. The FI phase has already been discussed by Plascak [3], and

[†]This chapter has been submitted to J. Phys. A

we will extend the calculation to include the other phases as well. It turns out that the behaviour of the MFRG for the XY and AI phases is fundamentally different from that for the FI phase.

Additional interest in the Hamiltonian (5.1.1) derives from the fact that it is equivalent to that of a lattice gas of interacting hard-core bosons [4, 5], and it has been used to describe both superfluidity and superconductivity.

5.2 The mean field renormalization group

In this section we will first describe the MFRG method as it applies to a simple Ising model, and then discuss the differences that arise when it is applied to the XXZ Hamiltonian (5.1.1). We calculate, for an Ising model with a coupling constant K and a magnetic field H , the magnetization m of a finite cluster containing N spins, e.g. one of the clusters shown in figure 5.1. The magnetization is calculated in the presence of a symmetry breaking boundary condition, so that the cluster is embedded in an effective magnetization m_0 , simulating the influence of the surrounding infinite lattice. Because of this effective magnetization the spins on the boundary of the cluster experience an extra effective surface field $H_{\text{eff}} = \alpha K m_0$, with α the number of lattice points outside the cluster that are adjacent to a boundary spin. (We only consider clusters, as in figure 5.1, where all spins are boundary spins, and all spins are equivalent. A generalization for a case where this is not so is easily made.) The basic idea of the MFRG is to repeat this calculation for a different cluster of N' spins ($N' < N$), with different parameters K' , H' , and m'_0 , and view the results as if they were related by a scaling transformation.

Postulating finite size scaling for the two clusters leads to the following relation for the singular part of the free energy per spin, $f = \beta F/N$, in d dimensions

$$f'(K', H', H'_{\text{eff}}) = \ell^d f(K, H, H_{\text{eff}}). \quad (5.2.1)$$

The length rescaling factor ℓ is discussed further on. The magnetization is given by $m = -\partial f / \partial H$, so differentiating (5.2.1) with respect to H we find

$$m'(K', H', H'_{\text{eff}}) = \ell^{d-y_H} m(K, H, H_{\text{eff}}), \quad (5.2.2)$$

with $H' = \ell^{y_H} H$, where y_H is the scaling exponent of the field H . Expanding (5.2.2) to first order in H and H_{eff} gives

$$\chi'(K') = \ell^{d-2y_H} \chi(K), \quad (5.2.3)$$

$$\alpha' K' \tilde{\chi}'(K') = \alpha K \tilde{\chi}(K), \quad (5.2.4)$$

where

$$\chi(K) \equiv \left. \frac{\partial m(K, H, 0)}{\partial H} \right|_{H=0}, \quad (5.2.5)$$

$$\tilde{\chi}(K) \equiv \left. \frac{\partial m(K, 0, H_{\text{eff}})}{\partial H_{\text{eff}}} \right|_{H_{\text{eff}}=0}. \quad (5.2.6)$$

In obtaining (5.2.4) m_0 is supposed to scale like m , i.e. $m'_0 = \ell^{d-y_H} m_0$, which in turn gives $H'_{\text{eff}} = \alpha' K' m'_0 = \alpha' K' m_0 \ell^{d-y_H}$.

If (5.2.4) has a fixed point $K' = K = K_c$, then (5.2.2) describes a scaling property of the magnetization near $K = K_c$ and $H = H_{\text{eff}} = 0$. This point is identified with the critical point, which is given by the equation

$$\alpha' \tilde{\chi}'(K_c) = \alpha \tilde{\chi}(K_c). \quad (5.2.7)$$

The scaling exponent y_H follows from (5.2.3) at $K' = K = K_c$. Because for the clusters that we use all spins are also boundary spins, we always have $\tilde{\chi}(K) = \chi(K)$. It then follows from (5.2.3) and (5.2.4) that y_H is given by

$$\ell^{2y_H} = \ell^d \frac{\tilde{\chi}'(K_c)}{\tilde{\chi}(K_c)} = \ell^d \frac{\alpha'}{\alpha}. \quad (5.2.8)$$

By differentiating (5.2.4) with respect to K at the fixed point one finds

$$\alpha' \left\{ \tilde{\chi}'(K_c) + K_c \frac{\partial \tilde{\chi}'(K')}{\partial K'} \Big|_{K'=K_c} \right\} \frac{\partial K'}{\partial K} \Big|_{K=K_c} = \alpha \left\{ \tilde{\chi}(K_c) + K_c \frac{\partial \tilde{\chi}(K)}{\partial K} \Big|_{K=K_c} \right\}. \quad (5.2.9)$$

The thermal exponent $y_T = 1/\nu$, defined by $\partial K'/\partial K|_{K=K_c} = \ell^{y_T}$, can be calculated from this equation.

It is not obvious what definition one should adopt for the length rescaling factor ℓ , especially for small clusters. We use the original choice of Indekeu et al., which is based on the number of spins in the cluster, $\ell = (N/N')^{1/d}$. It is argued by Slotte [6] that the estimates of the critical exponents are improved if one considers the number of interactions instead, which leads to a different value for ℓ . We will comment on this in the discussion.

A refinement of the MFRG method was proposed by Indekeu et al. [2], who showed that, for large clusters, the effective magnetization m_0 should scale like $m'_0 = \ell^{y_H S} m_0$, with y_{HS} the scaling exponent for a surface field. Combining this relation with (5.2.2) leads to

$$\alpha' K' \tilde{\chi}'(K') = \ell^{d-y_H-y_{HS}} \alpha K \tilde{\chi}(K), \quad (5.2.10)$$

instead of (5.2.4), while (5.2.3) still holds. Because of the introduction of an extra unknown in (5.2.10), one needs two equations to determine both $d - y_H - y_{HS}$ and the fixed point self-consistently. These are obtained by considering three clusters of sizes N , N' , and N'' , and imposing the scaling relations

$$\begin{aligned} m'(K', H', H'_{\text{eff}}) &= \ell_1^{d-y_H} m(K, H, H_{\text{eff}}), \\ m''(K'', H'', H''_{\text{eff}}) &= \ell_2^{d-y_H} m'(K', H', H'_{\text{eff}}), \end{aligned} \quad (5.2.11)$$

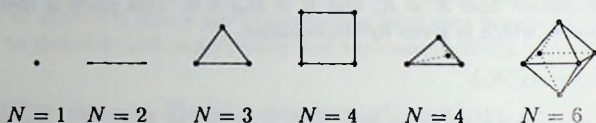


Fig. 5.1. The clusters that are used in the calculation. The single site and the pair are used for all lattices; the triangle for the triangular and fcc lattices; the square for the square and cubic lattices; the tetrahedron and the octahedron for the fcc lattice.

and $m'_0 = \ell_1^{y_{HS}} m_0$, $m''_0 = \ell_2^{y_{HS}} m'_0$. This leads to unique values for $\hat{c} = y_T - y_{HS}$ and the fixed point, but for y_T , y_H , and y_{HS} one finds slightly different results from the two equations (5.2.11).

When applying this method to the XXZ model, several changes take place. First, different ordered phases can occur in this model. The magnetization m must then be replaced by the order parameter of the phase under consideration; this can be the magnetization in either the z -direction or in the x - y plane, or the staggered magnetization. The field H couples to the order parameter, so it can be a magnetic field along the z -axis or in the x - y plane, or a staggered field. In all cases, the order parameter is given by $m = -\partial f / \partial H$. Second, the single coupling constant K is replaced by the pair (K, K_z) . One now finds a fixed line $K(K_z)$ in the space of the two coupling constants instead of a single fixed point. As in the case of phenomenological renormalization [7, 8], this fixed line converges to the critical line for large cluster sizes. The values of y_H and y_T one finds from (5.2.3) and (5.2.9) will in general depend on the ratio K_z/K . This dependence, which is not in accordance with universality, should disappear when the cluster sizes increase. In addition, the value one finds for y_T also depends on the way $\partial K' / \partial K$ is defined in the (K, K_z) plane. We will always take the derivative along a line $K_z/K = \text{constant}$, but for large enough clusters any choice should lead to the correct value [8].

5.3 Results of the two-cluster method

The clusters we use are shown in figure 5.1. With these clusters we apply the MFRG method to the two-dimensional triangular and square lattices, and to the three-dimensional cubic and fcc lattices. We start by employing the simpler scheme using two clusters, since that gives more possibilities to compare results for different sets of clusters. Also, it is reasonably well behaved, in contrast to the three-cluster scheme,

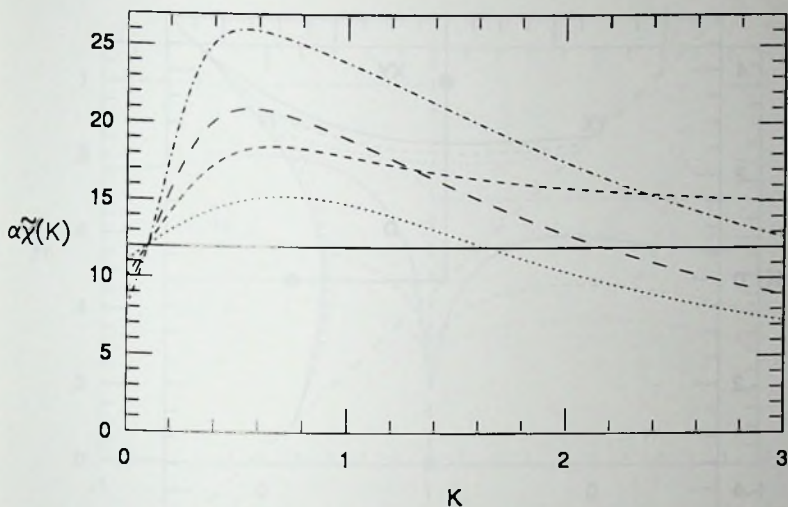


Fig. 5.2. The behaviour of $\alpha\tilde{\chi}(K)$ for several clusters in the fcc lattice. $N = 1$: solid line; $N = 2$: dotted line; $N = 3$: short dashes; $N = 4$: long dashes; $N = 6$: dot-dashed. The intersections near $K = 0.1$ give the various approximations for K_c ; the intersections at higher K are the additional fixed points discussed in the text.

which turns out to give unacceptable results in some cases when applied to the small clusters we use here.

On applying the two-cluster scheme to the Hamiltonian (5.1.1), one immediately notices a difference in the behaviour of $\tilde{\chi}(K)$ for the FI phase on the one hand, and the XY and AI phases on the other hand. In the FI phase, for the clusters in figure 5.1, $\tilde{\chi}(K)$ is monotonously increasing from one at $K = 0$ to some constant value for $K \rightarrow \infty$. In the AI and XY phases it has a maximum, after which it decreases to either zero (even N), or to some non-zero value (odd N). This reflects the fact that for the FI phase the ground state of a cluster has the largest "susceptibility" $\tilde{\chi}$, while the ground states for the XY and AI phases have either $\tilde{\chi} = 0$, or a relatively small non-zero value. As a consequence, when comparing $\alpha\tilde{\chi}(K)$ for different clusters, as in (5.2.7), there can be additional fixed points apart from the one indicating the phase transition, caused by the re-crossing of $\alpha\tilde{\chi}(K)$ for large K . In most cases there is a clear distinction between a solution of (5.2.7) indicating the phase transition, which clearly moves towards some limit for larger clusters, and the other zeros, which do not have this scaling behaviour (see figure 5.2 where $\alpha\tilde{\chi}(K)$ is shown for the fcc lattice

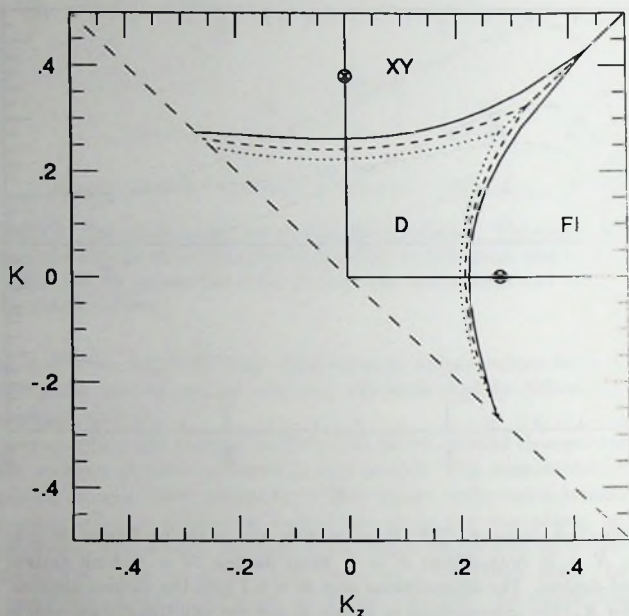


Fig. 5.3. The phase diagram for the triangular lattice. The dotted line is the result for $N' = 1, N = 2$, the dashed line for $N' = 1, N = 3$, and the solid line for $N' = 2, N = 3$. The crossed circles represent exact and series expansion [9] results. The lower left half of the phase diagram, where the dominant interaction is antiferromagnetic and where frustration effects play a role, is not treated here.

for various clusters). Moreover, these spurious zeros usually lie at such large values of K that they are far removed from the region where the phase transition takes place, and they will in general not show up in the phase diagrams shown. (An exception to this is the square lattice case, which is discussed further on.)

5.3.1 The triangular lattice

The phase diagram obtained with the two-cluster method for the triangular lattice is drawn in figure 5.3. Around $K = K_z = 0$ the system is in the disordered phase (D). When K_z is increased, ferromagnetic Ising order sets in (FI), while for increasing K the system enters the x - y ordered phase (XY). The parts of the phase diagram

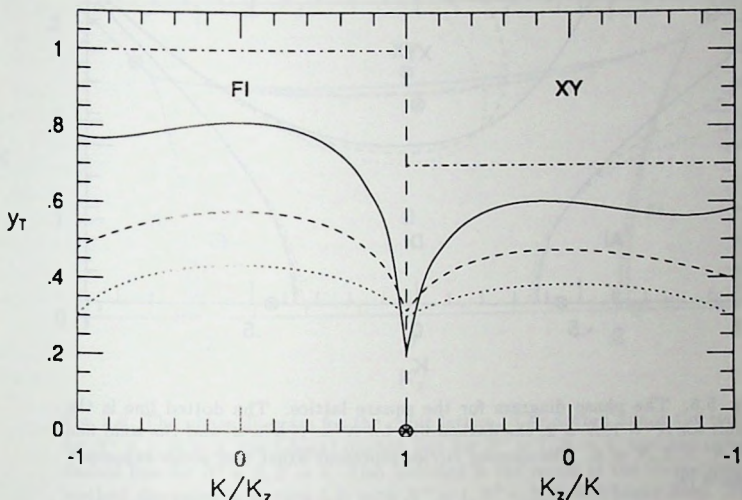


Fig. 5.4. The exponent y_T for the triangular lattice, plotted along the phase boundaries in figure 5.3. The dotted line is the result for $N' = 1, N = 2$, the dashed line for $N' = 1, N = 3$, and the solid line for $N' = 2, N = 3$. The exact and series [9] results are given by the dot-dashed lines and the crossed circle.

where an antiferromagnetic interaction dominates have been left blank, since we do not consider phases where frustration effects play a role. As was already shown in [3], the results for the FI boundary improve as the cluster size is increased. Although the critical coupling for the isotropic Heisenberg model ($K = K_z$) remains finite, it increases rapidly with cluster size, tending towards the exact result $K_c = \infty$. The XY phase boundary is also seen to move towards the series result for larger clusters [9].

The critical exponent y_T is shown in figure 5.4. Again, the result improves with increasing cluster size, roughly approaching the exact result $y_T = 1$ for the FI transition, $y_T = 0$ for the isotropic Heisenberg case, and the series result $y_T = 0.7$ for the XY phase [9]. Except for the region near $K = K_z$ where the cross-over between different values of y_T takes place, the dependence on the anisotropy is slight. From (5.2.8) it is seen that in the two-cluster method y_H does not depend on the coupling constants K and K_z . The best estimate for the triangular lattice ($N' = 2, N = 3$) gives $y_H = 1.55$, compared with the exact result $y_H = 1.875$ for the FI boundary, and a similar value from series expansions for the XY transition.

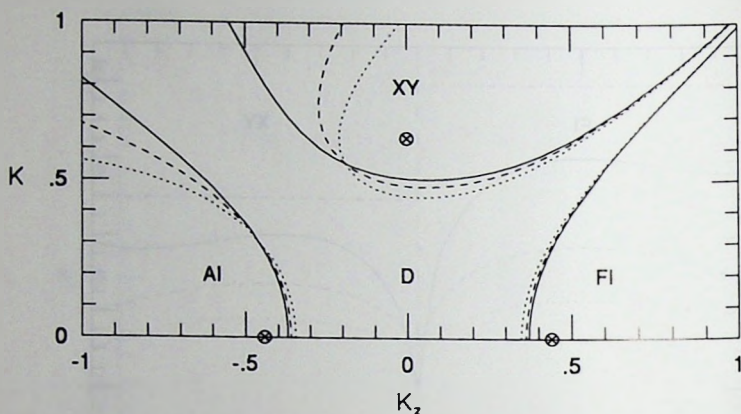


Fig. 5.5. The phase diagram for the square lattice. The dotted line is the result for $N' = 1, N = 2$, the dashed line for $N' = 1, N = 4$, and the solid line for $N' = 2, N = 4$. The crossed circles represent exact and series expansion results [9].

5.3.2 The square lattice

For the square lattice we obtain the phase diagram shown in figure 5.5. It also includes the antiferromagnetic Ising phase (AI), which occurs for large negative K_z . We only plot the upper half of the phase diagram, which is symmetric under reflection in the line $K = 0$. Here again, the location of the FI boundary improves as the cluster sizes are increased. The isotropic Heisenberg model has $T_c = 0$, which is the exact result, for all cluster sizes. For the XY phase the spurious fixed points discussed above show up in the phase diagram. For the combinations $N' = 1, N = 2$ and $N' = 1, N = 4$ the XY phase boundary curves back for large K , thus suggesting that the system re-enters the disordered phase at low temperature. For these values of N' and N the MFRG for the XY phase does not have a fixed point at $T = 0$. Instead, for a constant ratio $K_z/K > -1$, there is, in addition to the repulsive fixed point indicating the phase transition, an attractive fixed point at lower T . As K_z/K is decreased towards -1 these points approach each other, and they eventually meet and are annihilated. The same happens for the AI phase where K_z/K approaches -1 from below. This leaves a gap in the phase diagram around $K_z \approx -K$. For $N' = 2, N = 4$ there is a fixed point at $T = 0$, so there is no re-entrance into the disordered phase. The gap around $K_z = -K$ has remained in roughly the same position, giving support to the conclusion that there is a region around $K_z = -K$, in this last approximation given by $-1.22 \lesssim K_z/K \lesssim -0.55$, where the disordered phase extends down to $T = 0$,

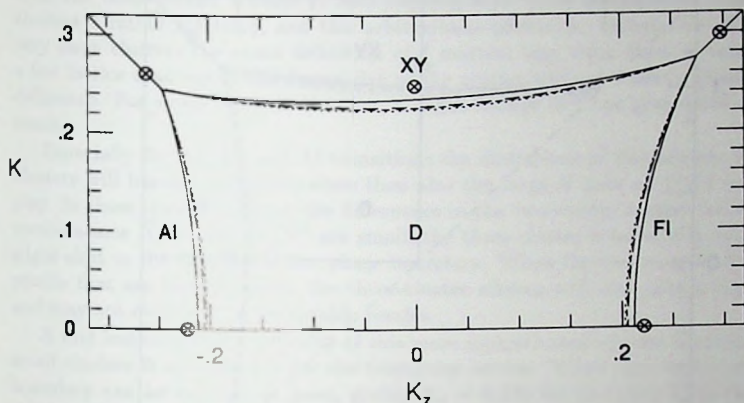


Fig. 5.6. The phase diagram for the cubic lattice. The dotted line is the result for $N' = 1, N = 2$, the (short) dashed line for $N' = 1, N = 4$, and the (long) dashed line for $N' = 2, N = 4$. Also included is the result of the three-cluster method discussed in section 5.4, with $N'' = 1, N' = 2, N = 4$ (solid line). The crossed circles represent the results of series expansions [11].

flanked by XY and AI phases.

The results for the exponent y_T are similar to those for the triangular lattice, showing a reasonably flat plateau for the FI, AI, and XY phases, at values around respectively 0.8, 0.8, and 0.5 in the best approximation ($N' = 2, N = 4$), and in this case dropping to zero for the isotropic Heisenberg model and in the region around $K = -K_z$. The best estimate for y_H gives $y_H = 1.59$.

5.3.3 The three-dimensional lattices

The phase diagrams for the three-dimensional lattices are shown in figures 5.6 and 5.7. For the cubic lattice there is some improvement as the cluster size is increased in most regions of the phase diagram. The exponent y_T again slowly varies along the phase boundary, assuming values of approximately 0.8, 0.7, and 0.6 for the FI, XY, and isotropic Heisenberg transitions in the best estimate ($N' = 2, N = 4$), while for the magnetic exponent we find $y_H = 1.98$. As a comparison, field theoretical methods, give $y_T = 1.59, 1.49$, and 1.42 , respectively, and $y_H = 2.48$ [10].

For the fcc lattice we find that, in contrast to the general trend, the inclusion of the largest cluster ($N = 6$) does not give better results. This confirms the observation that, especially in lattices with high coordination numbers, the improvement is not

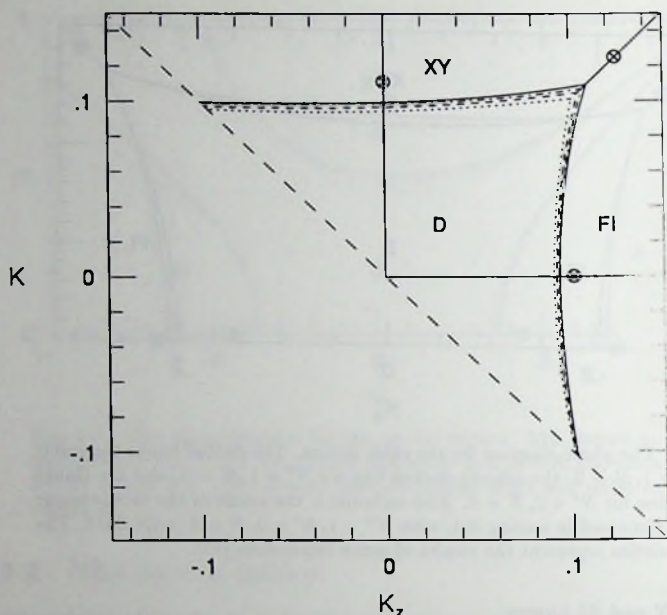


Fig. 5.7. The phase diagram for the fcc lattice. The dotted line is the result for $N' = 1, N = 2$, the dashed line for $N' = 2, N = 3$, the solid line for $N' = 3, N = 4$, and the dot-dashed line for $N' = 4, N = 6$. The crossed circles represent the results of series expansions [11].

always monotonic as the cluster size is increased [2, 12]. For the exponents we find values that are slightly better than those for the cubic lattice.

5.4 Results of the three-cluster method

When applying the scheme using three clusters to the situations discussed above, one cannot a priori expect the results to be an improvement. Although this scheme does put the MFRG method on a sounder footing, and guarantees the convergence of large-cluster results, it is not necessarily an improvement for the small clusters used in the present calculation. In the first place, the assertion that the effective order parameter m_0 scales like a surface field only holds for large clusters. Second, whereas the location of K_c in the simpler method is independent of the length rescaling factor

ℓ , in the three-cluster scheme it does depend on ℓ . The definition of ℓ for small clusters is rather arbitrary, and this arbitrariness affects the calculation of K_c . For very large clusters the exact definition of ℓ matters less, since there a variation of a few lattice spacings in the linear size of the cluster will not make a great deal of difference. For small clusters, however, a slight change in ℓ can give quite different results.

Especially for the XY and AI transitions the limitations of this scheme for small clusters will become apparent, since then also the large- K tails of $\bar{\chi}(K)$ come into play. In those instances where the differences in the two-cluster scheme between the combinations N, N' and N'', N'' are small, the three-cluster scheme will only give a slight shift in the location of the phase boundary. When the two combinations give results that are further apart, the three-cluster scheme will also give a large shift, and may not even lead to acceptable results.

A first instance of the difficulty of this more sophisticated scheme in dealing with small clusters is encountered for the triangular lattice. While the result for the FI boundary can be considered good, giving $K_c = 0.235$ for the pure Ising case, and shifting K_c for the isotropic Heisenberg model to infinity, even here we find some trouble, in the shape of an additional fixed point at high K , for the pure Ising model located at $K \approx 1.2$. This point can be dismissed as clearly being outside the region of the real phase transition; the same can not be said of the phase boundary one finds for the XY phase. This line describes a zig-zag in the region between $K_z/K = 1$ and $K_z/K = -1$, which is clearly not a very sensible result. It shows that in this case the results of the three-cluster scheme for small clusters should not be taken too seriously. Similar behaviour is found for the square lattice, where the differences in behaviour for the various combinations of cluster sizes are even greater than for the triangular lattice.

For the three-dimensional lattices the differences between the various combinations of clusters were rather small, and consequently the three-cluster method is better behaved for these lattices, only giving a small shift in the location of the phase boundary. For the cubic lattice, the resulting phase diagram is shown in figure 5.6, which does show an improvement over the two-cluster method. In contrast to the two-cluster case, (5.2.8) does not hold now, so the exponent y_H varies slightly along the phase boundary. Its value does not improve noticeably when compared with the previous results, and neither does the estimate for the exponent y_T . For the surface exponent one finds $y_{HS} \approx 1.1$, compared with the field theoretical value 0.8 [13].

The phase diagram for the fcc lattice, figure 5.8, is also better than the result of the two-cluster method. As in the previous section, we see that the combination of the largest clusters does not necessarily give the best result. While for $N'' = 2, N' = 3, N = 4$ we find phase boundaries that are quite close to the series expansion estimates, the agreement becomes worse for $N'' = 2, N' = 4, N = 6$, and the combination $N'' = 3, N' = 4, N = 6$ fails to give a fixed line that one can identify with the phase boundary. The best estimates for the exponents are similar to those

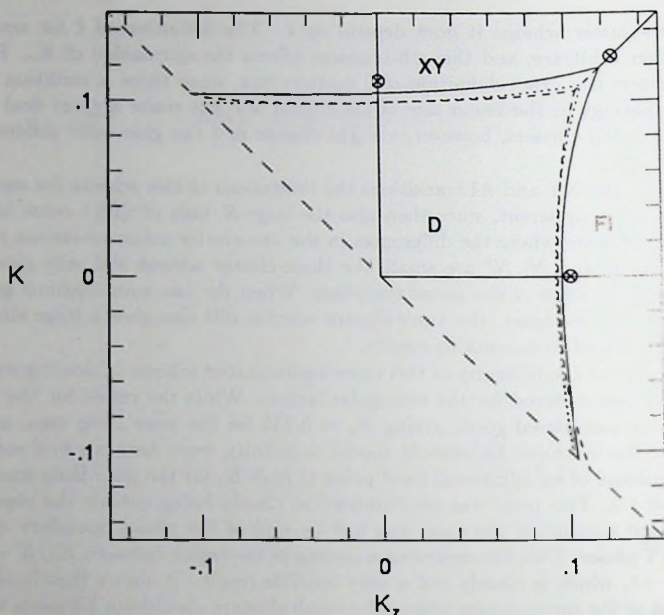


Fig. 5.8. The phase diagram for the fcc lattice. The dotted line is the result for $N'' = 1, N' = 2, N = 3$, the solid line for $N'' = 2, N' = 3, N = 4$, and the dashed line for $N'' = 2, N' = 4, N = 6$. The crossed circles represent the results of series expansions [11].

for the cubic lattice, and no great improvement over the two-cluster results.

5.5 Discussion

We have seen that applying the two-cluster version of the MFRG method to the XXZ model leads to quite good results for the phase diagram. It is certainly an improvement over the mean-field approximation, which gives the critical lines $K = 1/z$ and $K_z = \pm 1/z$. Both the value of the critical coupling (see table 5.1 for an example) and the overall shape of the phase diagram are greatly improved when compared with this approximation. It is especially striking that for small clusters, where the computational effort is relatively small, the improvement over mean-field is already considerable. For larger clusters the results improve even further, but the

	MF	MFRG2 1,2	MFRG2 1,4	MFRG2 2,4	MFRG3 1,2,4	series
K_c	0.167	0.224	0.226	0.227	0.235	0.248

Table 5.1. The critical coupling K_c of a pure XY-model ($K_z = 0$) on a cubic lattice, according to the mean field (MF), two-cluster MFRG (MFRG2 N', N), three-cluster MFRG (MFRG3) approximations, and the series result [11].

convergence is not very fast. Also, especially for lattices with a high coordination number, where there are many possible ways to form larger clusters, the improvement is not always monotonic [2, 12]. The critical exponents that one finds as a by-product of this method are only rough estimates; much more accurate values can be found by field-theoretical methods. The nature of the ordered phases is determined by the boundary condition employed to break the symmetry. So, the XY phase is an ordered phase with a non-zero magnetization, while it is known that two-dimensional XY models exhibit a different type of long range order. Nevertheless, the MFRG result can be expected to give some indication of the location of the phase boundary.

Thus the performance of the MFRG method for the XXZ model, which exhibits different types of ordering, and is an essentially quantum mechanical model, is about the same as for the classical Ising model. There are some differences, though, which mostly become apparent at low temperatures. For the XY and AI phases one might find additional fixed points, as discussed in section 5.3. These points lie at high values of K , and usually do not interfere with the phase diagram. But for low dimensions and/or low coordination numbers, when K_c itself is relatively high, as in the case of the square lattice, they do show up in the phase diagram for some combinations of clusters. Even there, the phase boundaries one finds for these clusters are not radically different from what one finds for a combination that does not lead to additional fixed points. It may be remarked that the appearance of spurious zeros is also noticed in the pair approximation of the cluster variation method [14, 15]. In fact, the case $N' = 1, N = 2$ of the MFRG is equivalent to this approximation, just as for the classical pure Ising model it is equivalent to the Bethe-Peierls approximation.

The three-cluster version of the MFRG method is less successful for the XXZ model. One reason for this is that the method is geared to the use of large clusters; neither the introduction of a surface exponent y_{HS} nor the role played by the length rescaling factor ℓ are compatible with the use of small clusters. If one examines the values of y_H and y_{HS} for the three-dimensional lattices, one finds that $y_{HS} \approx d - y_H$, which is the relation that would follow from the method without a surface exponent. So for small clusters the effective field does not really scale as a surface field. Also, the arbitrariness in defining ℓ for small clusters affects the location of the phase boundary.

In the case of the XXZ model there is the extra complication of the spurious fixed points that occur at high K . Especially for the two-dimensional lattices, where they

are closest to the region of the phase transition, this has an effect on the calculation of the phase boundary. For example, combining the approximations with $N' = 1, N = 2$ and $N' = 2, N = 4$ for the square lattice, which behave differently for large K , cannot be expected to give a consistent result. In three dimensions the influence of these fixed points is less noticeable, since they are farther removed from K_c .

A suggestion has been made [6] for a different estimate for ℓ , which would improve the value for the exponents. According to this definition, one should consider the number of interactions in a cluster, including the ones with the surrounding effective magnetization. The resulting value for ℓ is in general smaller than the one following from the definition that we used, and consequently the exponents are larger and closer to the expected values. However, if one tries to use this new definition of ℓ in the three-cluster scheme, where the location of the phase boundary depends on it, the phase diagram is totally distorted and the original definition turns out to be far superior.

References

- [1] J.O. Indekeu, A. Maritan, and A.L. Stella, *J. Phys. A* **15** (1982) L291
- [2] J.O. Indekeu, A. Maritan, and A.L. Stella, *Phys. Rev. B* **35** (1987) 305
- [3] J.A. Plascak, *J. Phys. A* **17** (1984) L597
- [4] T. Matsubara and H. Matsuda, *Prog. Theor. Phys.* **16** (1956) 569;
H. Matsuda and T. Matsubara, *Prog. Theor. Phys.* **17** (1957) 19
- [5] M.E. Fisher, *Rep. Prog. Phys.* **30** (1967) 615
- [6] P.A. Slotte, *J. Phys. A* **20** (1987) L177
- [7] M.P. Nightingale, *Physica A* **83** (1976) 561
- [8] T.W. Burkhardt and J.M.J. van Leeuwen, in: *Real Space Renormalization* (T.W. Burkhardt and J.M.J. van Leeuwen, eds.), Springer, Berlin, 1982
- [9] J. Rogiers, E.W. Grundke, and D.D. Betts, *Can. J. Phys.* **57** (1979) 1719
- [10] J.C. Le Guillou and J. Zinn-Justin, *Phys. Rev. B* **21** (1980) 3976
- [11] C. Domb, in: *Phase Transitions and Critical Phenomena*, Vol. 3 (C. Domb and M.S. Green, eds.), Academic Press, London, 1974; D.D. Betts, *ibid.* Vol. 3; G.S. Rushbrooke, G.A. Baker, Jr., and P.J. Wood, *ibid.* Vol. 3;
- [12] J.O. Indekeu, private communication

- [13] H.W. Diehl, in: *Phase Transitions and Critical Phenomena*, Vol. 10 (C. Domb and J.L. Lebowitz, eds.), Academic Press, London, 1986
- [14] S. Katsura and K. Shimada, *phys. stat. sol. (b)* **102** (1980) 163
- [15] D.J. Bukman, G. An, and J.M.J. van Leeuwen, *Phys. Rev. B* **43** (1991) 13352

The t -matrix for collisions of hard spheres in d spatial dimensions

6.1. Introduction

The t -matrix for collisions of hard spheres in d spatial dimensions is derived. The derivation proceeds by means of the t -matrix of the hard sphere in one dimension. In making the derivation, we use the t -matrix of the hard sphere in one dimension as a starting point. The t -matrix of the hard sphere in one dimension is derived by means of the t -matrix of the hard sphere in one dimension. The t -matrix of the hard sphere in one dimension is derived by means of the t -matrix of the hard sphere in one dimension. The t -matrix of the hard sphere in one dimension is derived by means of the t -matrix of the hard sphere in one dimension.

The advantage of the hard sphere in one dimension is that the t -matrix is simple. The t -matrix of the hard sphere in one dimension is derived by means of the t -matrix of the hard sphere in one dimension. The t -matrix of the hard sphere in one dimension is derived by means of the t -matrix of the hard sphere in one dimension. The t -matrix of the hard sphere in one dimension is derived by means of the t -matrix of the hard sphere in one dimension.

Using the t -matrix of the hard sphere in one dimension, we derive the t -matrix of the hard sphere in d spatial dimensions. The t -matrix of the hard sphere in d spatial dimensions is derived by means of the t -matrix of the hard sphere in one dimension. The t -matrix of the hard sphere in d spatial dimensions is derived by means of the t -matrix of the hard sphere in one dimension. The t -matrix of the hard sphere in d spatial dimensions is derived by means of the t -matrix of the hard sphere in one dimension.

Support for this work is from the National Science Foundation under Grant No. DMR-85-11584. The authors would like to thank the National Science Foundation for its support of this work.

*Originally published in *Phys. Rev. B*, **43**, 13352 (1991).

The first part of the paper discusses the importance of the study and the objectives of the research. It also provides a brief overview of the methodology used in the study.

The second part of the paper presents the results of the study. It discusses the findings of the research and compares them with the existing literature.

The third part of the paper discusses the implications of the study and provides recommendations for future research.

References

- [1] J. A. Smith, "The importance of the study," *Journal of Research*, vol. 1, no. 1, pp. 1-10, 1998.
- [2] J. B. Jones, "The methodology used in the study," *Journal of Research*, vol. 1, no. 1, pp. 11-20, 1998.
- [3] J. C. Brown, "The findings of the research," *Journal of Research*, vol. 1, no. 1, pp. 21-30, 1998.
- [4] J. D. Green, "The implications of the study," *Journal of Research*, vol. 1, no. 1, pp. 31-40, 1998.
- [5] J. E. White, "The recommendations for future research," *Journal of Research*, vol. 1, no. 1, pp. 41-50, 1998.
- [6] J. F. Black, "The importance of the study," *Journal of Research*, vol. 1, no. 1, pp. 51-60, 1998.
- [7] J. G. Gray, "The methodology used in the study," *Journal of Research*, vol. 1, no. 1, pp. 61-70, 1998.
- [8] J. H. King, "The findings of the research," *Journal of Research*, vol. 1, no. 1, pp. 71-80, 1998.
- [9] J. I. Lee, "The implications of the study," *Journal of Research*, vol. 1, no. 1, pp. 81-90, 1998.
- [10] J. J. Scott, "The recommendations for future research," *Journal of Research*, vol. 1, no. 1, pp. 91-100, 1998.

Chapter 6

The t -matrix for collisions of hard spheres in a layer geometry[†]

6.1 Introduction

The dynamics of helium can be qualitatively represented by a hard sphere system. The interaction potential between He atoms is of the 12-6 Lennard-Jones type. In making the connection with hard spheres the attraction is represented by a uniform background potential giving the system its density (see e.g. Lee et al. [1]). Such a model fails of course to describe the transition from the dilute gaseous phase to the dense liquid phase, for which the attraction is crucial, but it is believed that e.g. the phase transition from normal fluid to superfluid is qualitatively the same for the hard sphere Bose gas as for ⁴He.

The advantage of the hard sphere Bose gas is that one single parameter, the diameter a , controls the interaction and that one can change this parameter from zero, where the gas becomes ideal, to a value σ corresponding to the ⁴He value in the Lennard-Jones interaction. In this way the properties can be continuously tuned from ideal behaviour to ⁴He-like behaviour. To cope with the fact that the potential is singular one has to use the t -matrix, which remains finite even for a hard sphere potential.

Since the interesting phenomena in helium occur at low temperatures, low momenta are dominant, which allows a further simplification of the interaction to its scattering length. Then the interaction is replaced by a δ -function with the scattering length as strength, thus ignoring all momentum structure in the matrix elements of the interaction. For a three-dimensional system ($d = 3$) the scattering length equals the diameter a of the hard spheres.

Superfluidity also occurs in lower dimensional systems such as thin layers of ⁴He. Popov [2] and Fisher and Hohenberg [3] have recently pointed out that the scattering length, or what would be its equivalent, behaves qualitatively different in two-

[†]Apart from some modifications, this chapter has appeared in *Physica A* 161 (1989) 63

dimensional systems. It is the purpose of this paper to show the continuous crossover from $d = 2$ to $d = 3$ behaviour when the thickness of the layer $2w$ varies from $w \ll a$ to $w \gg a$.

The notion of scattering length may be most easily illustrated by considering scattering of a particle in an external spherical potential $V(r)$. The t -operator is defined by the equation

$$t(z) = V + V \frac{1}{z - \mathcal{H}_0} t(z). \quad (6.1.1)$$

Here \mathcal{H}_0 is the kinetic energy operator and z is a complex parameter with the dimension of an energy. We will always take $\text{Im } z > 0$. It is useful to introduce the so-called Møller wave operator $\Omega(z)$ [4], defined as

$$V\Omega(z) = t(z) \quad (6.1.2)$$

satisfying the equation

$$(z - \mathcal{H}_0 - V)\Omega(z) = z - \mathcal{H}_0. \quad (6.1.3)$$

This equation is conveniently analyzed in the mixed representation $\langle \mathbf{r} | \Omega(z) | \mathbf{k} \rangle$ where, for a particle of mass μ , $|\mathbf{k}\rangle$ is a state with kinetic energy $\hbar^2 k^2 / 2\mu$ and $|\mathbf{r}\rangle$ one with position \mathbf{r} . In this representation (6.1.3) obtains the form of an inhomogeneous Schrödinger equation

$$\left(z + \frac{\hbar^2}{2\mu} \nabla^2 - V(\mathbf{r}) \right) \langle \mathbf{r} | \Omega(z) | \mathbf{k} \rangle = \left(z - \frac{\hbar^2 k^2}{2\mu} \right) \langle \mathbf{r} | \mathbf{k} \rangle, \quad (6.1.4)$$

which has to be solved with the boundary condition that $\langle \mathbf{r} | \Omega(z) | \mathbf{k} \rangle$ remains finite when r goes to infinity. This boundary condition derives from the interpretation of $\langle \mathbf{r} | \Omega(z) | \mathbf{k} \rangle$, for $z = \hbar^2 k^2 / 2\mu + i\epsilon$ with $\epsilon \downarrow 0$, as [4]

$$\langle \mathbf{r} | \Omega(z) | \mathbf{k} \rangle = \langle \mathbf{r} | \mathbf{k} + \rangle, \quad (6.1.5)$$

with $|\mathbf{k} + \rangle$ the outgoing state which follows from the incoming state $|\mathbf{k}\rangle$ when it is scattered by the potential V . Once $\langle \mathbf{r} | \Omega(z) | \mathbf{k} \rangle$ is obtained it leads with (6.1.2) to the t -matrix

$$\langle \mathbf{k}' | t(z) | \mathbf{k} \rangle = \int d\mathbf{r} \langle \mathbf{k}' | \mathbf{r} \rangle V(\mathbf{r}) \langle \mathbf{r} | \Omega(z) | \mathbf{k} \rangle. \quad (6.1.6)$$

In $d = 3$ the zero-momentum, zero-energy limit of the t -matrix is proportional to the scattering length a

$$\langle \mathbf{0} | t(0) | \mathbf{0} \rangle = \frac{\hbar^2 a}{4\mu \pi^2}. \quad (6.1.7)$$

In a $d = 2$ system this limit vanishes, leading to additional complications in the many body theory for hard disks.

It is well known that the scattering of two particles of mass m is equivalent to the scattering of one particle of mass $m/2$ by an external potential. Therefore we can easily adapt the previous equations to describe the scattering of two particles by substituting $\mu = m/2$. The kinetic energy of the center of mass, being a conserved quantity, only causes a shift in z , leading to a new parameter α

$$\frac{\hbar^2}{m}\alpha^2 = z - z_{cm}. \quad (6.1.8)$$

The external potential V is in this case equal to the interparticle potential, while \mathcal{H}_0 is the kinetic energy with respect to the center of mass. The states $|\mathbf{k}\rangle$ and $|\mathbf{r}\rangle$ are now eigenstates of \mathcal{H}_0 and the relative position operator, respectively. With these substitutions (6.1.4) becomes

$$\left(\frac{\hbar^2}{m}\alpha^2 + \frac{\hbar^2}{m}\nabla^2 - V(r)\right) \langle \mathbf{r} | \Omega(\alpha) | \mathbf{k} \rangle = \frac{\hbar^2}{m}(\alpha^2 - k^2) \langle \mathbf{r} | \mathbf{k} \rangle. \quad (6.1.9)$$

For general \mathbf{k} , \mathbf{k}' and α (6.1.6) is the off-shell t -matrix [4]. If $k^2 = k'^2$ and $\alpha^2 = k^2 + i\epsilon$ with ϵ positive and infinitesimal it becomes the on-shell t -matrix, which is proportional to the scattering amplitude. In this paper we will investigate scattering at low energy and low momenta. In particular we will calculate the term that is lowest order in the particle momentum, which is obtained by setting $\mathbf{k} = \mathbf{k}' = \mathbf{k}_0$, with $|\mathbf{k}_0\rangle$ the lowest-momentum eigenstate of \mathcal{H}_0 , which also has the lowest energy. We will then examine what happens when α^2 approaches $k_0^2 + i\epsilon$.

We will do these calculations for a system of hard spheres moving in a layer. The particles can move freely in the x - and y -directions, but in the z -direction they are confined to the thickness $2w$ of the layer. The boundary condition for this system would be that the wave function is zero whenever one of the two particles hits the layer boundary. Unfortunately, this cannot be written as two separate boundary conditions for the relative and center of mass coordinates \mathbf{r} and \mathbf{R} , and we would not be able to separate the center of mass motion. Therefore we turn to a slightly different system where we do split off the center of mass motion, and impose boundary conditions on $\langle \mathbf{r} | \Omega(\alpha) | \mathbf{k} \rangle$.

In sections 6.5 and 6.6 we will discuss two different boundary conditions, one where $\langle \mathbf{r} | \Omega(\alpha) | \mathbf{k} \rangle$ is periodic with period $2w$ and one where it is zero for $|z| = w$. In sections 6.3 and 6.4 we will consider the two limits of a layer geometry, those of infinite and zero thickness. Since these cases are relatively easy we will calculate the off-shell t -matrix for general \mathbf{k} , \mathbf{k}' and α and then see what happens in the on-shell, low energy and low momentum limit. In sections 6.5 and 6.6 though, we will immediately set $\mathbf{k} = \mathbf{k}' = \mathbf{k}_0$ and $\alpha^2 = k_0^2 + i\epsilon$ in order to simplify the calculation. But first, in section 6.2, we will make some simplifications that are due to the fact that we are considering hard spheres.

6.2 The hard sphere t -matrix

The particles that we describe are hard spheres with diameter a , so the limiting potential is

$$V(r) = \begin{cases} \infty & \text{for } r \leq a \\ 0 & \text{for } r > a. \end{cases} \quad (6.2.1)$$

Since $\langle \mathbf{r} | \Omega(\alpha) | \mathbf{k} \rangle$ is finite everywhere the term $V(r) \langle \mathbf{r} | \Omega(\alpha) | \mathbf{k} \rangle$ in (6.1.9) is zero for $r > a$. In order for this product to be finite for $r \leq a$ we must also have

$$\langle \mathbf{r} | \Omega(\alpha) | \mathbf{k} \rangle = 0 \quad \text{for } r \leq a. \quad (6.2.2)$$

Then we only need to solve (6.1.9) for $r > a$:

$$(\alpha^2 + \nabla^2) \langle \mathbf{r} | \Omega(\alpha) | \mathbf{k} \rangle = (\alpha^2 - k^2) \langle \mathbf{r} | \mathbf{k} \rangle \quad \text{for } r > a. \quad (6.2.3)$$

The region $r \leq a$ is taken care of by demanding that $\langle \mathbf{r} | \Omega(\alpha) | \mathbf{k} \rangle$ is zero on the surface $r = a$.

The solution of (6.2.3) can be written as the sum of the special solution $\Omega_s(\alpha)$ of (6.2.3) and the general solution $\Omega_h(\alpha)$ of the corresponding homogeneous equation, so

$$\langle \mathbf{r} | \Omega(\alpha) | \mathbf{k} \rangle = \langle \mathbf{r} | \Omega_s(\alpha) | \mathbf{k} \rangle + \langle \mathbf{r} | \Omega_h(\alpha) | \mathbf{k} \rangle, \quad (6.2.4)$$

where the last term satisfies

$$(\alpha^2 + \nabla^2) \langle \mathbf{r} | \Omega_h(\alpha) | \mathbf{k} \rangle = 0. \quad (6.2.5)$$

The special solution can always be taken as

$$\langle \mathbf{r} | \Omega_s(\alpha) | \mathbf{k} \rangle = \langle \mathbf{r} | \mathbf{k} \rangle \quad (6.2.6)$$

and the condition on the surface $r = a$ now reads

$$\langle \mathbf{r} | \Omega_h(\alpha) | \mathbf{k} \rangle = -\langle \mathbf{r} | \mathbf{k} \rangle \quad \text{at } r = a. \quad (6.2.7)$$

The fact that $V(r)$ is zero for $r > a$ and that $\langle \mathbf{r} | \Omega(\alpha) | \mathbf{k} \rangle$ is zero for $r \leq a$ can be used to rewrite (6.1.6). Before taking the limiting behaviour (6.2.1) we multiply (6.1.9) by $\langle \mathbf{k}' | \mathbf{r} \rangle$ and integrate over the sphere U with $r \leq a$. This yields

$$\begin{aligned} \frac{\hbar^2}{m} \alpha^2 \int_U d\mathbf{r} \langle \mathbf{k}' | \mathbf{r} \rangle \langle \mathbf{r} | \Omega(\alpha) | \mathbf{k} \rangle + \frac{\hbar^2}{m} \int_U d\mathbf{r} \langle \mathbf{k}' | \mathbf{r} \rangle \nabla^2 \langle \mathbf{r} | \Omega(\alpha) | \mathbf{k} \rangle \\ - \int_U d\mathbf{r} \langle \mathbf{k}' | \mathbf{r} \rangle V(r) \langle \mathbf{r} | \Omega(\alpha) | \mathbf{k} \rangle = \frac{\hbar^2}{m} (\alpha^2 - k^2) \mathcal{J}(\mathbf{k}', \mathbf{k}), \end{aligned} \quad (6.2.8)$$

where $\mathcal{J}(\mathbf{k}', \mathbf{k})$ is defined as

$$\mathcal{J}(\mathbf{k}', \mathbf{k}) \equiv \int_U d\mathbf{r} \langle \mathbf{k}' | \mathbf{r} \rangle \langle \mathbf{r} | \mathbf{k} \rangle. \quad (6.2.9)$$

In the limit (6.2.1) the first term in (6.2.8) is zero, because then $\langle \mathbf{r} | \Omega(\alpha) | \mathbf{k} \rangle$ is zero inside U by (6.2.2). Because $V(\mathbf{r})$ is zero outside U , we see from (6.1.6) that the third term is equal to $-\langle \mathbf{k}' | t(\alpha) | \mathbf{k} \rangle$, and (6.2.8) becomes

$$\langle \mathbf{k}' | t(\alpha) | \mathbf{k} \rangle = \frac{\hbar^2}{m} \int_U d\mathbf{r} \langle \mathbf{k}' | \mathbf{r} \rangle \nabla^2 \langle \mathbf{r} | \Omega(\alpha) | \mathbf{k} \rangle + \frac{\hbar^2}{m} (k^2 - \alpha^2) \mathcal{J}(\mathbf{k}', \mathbf{k}). \quad (6.2.10)$$

The first term on the right hand side of (6.2.10) can, by partial integration and using Gauss's theorem and (6.2.2), be rewritten as an integral over the surface S of U . The result is

$$\langle \mathbf{k}' | t(\alpha) | \mathbf{k} \rangle = \frac{\hbar^2}{m} \int_S d\mathbf{s} \cdot \langle \mathbf{k}' | \mathbf{r} \rangle \nabla \langle \mathbf{r} | \Omega(\alpha) | \mathbf{k} \rangle + \frac{\hbar^2}{m} (k^2 - \alpha^2) \mathcal{J}(\mathbf{k}', \mathbf{k}). \quad (6.2.11)$$

If we substitute (6.2.4) and (6.2.6) and use the fact that

$$\begin{aligned} \int_S d\mathbf{s} \cdot \langle \mathbf{k}' | \mathbf{r} \rangle \nabla \langle \mathbf{r} | \Omega_s(\alpha) | \mathbf{k} \rangle &= \int_S d\mathbf{s} \cdot \langle \mathbf{k}' | \mathbf{r} \rangle \nabla \langle \mathbf{r} | \mathbf{k} \rangle \\ &= \int_U d\mathbf{r} \langle \mathbf{k}' | \mathbf{r} \rangle \nabla^2 \langle \mathbf{r} | \mathbf{k} \rangle + \int_U d\mathbf{r} \nabla \langle \mathbf{k}' | \mathbf{r} \rangle \cdot \nabla \langle \mathbf{r} | \mathbf{k} \rangle \\ &= -k^2 \mathcal{J}(\mathbf{k}', \mathbf{k}) + \mathcal{L}(\mathbf{k}', \mathbf{k}), \end{aligned} \quad (6.2.12)$$

where we defined

$$\mathcal{L}(\mathbf{k}', \mathbf{k}) \equiv \int_U d\mathbf{r} \nabla \langle \mathbf{k}' | \mathbf{r} \rangle \cdot \nabla \langle \mathbf{r} | \mathbf{k} \rangle, \quad (6.2.13)$$

we see that the term proportional to $k^2 \mathcal{J}(\mathbf{k}', \mathbf{k})$ in (6.2.11) is cancelled. This reduces the equation to

$$\langle \mathbf{k}' | t(\alpha) | \mathbf{k} \rangle = \mathcal{K} + \mathcal{G} + \mathcal{F}_h, \quad (6.2.14)$$

where we have two terms that are just integrals over the eigenstates $\langle \mathbf{r} | \mathbf{k} \rangle$,

$$\mathcal{K} \equiv \frac{\hbar^2}{m} \mathcal{L}(\mathbf{k}', \mathbf{k}) \quad (6.2.15)$$

and

$$\mathcal{G} \equiv -\frac{\hbar^2}{m} \alpha^2 \mathcal{J}(\mathbf{k}', \mathbf{k}), \quad (6.2.16)$$

and where the most important term is the one containing $\langle \mathbf{r} | \Omega_h(\alpha) | \mathbf{k} \rangle$,

$$\mathcal{F}_h \equiv \frac{\hbar^2}{m} \int_S d\mathbf{s} \cdot \langle \mathbf{k}' | \mathbf{r} \rangle \nabla \langle \mathbf{r} | \Omega_h(\alpha) | \mathbf{k} \rangle. \quad (6.2.17)$$

In the limit of low momentum and low energy the terms \mathcal{G} and \mathcal{K} will in general turn out to be either zero or equal to a constant that is cancelled by a term in \mathcal{F}_h . Therefore most of the effort of computing the t -matrix goes into calculating (6.2.17).

6.3 A layer of infinite width

In this section we will consider particles moving in a layer of infinite width, or in other words in three-dimensional space (see also van Leeuwen and Reiner [5]). In that case the eigenstates of \mathcal{H}_0 are plane waves

$$\langle \mathbf{r} | \mathbf{k} \rangle = \frac{e^{i\mathbf{k} \cdot \mathbf{r}}}{(2\pi)^{3/2}}. \quad (6.3.1)$$

The eigenstate with lowest energy and momentum, $|\mathbf{k}_0\rangle$, has $\mathbf{k}_0 = 0$.

On writing the homogeneous equation (6.2.5) in spherical coordinates we find that $\langle \mathbf{r} | \Omega_h(\alpha) | \mathbf{k} \rangle$ can be expressed as a combination of spherical Hankel functions of the first kind, $h_l^+(x)$, and spherical harmonics $Y_{lm}(\hat{\mathbf{x}})$

$$\langle \mathbf{r} | \Omega_h(\alpha) | \mathbf{k} \rangle = \sum_{l=0}^{\infty} \sum_{m=-l}^l B_{lm} h_l^+(\alpha r) Y_{lm}(\hat{\mathbf{r}}) Y_{lm}^*(\hat{\mathbf{k}}). \quad (6.3.2)$$

Hankel functions of the first kind have been used because they satisfy the boundary condition for $r \rightarrow \infty$ in the case $\text{Im } \alpha > 0$ (see appendix 6.A).

The coefficients B_{lm} are fixed by (6.2.7). Using the expansion of (6.3.1) in spherical waves,

$$\frac{e^{i\mathbf{k} \cdot \mathbf{r}}}{(2\pi)^{3/2}} = \sum_{l=0}^{\infty} \sum_{m=-l}^l \sqrt{\frac{2}{\pi}} i^l j_l(kr) Y_{lm}(\hat{\mathbf{r}}) Y_{lm}^*(\hat{\mathbf{k}}), \quad (6.3.3)$$

and the orthogonality of the spherical harmonics we find the coefficients B_{lm}

$$B_{lm} = -\sqrt{\frac{2}{\pi}} i^l \frac{j_l(ka)}{h_l^+(\alpha a)}. \quad (6.3.4)$$

To calculate the t -matrix element we first note that, since in this case S is a spherical surface, the surface element $d\mathbf{s}$ points in the radial direction, so the gradient in (6.2.17) may be replaced by the radial derivative, giving

$$\mathcal{F}_h = \frac{\hbar^2}{m} a^2 \int_S d\hat{\mathbf{r}} \langle \mathbf{k}' | \mathbf{r} \rangle \frac{\partial}{\partial r} \langle \mathbf{r} | \Omega_h(\alpha) | \mathbf{k} \rangle. \quad (6.3.5)$$

Substituting (6.3.1), (6.3.2), (6.3.3), and (6.3.4) and using the orthonormality of spherical harmonics this yields

$$\mathcal{F}_h = -\frac{2\hbar^2 a}{m\pi} \sum_{l=0}^{\infty} \sum_{m=-l}^l j_l(ka) j_l(k'a) \alpha a \frac{h_l^+(\alpha a)}{h_l^+(\alpha a)} Y_{lm}^*(\hat{\mathbf{k}}) Y_{lm}(\hat{\mathbf{k}}'), \quad (6.3.6)$$

where $f'(q) = (df/dx)_{x=q}$.

Combining (6.3.1) with (6.2.9) and (6.2.13) one finds that

$$\mathcal{J}(\mathbf{k}', \mathbf{k}) = \frac{1}{2\pi^2 |\mathbf{k} - \mathbf{k}'|^2} \left\{ \frac{\sin |\mathbf{k} - \mathbf{k}'| a}{|\mathbf{k} - \mathbf{k}'|} - a \cos |\mathbf{k} - \mathbf{k}'| a \right\} \quad (6.3.7)$$

and

$$\mathcal{L}(\mathbf{k}', \mathbf{k}) = \mathbf{k}' \cdot \mathbf{k} \mathcal{J}(\mathbf{k}', \mathbf{k}), \quad (6.3.8)$$

so

$$\mathcal{K} + \mathcal{G} = -\frac{\hbar^2}{m} (\alpha^2 - \mathbf{k}' \cdot \mathbf{k}) \mathcal{J}(\mathbf{k}', \mathbf{k}). \quad (6.3.9)$$

Substituting (6.3.6) and (6.3.9) in (6.2.14) we find (cf. [5])

$$\langle \mathbf{k}' | t(\alpha) | \mathbf{k} \rangle = -\frac{\hbar^2}{m} \left\{ (\alpha^2 - \mathbf{k}' \cdot \mathbf{k}) \mathcal{J}(\mathbf{k}', \mathbf{k}) + \frac{2a}{\pi} \sum_{l=0}^{\infty} \sum_{m=-l}^l j_l(ka) j_l(k'a) \alpha a \frac{h_l^{+'}(\alpha a)}{h_l^{+'}(\alpha a)} Y_{lm}^*(\hat{\mathbf{k}}) Y_{lm}(\hat{\mathbf{k}}') \right\}. \quad (6.3.10)$$

This is the t -matrix element for general \mathbf{k} , \mathbf{k}' and α . To find the low-energy, low-momentum behaviour we first let \mathbf{k} and \mathbf{k}' go to $\mathbf{k}_0 = \mathbf{0}$. With (6.A.1) and (6.A.3) we see that (6.3.10) reduces to

$$\langle \mathbf{0} | t(\alpha) | \mathbf{0} \rangle = -\frac{\hbar^2}{m} \left\{ \frac{1}{6\pi^2} \alpha^2 a^3 - \frac{1}{2\pi^2} \alpha a^2 \frac{h_1^+(\alpha a)}{h_0^+(\alpha a)} \right\}. \quad (6.3.11)$$

For the on-shell t -matrix we set $\alpha^2 = k_0^2 + i\epsilon = i\epsilon$ with $\epsilon \downarrow 0$. Consequently $\alpha \rightarrow 0$ and $|\alpha a| \ll 1$. Using (6.A.4), (6.3.11) for small αa becomes

$$\langle \mathbf{0} | t(\alpha) | \mathbf{0} \rangle = \frac{\hbar^2 a}{2m \pi^2}. \quad (6.3.12)$$

This is the familiar result (6.1.7) that in three dimensions the t -matrix approaches a constant value in the limit of low momentum and low energy. This value is proportional to the scattering length, which for hard spheres is equal to the diameter a .

6.4 A layer of zero width

For the case of a layer of zero width we just repeat the calculation of the previous section in two dimensions (quantum scattering in two dimensions is discussed by e.g. Lapidus [6] and Adhikari [7]). The vectors \mathbf{k} and \mathbf{r} in this section are all two-dimensional and the eigenstates of \mathcal{H}_0 are

$$\langle \mathbf{r} | \mathbf{k} \rangle = \frac{e^{i\mathbf{k} \cdot \mathbf{r}}}{2\pi} \quad (6.4.1)$$

and again $\mathbf{k}_0 = \mathbf{o}$.

If we express (6.2.5) in polar coordinates we can write $\langle \mathbf{r} | \Omega_h(\alpha) | \mathbf{k} \rangle$ as a combination of Hankel functions of the first kind, $H_m^+(x)$, and phase factors $e^{im\phi}$

$$\langle \mathbf{r} | \Omega_h(\alpha) | \mathbf{k} \rangle = \sum_{m=-\infty}^{\infty} B_m H_m^+(\alpha r) e^{im(\phi-\phi_k)}, \quad (6.4.2)$$

where ϕ and ϕ_k are the angles between \mathbf{r} and \mathbf{k} , respectively, and the x -axis. This expression satisfies the boundary conditions for $r \rightarrow \infty$ when $\text{Im } \alpha > 0$. Making use of the expansion

$$\frac{e^{i\mathbf{k}\cdot\mathbf{r}}}{2\pi} = \sum_{m=-\infty}^{\infty} \frac{i^m}{2\pi} J_m(kr) e^{im(\phi-\phi_k)} \quad (6.4.3)$$

we find the B_m from (6.2.7)

$$B_m = -\frac{i^m J_m(ka)}{2\pi H_m^+(\alpha a)}. \quad (6.4.4)$$

In two dimensions (6.3.5) becomes

$$\mathcal{F}_h = \frac{\hbar^2}{m} a \int_S d\phi \langle \mathbf{k}' | \mathbf{r} \rangle \frac{\partial}{\partial r} \langle \mathbf{r} | \Omega_h(\alpha) | \mathbf{k} \rangle, \quad (6.4.5)$$

where S is a circle of radius a , and with (6.4.1), (6.4.2), (6.4.3) and (6.4.4) we find

$$\mathcal{F}_h = -\frac{\hbar^2}{2m\pi} \sum_{m=-\infty}^{\infty} J_m(ka) J_m(k'a) \alpha a \frac{H_m^{+'}(\alpha a)}{H_m^+(\alpha a)} e^{im(\phi_{k'}-\phi_k)}. \quad (6.4.6)$$

Similar to (6.3.9) we have

$$\mathcal{K} + \mathcal{G} = -\frac{\hbar^2}{m} (\alpha^2 - \mathbf{k}' \cdot \mathbf{k}) \mathcal{J}(\mathbf{k}', \mathbf{k}). \quad (6.4.7)$$

Combining (6.4.6) and (6.4.7) and setting $\mathbf{k} = \mathbf{k}' = \mathbf{k}_0 = \mathbf{o}$ yields

$$\langle \mathbf{o} | t(\alpha) | \mathbf{o} \rangle = -\frac{\hbar^2}{m} \left\{ \frac{1}{4\pi} \alpha^2 a^2 - \frac{1}{2\pi} \alpha a \frac{H_1^{+'}(\alpha a)}{H_0^+(\alpha a)} \right\}, \quad (6.4.8)$$

where we have also used (6.A.5) and (6.A.9). We again set $\alpha^2 = i\epsilon$, and with (6.A.11) we see that for small αa (6.4.8) becomes

$$\langle \mathbf{o} | t(\alpha) | \mathbf{o} \rangle = -\frac{\hbar^2}{2m} \frac{2i}{\pi^2} \frac{1}{H_0^+(\alpha a)} \quad (6.4.9)$$

or, with (6.A.10)

$$\langle \mathbf{o} | t(\alpha) | \mathbf{o} \rangle = -\frac{\hbar^2}{2m} \frac{1}{\pi} \left[\ln(\alpha a) + \frac{\pi}{2i} + \gamma - \ln 2 \right]^{-1}. \quad (6.4.10)$$

This shows that in two dimensions the on-shell t -matrix element vanishes in the limit of low momentum and low energy.

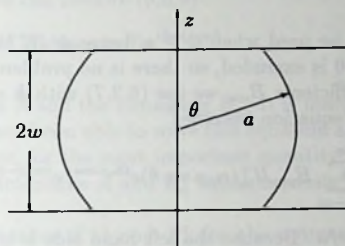


Fig. 6.1. The geometry of the problem for $w < a$

6.5 A finite layer with periodic boundary conditions

We now consider a layer of finite width $2w$, and in this section we will take as boundary condition that $\langle \mathbf{r} | \Omega(\alpha) | \mathbf{k} \rangle$ is periodic in z , as we explained in the introduction. A suitable set of eigenstates of \mathcal{H}_0 is

$$\langle \mathbf{r} | \mathbf{k} \rangle = \frac{e^{i\mathbf{k} \cdot \mathbf{r}}}{2\pi\sqrt{2w}}, \quad (6.5.1)$$

where $\mathbf{r} = (\rho, z)$ with $-w \leq z \leq w$, and $\mathbf{k} = (k_{\parallel}, k_z)$, where k_z must equal $k_n = n\pi/w$ for some n ($n = 0, \pm 1, \pm 2, \dots$) to ensure periodicity. Of course, $|\mathbf{k}_0\rangle$ has $k_{\parallel} = 0$, $k_z = 0$.

As before we are interested in the low energy and low momentum behaviour of the t -matrix. In contrast to the previous sections we will not use general \mathbf{k} , \mathbf{k}' and α but take $\mathbf{k} = \mathbf{k}' = \mathbf{k}_0 = \mathbf{0}$ and $|\alpha| \ll 1$ from the start, since this considerably simplifies the equations. In order to solve the homogeneous equation (6.2.5) we must discriminate between the cases $w < a$ and $w \geq a$. First we will treat the case $w < a$.

6.5.1 The case $w < a$

The geometry of the problem for $w < a$ is sketched in figure 6.1. Writing (6.2.5) in cylinder coordinates we see that the solution which is finite for $\rho \rightarrow \infty$ and periodic in z can be written as

$$\langle \mathbf{r} | \Omega_h(\alpha) | \mathbf{0} \rangle = \sum_{m=-\infty}^{\infty} \sum_{n=-\infty}^{\infty} B_{mn} H_m^+(\alpha_n \rho) e^{ik_n z} e^{im(\phi - \phi_k)}, \quad (6.5.2)$$

where α_n is defined as

$$\alpha_n^2 = \alpha^2 - k_n^2. \quad (6.5.3)$$

Note that (6.5.2) cannot be used when $w \geq a$, because $H_m^+(\alpha_n \rho)$ diverges for $\rho = 0$. For $w < a$ the value $\rho = 0$ is excluded, so there is no problem.

To determine the coefficients B_{mn} we use (6.2.7) with $\mathbf{k} = \mathbf{o}$. Writing $\rho = r \sin \theta$ and $z = r \cos \theta$ the basic equation becomes

$$\frac{-1}{2\pi\sqrt{2w}} = \sum_{m=-\infty}^{\infty} \sum_{n=-\infty}^{\infty} B_{mn} H_m^+(\alpha_n a \sin \theta) e^{ik_n a \cos \theta} e^{im(\phi - \phi_k)}, \quad (6.5.4)$$

where $-w/a \leq \cos \theta \leq w/a$. Because the left hand side is independent of ϕ we can take

$$B_{mn} = B_n \delta_{m,0} \quad (6.5.5)$$

and (6.5.4) reduces to

$$\frac{-1}{2\pi\sqrt{2w}} = \sum_{n=-\infty}^{\infty} B_n H_0^+(\alpha_n a \sin \theta) e^{ik_n a \cos \theta}. \quad (6.5.6)$$

Because $|\alpha_0 a| = |\alpha a| \ll 1$, as we can see from (6.5.3), the term $n = 0$ plays a special role. To prevent the right-hand side of (6.5.6) from becoming divergent for $\alpha_0 a \rightarrow 0$, see (6.A.10), we define

$$B_n = \frac{(2\pi\sqrt{2w})^{-1} B'_n}{H_0^+(\alpha a) + 2iA/\pi}, \quad (6.5.7)$$

where A is an unknown constant. If we substitute (6.5.7) in (6.5.6) and multiply by $2\pi\sqrt{2w} [H_0^+(\alpha a) + 2iA/\pi]$ we obtain

$$-H_0^+(\alpha a) - \frac{2i}{\pi} A = \sum_{n=-\infty}^{\infty} B'_n H_0^+(\alpha_n a \sin \theta) e^{ik_n a \cos \theta}. \quad (6.5.8)$$

Separating the term with $n = 0$ and using (6.A.10) for small αa , this yields

$$\begin{aligned} & -\frac{2i}{\pi} \ln \alpha a - 1 - \frac{2i}{\pi} (\gamma - \ln 2) - \frac{2i}{\pi} A = \\ & B'_0 \left[\frac{2i}{\pi} (\ln \alpha a + \ln \sin \theta) + 1 + \frac{2i}{\pi} (\gamma - \ln 2) \right] \\ & + \sum_{n \neq 0} B'_n H_0^+(\alpha_n a \sin \theta) e^{ik_n a \cos \theta}. \end{aligned} \quad (6.5.9)$$

We get rid of the divergent term $\ln \alpha a$ by taking $B'_0 = -1$. From (6.5.3) we see that for small αa

$$\alpha_n a = a\sqrt{\alpha^2 - k_n^2} = ik_n a \quad (n \neq 0). \quad (6.5.10)$$

Using this and (6.A.6) we can rewrite (6.5.9)

$$\ln \sin \theta = A - \sum_{n \neq 0} B'_n K_0(k_n a \sin \theta) e^{ik_n a \cos \theta}. \quad (6.5.11)$$

This equation determines A and the remaining B'_n . It is independent of α , and so are A and the B'_n . We have not been able to solve this equation analytically, in particular to find a closed expression for the most important quantity A as a function of w/a . A numerical scheme to determine A and B'_n simultaneously could however easily be worked out.

Leaving the determination of A and B'_n for the moment, we turn to the computation of the \mathcal{F}_h matrix. For small αa we can now write (6.5.2), using (6.5.5) and (6.5.7)

$$\langle \mathbf{r} | \Omega_h(\alpha) | \alpha \rangle = \frac{(2\pi\sqrt{2w})^{-1}}{H_0^+(\alpha a) + 2iA/\pi} \left\{ -H_0^+(\alpha\rho) + \sum_{n \neq 0} B'_n H_0^+(ik_n \rho) e^{ik_n z} \right\}. \quad (6.5.12)$$

To calculate \mathcal{F}_h we must integrate over the surface S that encloses U which is, for $w < a$, a truncated sphere. On the spherical part S' of this surface we may again replace the gradient by the radial derivative, because the surface element ds points in the radial direction. On the top and bottom planes, at $|z| = w$, the gradient may be replaced by the z -derivative, and because $\langle \mathbf{r} | \Omega(\alpha) | \alpha \rangle$ is periodic this derivative is zero. So we only need to integrate over S'

$$\mathcal{F}_h = \frac{\hbar^2}{m} a^2 \int_{S'} d\mathbf{r} \langle \alpha | \mathbf{r} \rangle \frac{\partial}{\partial r} \langle \mathbf{r} | \Omega_h(\alpha) | \alpha \rangle. \quad (6.5.13)$$

From (6.5.12) and (6.5.13) and using (6.A.10) we find for small αa

$$\mathcal{F}_h = \frac{\hbar^2}{m} a^2 \int_0^{2\pi} d\phi \int_{-w/a}^{w/a} \sin \theta d\theta \frac{(2\pi)^{-2} (2w)^{-1}}{H_0^+(\alpha a) + 2iA/\pi} \left\{ -\frac{2i}{\pi a} + \frac{\partial}{\partial r} \left[\sum_{n \neq 0} B'_n H_0^+(ik_n r \sin \theta) e^{ik_n r \cos \theta} \right]_{r=a} \right\} \quad (6.5.14)$$

or, with the definition

$$M_n(s) \equiv \int_{-s}^s dx \frac{\partial}{\partial y} \left\{ H_0^+(in\pi y \sqrt{1-x^2}) e^{in\pi y x} \right\}_{y=1/s}, \quad (6.5.15)$$

we find

$$\mathcal{F}_h = \frac{\hbar^2}{m} \left[H_0^+(\alpha a) + \frac{2i}{\pi} A \right]^{-1} \left\{ -\frac{i}{\pi^2} + \frac{a^2}{4\pi w^2} \sum_{n \neq 0} B'_n M_n(w/a) \right\}. \quad (6.5.16)$$

The other two contributions to $\langle \mathbf{o} | t(\alpha) | \mathbf{o} \rangle$ are easy; from (6.5.1) we immediately see that with $\mathbf{k} = \mathbf{k}' = \mathbf{k}_0 = \mathbf{o}$ (6.2.15) gives

$$\mathcal{K} = \frac{\hbar^2}{m} k_0^2 \mathcal{J}(\mathbf{k}_0, \mathbf{k}_0) = 0 \quad (6.5.17)$$

and it is simple to show that

$$\mathcal{G} = -\frac{\hbar^2}{m} \alpha^2 \mathcal{J}(\mathbf{o}, \mathbf{o}) = -\frac{\hbar^2 \alpha^2}{m 4\pi} \left(a^2 - \frac{w^2}{3} \right). \quad (6.5.18)$$

Consequently for small αa the only contribution to the t -matrix is (6.5.16), so

$$\langle \mathbf{o} | t(\alpha) | \mathbf{o} \rangle = \frac{\hbar^2}{m} \left[H_0^+(\alpha a) + \frac{2i}{\pi} A \right]^{-1} \left\{ -\frac{i}{\pi^2} + \frac{1}{4\pi} \frac{a^2}{w^2} \sum_{n \neq 0} B'_n K_0(n\pi \frac{a}{w}) \right\}. \quad (6.5.19)$$

In (6.5.19) A and the B'_n , which are found by solving (6.5.11), are independent of α . Therefore the only α dependence in (6.5.19) is in the factor in front, and we see that, just as in the two-dimensional case, the on-shell t -matrix vanishes for low momentum and low energy.

The result (6.4.9) can in fact be recovered exactly by letting $w/a \rightarrow 0$. If in (6.5.11) we substitute $\cos \theta = (w/a)\beta$ with $-1 \leq \beta \leq 1$, we find

$$\ln \sqrt{1 - \frac{w^2}{a^2} \beta^2} = A - \sum_{n \neq 0} B'_n K_0(n\pi \frac{a}{w} \sqrt{1 - \frac{w^2}{a^2} \beta^2}) e^{in\pi\beta}. \quad (6.5.20)$$

Using (6.A.8) we can write this for small w/a

$$-\frac{1}{2} \frac{w^2}{a^2} \beta^2 = A - \sum_{n \neq 0} B'_n \frac{1}{\sqrt{2n}} \sqrt{\frac{w}{a}} e^{-n\pi \frac{a}{w} + in\pi\beta}. \quad (6.5.21)$$

Scaling A and B'_n as follows

$$A = \tilde{A} \frac{w^2}{a^2} \quad (6.5.22)$$

$$B'_n = \tilde{B}_n \sqrt{2n} \left(\frac{w}{a} \right)^{3/2} e^{n\pi \frac{a}{w}} \quad (6.5.23)$$

we obtain

$$\beta^2 = -2\tilde{A} + 2 \sum_{n \neq 0} \tilde{B}_n e^{in\pi\beta}. \quad (6.5.24)$$

The constants \tilde{A} and \tilde{B}_n are simply the Fourier coefficients of β^2 , which can be calculated straightforwardly, and with (6.5.22) and (6.5.23) we find that to lowest order in w/a

$$A = -\frac{1}{6} \frac{w^2}{a^2} \quad (6.5.25)$$

$$B'_n = \frac{(-1)^n}{\pi^2} \sqrt{\frac{2}{n^3}} \left(\frac{w}{a}\right)^{3/2} e^{n\pi \frac{a}{w}}. \quad (6.5.26)$$

Also, for small w/a

$$M_n(w/a) = \left(\frac{w}{a}\right)^{3/2} e^{-n\pi \frac{a}{w}} C_n, \quad (6.5.27)$$

with C_n a constant independent of w/a . Substituting (6.5.25), (6.5.26), and (6.5.27) in (6.5.19) yields

$$\begin{aligned} \langle \alpha | t(\alpha) | \alpha \rangle &= \frac{\hbar^2}{m} \left[H_0^+(\alpha a) - \frac{i}{3\pi} \frac{w^2}{a^2} \right]^{-1} \\ &\times \left\{ -\frac{i}{\pi^2} + \frac{1}{4\pi^3} \frac{w}{a} \sum_{n \neq 0} (-1)^n \sqrt{\frac{2}{n^3}} C_n \right\}. \end{aligned} \quad (6.5.28)$$

And for $w/a \rightarrow 0$ this reduces to

$$\langle \alpha | t(\alpha) | \alpha \rangle = -\frac{\hbar^2}{2m} \frac{2i}{\pi^2} \frac{1}{H_0^+(\alpha a)}, \quad (6.5.29)$$

which is exactly equal to the two-dimensional result (6.4.9).

If, on the other hand, we consider the limit $w/a = 1$ it can be shown that

$$M_n(1) = 0 \quad \text{for } n = \pm 1, \pm 2, \dots \quad (6.5.30)$$

and (6.5.19) simplifies to

$$\langle \alpha | t(\alpha) | \alpha \rangle = -\frac{\hbar^2}{2m} \frac{2i}{\pi^2} \frac{1}{H_0^+(\alpha a) + 2iA/\pi}. \quad (6.5.31)$$

Numerically solving (6.5.11) suggests with remarkable precision that for $w = a$

$$A = \ln \frac{\pi}{2} - \gamma, \quad (6.5.32)$$

which we have not been able to reproduce analytically. Now we turn to the case $w \geq a$.

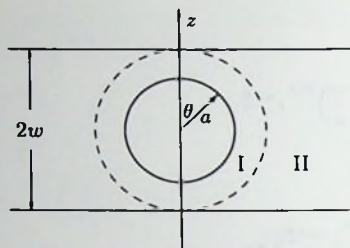


Fig. 6.2. The geometry of the problem for $w \geq a$.

6.5.2 The case $w \geq a$

When $w \geq a$ we cannot use the expansion (6.5.2) in the region $a \leq r \leq w$ because there ρ can become zero. So we divide space into two regions (see figure 6.2):

Region I : $a \leq r \leq w$

Region II : $r > w$.

In region I we write (6.2.5) in spherical coordinates, and since neither $r \rightarrow \infty$ nor $r = 0$ in this region, the solution can be written as follows

$$\langle \mathbf{r} | \Omega_h^I(\alpha) | \mathbf{o} \rangle = \sum_{l=0}^{\infty} \sum_{m=-l}^l \{ B_{lm}^+ j_l(\alpha r) + B_{lm}^- n_l(\alpha r) \} Y_{lm}(\hat{\mathbf{r}}). \quad (6.5.33)$$

In region II we still use the expansion (6.5.2), and we can again take $B_{mn} = B_n \delta_{m,0}$. One of the equations that determines the coefficients B_{lm}^+ , B_{lm}^- , and B_n is (6.2.7). At $r = a$ we use (6.5.33) and for the coefficients B_{lm}^\pm this yields, using the cylinder symmetry of the problem

$$B_{lm}^\pm = \frac{B_l^\pm}{2\pi\sqrt{2w}} \delta_{m,0} \quad (6.5.34)$$

and

$$B_l^- n_l(\alpha a) = -\delta_{l,0} - B_l^+ j_l(\alpha a), \quad (6.5.35)$$

so we can rewrite (6.5.33)

$$\langle \mathbf{r} | \Omega_h^I(\alpha) | \mathbf{o} \rangle = \sum_{l=0}^{\infty} \frac{B_l^+}{2\pi\sqrt{2w}} \left\{ j_l(\alpha r) - \frac{j_l(\alpha a)}{n_l(\alpha a)} n_l(\alpha r) \right\} P_l(\cos \theta) - \frac{1}{2\pi\sqrt{2w}} \frac{n_0(\alpha r)}{n_0(\alpha a)}. \quad (6.5.36)$$

We still need two equations to fix the remaining B_l^+ and B_n . These equations follow from the fact that $\langle \mathbf{r} | \Omega_h(\alpha) | \mathbf{o} \rangle$ and its radial derivative must be continuous at $r = w$. So the two equations are

$$\langle \mathbf{r} | \Omega_h^I(\alpha) | \mathbf{o} \rangle = \langle \mathbf{r} | \Omega_h^{II}(\alpha) | \mathbf{o} \rangle \quad \text{at } r = w \quad (6.5.37)$$

$$\frac{\partial}{\partial r} \langle \mathbf{r} | \Omega_h^I(\alpha) | \mathbf{o} \rangle = \frac{\partial}{\partial r} \langle \mathbf{r} | \Omega_h^{II}(\alpha) | \mathbf{o} \rangle \quad \text{at } r = w. \quad (6.5.38)$$

To solve these equations we again use an ansatz like (6.5.7)

$$B_r = \frac{(\sqrt{2w})^{-1} B_n'}{H_0^+(\alpha w) + 2iA/\pi} \quad (6.5.39)$$

$$B_l^+ = \frac{B_l^{+'}}{H_0^+(\alpha w) + 2iA/\pi} - \delta_{l,0}. \quad (6.5.40)$$

The equations one obtains after substituting (6.5.2), (6.5.33), (6.5.39), and (6.5.40) into (6.5.37) and (6.5.38) are rather long and cumbersome, and they are treated in appendix 6.B. The important results that we find are

$$B_0' = -1 \quad (6.5.41)$$

and

$$B_0^{+'} = -\frac{2i w}{\pi a}. \quad (6.5.42)$$

In addition we get two equations that determine, in principle, the values of the remaining coefficients A , B_n' , and $B_l^{+'}$ for n and $l \neq 0$.

Turning to the t -matrix, we need to calculate \mathcal{F}_h . When $w \geq a$ the surface S is a sphere. Consequently we get the same expression as in section 6.3

$$\mathcal{F}_h = \frac{\hbar^2 a^2}{m} \int_S d\hat{\mathbf{r}}(\mathbf{o} | \mathbf{r}) \frac{\partial}{\partial r} \langle \mathbf{r} | \Omega_h^I(\alpha) | \mathbf{o} \rangle. \quad (6.5.43)$$

We now substitute (6.5.36), (6.5.40), and (6.5.42), and with the orthonormality of the Legendre polynomials and using (6.A.3) and (6.A.4) we find for small αa

$$\mathcal{F}_h = -\frac{\hbar^2}{m} \left[H_0^+(\alpha w) + \frac{2i}{\pi} A \right]^{-1} \frac{i}{\pi^2}. \quad (6.5.44)$$

Of course we still have

$$\mathcal{K} = 0 \quad (6.5.45)$$

and now

$$\mathcal{G} = -\frac{\hbar^2}{m} \alpha^2 \mathcal{J}(\mathbf{o}, \mathbf{o}) = -\frac{\hbar^2 \alpha^2 a^3}{m \pi w}. \quad (6.5.46)$$

For $|\alpha a| \ll 1$ the t -matrix is

$$\langle \mathbf{0} | t(\alpha) | \mathbf{0} \rangle = -\frac{\hbar^2 2i}{2m \pi^2 H_0^+(\alpha w) + 2iA/\pi}. \quad (6.5.47)$$

This formula is very similar to (6.5.31), only the argument of H_0^+ is αw instead of αa and A still depends on w/a . For $w = a$, of course it is the same as (6.5.31). So, for any finite w , the behaviour of the t -matrix is still the same as in two dimensions: it vanishes in the on-shell, low momentum and low energy limit. Only when $w/a \rightarrow \infty$ do we recover the three-dimensional behaviour.

If we let $w/a \rightarrow \infty$, we first of all need to change the normalization factor in (6.5.1) to $(2\pi)^{-3/2}$ to get the same result as in section 6.3. For the t -matrix this implies multiplying it by w/π . Then we need to find the behaviour of A for large w/a . If we take (6.B.4), substitute (6.5.42) and integrate all terms over $\cos \theta$ from -1 to 1 , all $P_l(\cos \theta)$ for $l > 0$ drop out because of the orthogonality of the Legendre polynomials. The remaining equation is

$$A = \ln 2 - \frac{w}{a} + \sum_{n \neq 0} B'_n S_n, \quad (6.5.48)$$

where

$$S_n \equiv \frac{i\pi}{4} \int_{-1}^1 dx H_0^+(in\pi\sqrt{1-x^2}) e^{in\pi x}. \quad (6.5.49)$$

Supposing the B'_n do not diverge for $w/a \rightarrow \infty$, we see that for large w/a

$$A = -\frac{w}{a}. \quad (6.5.50)$$

If we substitute this in (6.5.47) and multiply by w/π we find

$$\langle \mathbf{0} | t(\alpha) | \mathbf{0} \rangle = -\frac{\hbar^2 2i}{2m \pi^3 H_0^+(\alpha w) - 2iw/\pi a} w \quad (6.5.51)$$

and in the limit $w/a \rightarrow \infty$ this is

$$\langle \mathbf{0} | t(\alpha) | \mathbf{0} \rangle = \frac{\hbar^2 a}{2m \pi^2}, \quad (6.5.52)$$

which is the same as (6.3.12).

6.6 A finite layer with zero boundary conditions

In this section we will adapt the calculation of the previous section to a different set of boundary conditions. Instead of periodic boundary conditions we take $\langle r|\Omega(\alpha)|k\rangle = 0$ at $|z| = w$. Since this requires the same general approach as before we will be somewhat less specific and stress the differences and similarities between this section and section 6.5. We will treat the case $w < a$ and for $w \geq a$ we will only quote the result. Eigenstates of \mathcal{H}_0 that are zero at $|z| = w$ are

$$\langle r|k\rangle = \frac{e^{i\bar{k}_z z}}{2\pi\sqrt{w}} \cos k_z z \quad \text{or} \quad \frac{e^{i\bar{k}_z z}}{2\pi\sqrt{w}} \sin \bar{k}_z z, \quad (6.6.1)$$

where k_z and \bar{k}_z must be equal to $k_n = (2n+1)\pi/2w$ and $\bar{k}_n = (n+1)\pi/w$, respectively, for some n ($n = 0, 1, 2, \dots$). The lowest energy eigenstate $|k_0\rangle$ is $k_{||} = 0$, $k_z = k_0 = \pi/2w$. Again we immediately set $k = k' = k_0$ and $\alpha^2 = k_0^2 + i\epsilon$, so $|\alpha^2 - k_0^2|a^2 \ll 1$.

For $w < a$ we can, in analogy to (6.5.2) and making use of the cylinder symmetry of the problem and the fact that $\langle r|k_0\rangle$ is even in z , write

$$\langle r|\Omega_h(\alpha)|k_0\rangle = \sum_{n=0}^{\infty} B_n H_0^+(\alpha_n \rho) \cos k_n z \quad (6.6.2)$$

with

$$\alpha_n^2 = \alpha^2 - k_n^2. \quad (6.6.3)$$

At $r = a$ we have (6.2.7), so

$$-\frac{\cos k_0 a \cos \theta}{2\pi\sqrt{w}} = \sum_{n=0}^{\infty} B_n H_0^+(\alpha_n a \sin \theta) \cos k_n a \cos \theta. \quad (6.6.4)$$

According to (6.6.3) $\alpha_0^2 = \alpha^2 - k_0^2$, and so $|\alpha_0 a| \ll 1$. Then we define as in (6.5.7)

$$B_n = \frac{(2\pi\sqrt{w})^{-1} B'_n}{H_0^+(\alpha_0 a) + 2iA/\pi}. \quad (6.6.5)$$

Substituting this in (6.6.4) and multiplying by $2\pi\sqrt{w}[H_0^+(\alpha_0 a) + 2iA/\pi]$ produces an equation similar to (6.5.8). Using (6.A.10) for $|\alpha_0 a| \ll 1$ we can again eliminate the divergent term $\ln \alpha_0 a$ by taking

$$B'_0 = -1. \quad (6.6.6)$$

If we then substitute, for $|\alpha_0 a| \ll 1$

$$\alpha_n a = a\sqrt{\alpha^2 - k_n^2} = a\sqrt{k_0^2 - k_n^2} \equiv i\beta_n a \quad (n \neq 0) \quad (6.6.7)$$

the remaining equation reads

$$\ln(\sin \theta) \cos(k_0 a \cos \theta) = A \cos(k_0 a \cos \theta) - \sum_{n>0} B'_n K_0(\beta_n a \sin \theta) \cos(k_n a \cos \theta), \quad (6.6.8)$$

where we have also used (6.A.6). This is again an equation independent of α from which A and the B'_n can be determined.

With (6.6.5) and (6.6.6) we now have for (6.6.2)

$$\langle \mathbf{r} | \Omega_h(\alpha) | \mathbf{k}_0 \rangle = \frac{(2\pi\sqrt{w})^{-1}}{H_0^+(\alpha_0 a) + 2iA/\pi} \left\{ -H_0^+(\alpha_0 \rho) \cos k_0 z + \sum_{n>0} B'_n H_0^+(i\beta_n \rho) \cos k_n z \right\} \quad (6.6.9)$$

In calculating \mathcal{F}_h we can again limit the integration to the spherical part S' of S , this time because at $|z| = w$ the eigenstates $\langle \mathbf{k}_0 | \mathbf{r} \rangle$ are zero. We find

$$\mathcal{F}_h = \frac{\hbar^2}{m} a^2 \int_{S'} d\hat{\mathbf{r}} \langle \mathbf{k}_0 | \mathbf{r} \rangle \frac{\partial}{\partial r} \langle \mathbf{r} | \Omega_h(\alpha) | \mathbf{k}_0 \rangle \quad (6.6.10)$$

or, with (6.6.9) and (6.A.10) for small $\alpha_0 a$

$$\mathcal{F}_h = \frac{\hbar^2}{m} \left[H_0^+(\alpha_0 a) + \frac{2i}{\pi} A \right]^{-1} \left\{ -\frac{i}{\pi^2} + \frac{1}{4\pi} \left[\frac{2i}{\pi} \ln \alpha_0 a + 1 + \frac{2i}{\pi} (\gamma - \ln 2) \right] + \frac{i}{8\pi^3} R(w/a) + \frac{a^2}{2\pi w^2} \sum_{n>0} B'_n Q_n(w/a) \right\} \quad (6.6.11)$$

with

$$R(s) \equiv \int_{-\pi}^{\pi} dx x \sin x \ln(1 - \frac{s^2}{\pi^2} x^2) \quad (6.6.12)$$

and

$$Q_n(s) \equiv \int_{-\pi}^{\pi} dx \cos\left(\frac{\pi y x}{2}\right) \frac{\partial}{\partial y} \left\{ H_0^+(i\sqrt{n^2 + \pi n y \sqrt{1-x^2}}) \times \cos\left((2n+1)\frac{\pi y x}{2}\right) \right\}_{y=1/s} \quad (6.6.13)$$

In this case \mathcal{K} is not zero, but

$$\mathcal{K} = -\frac{\hbar^2}{m} \frac{1}{4\pi} + \frac{\hbar^2}{m} k_0^2 \mathcal{J}(\mathbf{k}_0, \mathbf{k}_0) \quad (6.6.14)$$

and

$$\mathcal{G} = -\frac{\hbar^2}{m} \alpha^2 \mathcal{J}(\mathbf{k}_0, \mathbf{k}_0), \quad (6.6.15)$$

so

$$\mathcal{K} + \mathcal{G} = -\frac{\hbar^2}{m} \left[\frac{1}{4\pi} + \alpha_0^2 \mathcal{J}(\mathbf{k}_0, \mathbf{k}_0) \right]. \quad (6.6.16)$$

For small α_0 the second term in (6.6.16) vanishes and we then have

$$\begin{aligned} \langle i\mathbf{k}_0 | t(\alpha) | \mathbf{k}_0 \rangle &= \mathcal{K} + \mathcal{G} + \mathcal{F}_h \\ &= -\frac{\hbar^2}{m} \frac{1}{4\pi} + \frac{\hbar^2}{m} \left[H_0^+(\alpha_0 a) + \frac{2i}{\pi} A \right]^{-1} \left\{ -\frac{i}{\pi^2} \right. \\ &\quad \left. + \frac{1}{4\pi} \left(\frac{2i}{\pi} \ln \alpha_0 a + 1 + \frac{2i}{\pi} (\gamma - \ln 2) \right) + \frac{i}{8\pi^3} R(w/a) \right. \\ &\quad \left. + \frac{a^2}{2\pi w^2} \sum_{n>0} B'_n Q_n(w/a) \right\}. \end{aligned} \quad (6.6.17)$$

Since for small $\alpha_0 a$ the term in parentheses is equal to $H_0^+(\alpha_0 a)$, it cancels the contribution of the first term on the right-hand side of (6.6.17). The remaining terms are all proportional to $[H_0^+(\alpha_0 a) + 2iA/\pi]^{-1}$:

$$\begin{aligned} \langle \mathbf{k}_0 | t(\alpha) | \mathbf{k}_0 \rangle &= -\frac{\hbar^2}{m} \left[H_0^+(\alpha_0 a) + \frac{2i}{\pi} A \right]^{-1} \left\{ \frac{i}{\pi^2} + \frac{iA}{2\pi^2} - \frac{i}{8\pi^3} R(w/a) \right. \\ &\quad \left. - \frac{a^2}{2\pi w^2} \sum_{n>0} B'_n Q_n(w/a) \right\}. \end{aligned} \quad (6.6.18)$$

All terms inside the braces are independent of α , so the behaviour of $\langle \mathbf{k}_0 | t(\alpha) | \mathbf{k}_0 \rangle$ is the same as for periodic boundary conditions. It can also be shown that for $w/a \rightarrow 0$ it exactly reproduces (6.5.29).

Thus we find that changing the boundary conditions considerably changes the problem; e.g. neither k_0 nor α vanish in the low energy, low momentum limit. This causes the equations to become more complicated than in the previous section. Nevertheless, the behaviour of the t -matrix is qualitatively the same: it vanishes in the on-shell, low momentum and low energy limit.

For the boundary conditions considered here the case $w < a$ seems rather unphysical: while the hard spheres do not fit into the layer, their wave functions are supposed to be zero on the boundary $|z| = w$. The case $w \geq a$ however is physical, and there we find the same behaviour of the t -matrix:

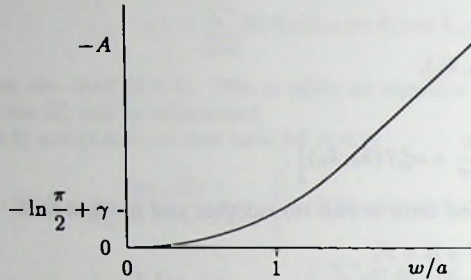


Fig. 6.3. The behaviour of A as a function of w/a for periodic boundary conditions

$$\langle \mathbf{k}_0 | t(\alpha) | \mathbf{k}_0 \rangle \propto \frac{1}{H_0^2(\alpha_0 w) + 2iA/\pi} \quad (6.6.19)$$

So for these different boundary conditions the result is the same.

6.7 Discussion

We have computed the t -matrix of two hard spheres confined to a thin layer in the limit of low momentum and energy. It is found that the t -matrix behaves as

$$\langle \mathbf{k}' | t(\alpha) | \mathbf{k} \rangle \approx -\frac{\hbar^2}{2m} \frac{1}{\pi} \left[\ln \alpha_0 s + \frac{\pi}{2i} + \gamma - \ln 2 + A \right]^{-1}, \quad (6.7.1)$$

where $s = \max(a, w)$ and A is a function of the ratio of the layer width $2w$ to the hard sphere diameter a . The parameter α_0 is related to the energy by (6.1.8) and (6.5.3). The function $A(w/a)$ depends on the boundary conditions which are imposed on the wave matrix $\langle \mathbf{r} | \Omega(\alpha) | \mathbf{k} \rangle$ from which the t -matrix is calculated by (6.1.6). In figure 6.3 a sketch is given of $A(w/a)$ for periodic boundary conditions.

The simplest case considered here refers to periodic boundary conditions in the relative motion of the two spheres. In this case the result (6.7.1) can be intuitively understood by considering the following electrical analogon. The equation for the homogeneous part (6.2.5)

$$(\alpha^2 + \nabla^2) \langle \mathbf{r} | \Omega_h(\alpha) | \mathbf{k} \rangle = 0 \quad (6.7.2)$$

becomes for $\alpha = 0$ the Laplace equation, and $\langle \mathbf{r} | \Omega_h(0) | \mathbf{k} \rangle$ may be considered as an electrical potential. It vanishes at infinity and on the sphere $r = a$ it satisfies, for small k , the condition

$$\langle \mathbf{r} | \Omega_h(0) | \mathbf{k} \rangle = -\langle \mathbf{r} | \mathbf{k} \rangle \approx -\frac{1}{2\pi\sqrt{2w}}. \quad (6.7.3)$$

The t -matrix for low momentum and energy follows from this "potential" as

$$\langle \mathbf{k}' | t(0) | \mathbf{k} \rangle = \int_S d\mathbf{s} \cdot \nabla \langle \mathbf{r} | \Omega_h(0) | \mathbf{k} \rangle, \quad (6.7.4)$$

or as the integral over the normal component of the electric "field" on the sphere, which equals the total "charge" on the sphere.

Thus the t -matrix is the total charge on the sphere for a potential which is zero at infinity and given by (6.7.3) on the sphere. The periodicity requirement transforms the problem into a row of spheres along the z -axis. From large distances this row manifests itself as a charged infinitely long cylinder. It is well known that this leads to a logarithmically divergent potential at infinity. Thus in order to keep the potential zero at infinity the charge on the sphere (or the t -matrix) must vanish. As α^{-1} may be interpreted as a cut-off length the vanishing of the t -matrix as given by (6.7.1) follows.

From this viewpoint it is surprising that the boundary condition where we require $\langle \mathbf{r} | \Omega_h(\alpha) | \mathbf{k} \rangle$ to vanish for $|z| = w$ leads to essentially the same result. The difference is that α does not vanish, but rather assumes the value $k_0^2 = (\pi/2w)^2$ which is not necessarily small. So the singular behaviour (6.7.1) occurs at the lowest energy possible in the layer. Thus one cannot use the interpretation of (6.7.2) as a potential equation.

Neither of the two boundary conditions treated here correspond fully to the boundary conditions appropriate to a real layer. As has been mentioned the requirement of the vanishing of the wave matrix $\langle \mathbf{r}_1 \mathbf{r}_2 | \Omega | \mathbf{k}_1 \mathbf{k}_2 \rangle$ when either of the two particles hits the boundary $|z_i| = w$ couples the relative motion to the center of mass motion. This makes the analytical treatment substantially more complex. The fact that two different boundary conditions in the relative space, which may be considered extreme opposites, lead to essentially the same result makes us confident that (6.7.1) also holds for the real case. The function $A(w/a)$ will then of course differ from the A calculated here.

Appendix 6.A: Bessel functions

In this paper we use the following properties of the spherical Bessel functions [8]:

$$\frac{d}{dx} h_0^+(x) = -h_1^+(x); \quad (6.A.1)$$

for $x \rightarrow \infty$:

$$h_l^+(x) \sim (-i)^{l+1} \frac{e^{ix}}{x}; \quad (6.A.2)$$

for $x \rightarrow 0$:

$$j_l(x) \approx \frac{x^l}{(2l+1)!!}, \quad (6.A.3)$$

$$n_l(x) \approx -ih_l^+(x) \approx -\frac{(2l-1)!!}{x^{l+1}}. \quad (6.A.4)$$

For the ordinary Bessel functions we use:

$$\frac{d}{dx} H_0^+(x) = -H_1^+(x); \quad (6.A.5)$$

$$K_0(x) \equiv \frac{i\pi}{2} H_0^+(ix); \quad (6.A.6)$$

for $x \rightarrow \infty$:

$$H_0^+(x) \sim \sqrt{\frac{2}{\pi x}} e^{ix}, \quad (6.A.7)$$

$$K_0(x) \sim \sqrt{\frac{\pi}{2x}} e^{-x}; \quad (6.A.8)$$

for $x \rightarrow 0$:

$$J_m(x) \approx \frac{x^m}{2^m m!}, \quad (6.A.9)$$

$$H_0^+(x) \approx \frac{2i}{\pi} \ln x + 1 + \frac{2i}{\pi} (\gamma - \ln 2), \quad (6.A.10)$$

$$H_m^+(x) \approx -i \frac{(m-1)!}{\pi} \left(\frac{2}{x}\right)^m \quad (m > 0), \quad (6.A.11)$$

where $\gamma = 0.57721566 \dots$ is Euler's constant.

Appendix 6.B: The continuity equations at $r = w$

We will show in this appendix how (6.5.37) and (6.5.38) lead to the results (6.5.41) and (6.5.42). After substituting (6.5.2), (6.5.33), (6.5.39), and (6.5.40) into (6.5.37) and multiplying by $2\pi\sqrt{2w} [H_0^+(\alpha w) + 2iA/\pi]$ we find

$$\begin{aligned} & - [H_0^+(\alpha w) + 2iA/\pi] \left(j_0(\alpha w) - \frac{j_0(\alpha a)}{n_0(\alpha a)} n_0(\alpha w) + \frac{n_0(\alpha w)}{n_0(\alpha a)} \right) \\ & + B_0^{+'} \left(j_0(\alpha w) - \frac{j_0(\alpha a)}{n_0(\alpha a)} n_0(\alpha w) \right) \\ & + \sum_{l=1}^{\infty} B_l^{+'} \left\{ j_l(\alpha w) - \frac{j_l(\alpha a)}{n_l(\alpha a)} n_l(\alpha w) \right\} P_l(\cos \theta) \\ & = B_0^+ H_0^+(\alpha w \sin \theta) + \sum_{n \neq 0} B_n^+ H_0^+(\alpha_n w \sin \theta) e^{ik_n w \cos \theta}. \end{aligned} \quad (6.B.1)$$

For $\alpha w \rightarrow 0$ we find, with (6.5.10) and (6.A.10)

$$\begin{aligned}
 & -\frac{2i}{\pi} \left(\ln \alpha w + \frac{\pi}{2i} + \gamma - \ln 2 + A \right) + B_0^{+'} \left(1 - \frac{a}{w} \right) \\
 & + \sum_{l=1}^{\infty} B_l^{+'} \left\{ j_l(\alpha w) - \frac{j_l(\alpha a)}{n_l(\alpha a)} n_l(\alpha w) \right\} P_l(\cos \theta) \\
 & = E_0' \frac{2i}{\pi} \left(\ln \alpha w \sin \theta + \frac{\pi}{2i} + \gamma - \ln 2 \right) \\
 & + \sum_{n \neq 0} B_n' H_0^{+'}(\alpha_n w \sin \theta) e^{ik_n w \cos \theta}. \tag{6.B.2}
 \end{aligned}$$

To get rid of the divergent term $\ln \alpha w$ we take

$$B_0' = -1. \tag{6.B.3}$$

The remaining equation is

$$\begin{aligned}
 & -\frac{2i}{\pi} A + \left(1 - \frac{a}{w} \right) B_0^{+'} + \sum_{l=1}^{\infty} B_l^{+'} \left\{ j_l(\alpha w) - \frac{j_l(\alpha a)}{n_l(\alpha a)} n_l(\alpha w) \right\} P_l(\cos \theta) \\
 & = -\frac{2i}{\pi} \ln \sin \theta + \sum_{n \neq 0} B_n' H_0^{+'}(\alpha_n w \sin \theta) e^{ik_n w \cos \theta}. \tag{6.B.4}
 \end{aligned}$$

A second relation follows from (6.5.38). With (6.B.3) we find

$$\begin{aligned}
 & - \left(\alpha j_0'(\alpha w) - \alpha \frac{j_0(\alpha a)}{n_0(\alpha a)} n_0'(\alpha w) + \alpha \frac{n_0'(\alpha w)}{n_0(\alpha a)} \right) [H_0^{+'}(\alpha w) + 2iA/\pi] \\
 & + B_0^{+'} \left(\alpha j_0'(\alpha w) - \alpha \frac{j_0(\alpha a)}{n_0(\alpha a)} n_0'(\alpha w) \right) \\
 & + \sum_{l=1}^{\infty} B_l^{+'} \alpha \left\{ j_l'(\alpha w) - \frac{j_l(\alpha a)}{n_l(\alpha a)} n_l'(\alpha w) \right\} P_l(\cos \theta) \\
 & = -H_0^{+'}(\alpha w \sin \theta) \alpha \sin \theta \\
 & + \sum_{n \neq 0} B_n' \frac{\partial}{\partial r} [H_0^{+'}(\alpha_n r \sin \theta) e^{ik_n r \cos \theta}]_{r=w}. \tag{6.B.5}
 \end{aligned}$$

Again letting $\alpha w \rightarrow 0$ this gives

$$\begin{aligned}
 & \frac{a}{w^2} B_0^{+'} + \sum_{l=1}^{\infty} B_l^{+'} \alpha \left\{ j_l'(\alpha w) - \frac{j_l(\alpha a)}{n_l(\alpha a)} n_l'(\alpha w) \right\} P_l(\cos \theta) \\
 & = -\frac{2i}{\pi} \frac{1}{w} + \sum_{n \neq 0} B_n' \frac{\partial}{\partial r} [H_0^{+'}(\alpha_n r \sin \theta) e^{ik_n r \cos \theta}]_{r=w}. \tag{6.B.6}
 \end{aligned}$$

Integrating this equation over $\cos \theta$ from -1 to 1 the terms with $l > 0$ vanish because of the orthogonality of the $P_l(\cos \theta)$. Thus we obtain

$$\frac{2a}{w^2} B_0^{+'} = -\frac{4i}{\pi} \frac{1}{w} + \sum_{n \neq 0} \frac{1}{w} B_n' M_n(1), \quad (6.B.7)$$

where the integral $M_n(x)$ is defined by (6.5.15). From (6.5.30) we know that $M_n(1) = 0$ for $n \neq 0$, so

$$B_0^{+'} = -\frac{2i}{\pi} \frac{w}{a}. \quad (6.B.8)$$

The other coefficients B_n' and $B_l^{+'}$ can be obtained by solving (6.B.4) and (6.B.6).

References

- [1] T.D. Lee, K. Huang, and C.N. Yang, *Phys. Rev.* **106** (1957) 1135
- [2] V.N. Popov, *Functional Integrals in Quantum Field Theory and Statistical Physics*, Reidel, Dordrecht, 1983, Chap. 6
- [3] D.S. Fisher and P.C. Hohenberg, *Phys. Rev. B* **37** (1988) 4936
- [4] J.R. Taylor, *Scattering Theory*, Wiley, New York, 1972
- [5] J.M.J. van Leeuwen and A.S. Reiner, *Physica* **27** (1961) 99
- [6] I.R. Lapidus, *Am. J. Phys.* **50** (1982) 45
- [7] S.K. Adhikari, *Am. J. Phys.* **54** (1986) 362
- [8] G. Arfken, *Mathematical Methods for Physicists*, Academic Press, Orlando, 1985, Chap. 11

Samenvatting

Het doel van de statistische mechanica is het beschrijven van het gedrag van een macroscopisch materiaal (gas, vloeistof, vaste stof), uitgaande van de eigenschappen van de samenstellende deeltjes (atomen, moleculen etc.). Hoewel deze eigenschappen vaak zeer goed bekend zijn, is het toch slechts zelden mogelijk om het gedrag van een zeer groot aantal van deze deeltjes hieruit exact af te leiden; die gevallen waarin dit wel mogelijk is betreffen in het algemeen een geïdealiseerde situatie en niet een werkelijk bestaand systeem. Daarom is het vrijwel altijd noodzakelijk benaderingen te maken om tot een resultaat te komen.

Het materiaal dat aanleiding heeft gegeven tot het onderzoek in dit proefschrift is helium en in het bijzonder de isotoop ${}^4\text{He}$. Onder normale omstandigheden is helium gasvormig, maar bij lage temperaturen is het een vloeistof. Het is het enige materiaal dat zelfs bij het absolute nulpunt slechts onder hoge druk vast wordt. De oorzaak hiervan is de sterke nulpuntsbeweging, die ook bij zeer lage temperaturen de zwakke aantrekkingskracht tussen de heliumatomen blijft tegenwerken. Dit geeft al aan dat quantummechanische effecten een grote invloed hebben op het gedrag van helium bij lage temperatuur. Een nog spectaculairder voorbeeld hiervan is het optreden van superfluiditeit.

Boven een temperatuur van 2.18 K is ${}^4\text{He}$ een normale vloeistof; daar beneden is het superfluïde. Superfluïde helium heeft verschillende bijzondere eigenschappen, waarvan de belangrijkste is dat het zonder weerstand kan stromen. De theoretische verklaring voor dit verschijnsel is het optreden van Bose-Einstein condensatie van de heliumatomen. Dit is een bijzonder soort fase-overgang, waarbij de quantummechanische beschrijving van de microscopische eigenschappen van de atomen ook tot uiting komt in het gedrag van de vloeistof op macroscopische schaal. Het treedt alleen op bij deeltjes die bosonen zijn, zoals ${}^4\text{He}$ -atomen. Dit is in overeenstemming met het feit dat de andere isotoop van helium, ${}^3\text{He}$, bestaande uit fermionen, een dergelijke superfluiditeit niet vertoont.

De wisselwerking tussen ${}^4\text{He}$ -atomen is goed bekend: op korte afstanden stoten zij elkaar sterk af, zodat zich geen twee atomen op dezelfde plaats kunnen bevinden, en op grotere afstanden trekken zij elkaar zwak aan. Op zeer grote afstand verdwijnt de wisselwerking vrijwel geheel. Toch is het ondoenlijk om deze eigenschappen te vertalen in eigenschappen van de vloeistof ${}^4\text{He}$. Alleen voor een ideaal, niet-wisselwerkend Bose-gas kan deze berekening uitgevoerd worden. Om de wis-

selwerking tussen de atomen in de berekening mee te kunnen nemen moet dus een benadering gemaakt worden.

Een mogelijke aanpak is om een gas van harde bollen als uitgangspunt te nemen en de aantrekkende wisselwerking te verwaarlozen. Dit kan door middel van storings-theorie. Een nadeel van deze methode is dat zij vooral geschikt is voor een gas bij lage dichtheid en niet bij dichtheden zoals die van ${}^4\text{He}$. Ook worden de berekeningen in deze benadering snel gecompliceerd, vooral als met bijzondere externe omstandigheden rekening gehouden moet worden. Dit blijkt uit de berekening in hoofdstuk 6, waar een belangrijke grootheid in deze methode, de t -matrix, wordt uitgerekend voor een systeem in een dunne laag.

In de overige hoofdstukken van dit proefschrift wordt voor een andere aanpak gekozen. In plaats van te proberen een realistisch model van wisselwerkende bosonen te behandelen, beschouwen wij een sterk vereenvoudigd model, dat niet min de essentiële eigenschappen van het werkelijke systeem bezit. Dit model bestaat uit bosonische deeltjes die op een rooster bewegen. Hun beweging is beperkt tot aangrenzende roosterplaatsen. De wisselwerking tussen de deeltjes wordt gerepresenteerd door een wisselwerking tussen twee deeltjes als zij op naburige roosterplaatsen zitten. Met de harde afstotende kern van de wisselwerking wordt rekening gehouden door te verbieden dat er meer dan één deeltje op een roosterplaats kan zitten. De eenvoud van dit model ligt in het feit dat de deeltjes, in plaats van door de hele ruimte te bewegen, zich slechts op discrete roosterpunten kunnen bevinden, en dat zowel de beweging als de interactie van de deeltjes zeer plaatselijk is.

Een bijkomend voordeel van het werken met een zeer vereenvoudigd roostermodel is dat het niet alleen ${}^4\text{He}$ beschrijft, maar ook talrijke deeltjessystemen die dezelfde essentiële eigenschappen hebben; bijvoorbeeld een gas van gaten in een vast ${}^4\text{He}$ -kristal, of paren van elektronen die voorkomen in sommige theorieën voor hoge-temperatuur supergeleiders. Om de berekeningen aan dit model te vergemakkelijken wordt in hoofdstuk 2 een equivalent model geïntroduceerd: het spin- $\frac{1}{2}$ XXZ model. In plaats van bewegende deeltjes op een rooster beschrijft dit model magnetische quantumspins op een rooster; eenvoudig kan aangetoond worden dat deze twee modellen equivalent zijn. Het introduceren van dit pseudospinmodel leidt dan ook niet tot andere uitkomsten, maar alleen tot een andere manier om de uitkomsten te beschrijven. Het geeft ook de mogelijkheid om deze resultaten toe te passen op modellen voor magnetische materialen en om ze te vergelijken met bekende gegevens voor zulke modellen.

Toch is zelfs het roostermodel te moeilijk om exact op te lossen, en in dit proefschrift worden verschillende benaderingstechnieken toegepast. De eerste benaderingstechniek is de cluster-variatiemethode, die in hoofdstuk 3 wordt geïntroduceerd. Met deze methode kan het fasediagram van het pseudospinmodel berekend worden. De specifieke kracht van deze benadering is, dat het effect van correlaties tussen naastelust-spins wordt meegenomen. Het resulterende fasediagram is een grote vooruitgang vergeleken met simpelere benaderingsmethoden. Ook is het goed in overeenstemming met wat al bekend was uit andere berekeningen. In het bijzonder de vorm en de sym-

metrie van het fase-diagram worden goed weergegeven.

Na de cluster-variantie-methode op homogene systemen in twee en drie dimensies toegepast te hebben, wordt in hoofdstuk 4 aandacht besteed aan systemen met een meer gecompliceerde geometrie. Eerst wordt een drie-dimensionaal systeem met een anisotrope wisselwerking behandeld en vervolgens een systeem in een dunne laag. Deze beide systemen kunnen zowel twee- als drie-dimensionaal gedrag vertonen en de overgang tussen die twee gevallen wordt bestudeerd. Ook is het mogelijk om grootheden te berekenen als functie van de diepte in de laag. Net als voor homogene systemen zijn de resulterende fase-diagrammen bevredigend, ondanks enkele inconsistenties in de beschrijving van de overgang van twee naar drie dimensies.

In hoofdstuk 5 wordt tenslotte de gemiddelde-veld renormalisatiegroep toegepast op systemen in twee en drie dimensies. De resultaten van de simpelste versie van deze methode zijn hetzelfde als die van de cluster-variantie-methode. Bij het verfijnen van de beschrijving blijkt echter dat dit slechts op toeval berust en dat er geen fundamentele overeenkomst tussen beide methoden bestaat. Het blijkt dat het toepassen van deze methode op quantumspins soms grote problemen kan opleveren, maar net als de cluster-variantie-methode geeft zij toch een goed beeld van het fase-diagram.

Tot de promotie wordt met het oog op de beperkte ruimte
in de Senaatskamer uitsluitend toegang verleend op
vertoon van een bewijs van toegang.

Receptie na afloop van de promotie
in het Academiegebouw,
Rapenburg 73, Leiden.

N.B. Met tijdrovende parkeermoeilijkheden bij het
Academiegebouw moet rekening gehouden worden.

Curriculum vitae

Op 29 september 1965 werd ik in Amstelveen geboren. Na in 1983 aan het Hermann Wesselink College in Amstelveen het eindexamen Gymnasium- β te hebben behaald, begon ik aan de studie Natuurkunde aan de Vrije Universiteit in Amsterdam. In augustus 1984 legde ik het propaedeutisch examen af. Mijn afstudeeronderzoek deed ik onder leiding van prof.dr. A. Lodder, in de werkgroep theorie van de vaste stof. De titel van mijn scriptie luidde "Symmetrie bij Bloch-elektronverstrooiing aan een Frenkelpaar in koper". In november 1987 legde ik het doctoraalexamen Natuurkunde af. Per 1 december 1987 trad ik in dienst van de stichting Fundamenteel Onderzoek der Materie, om bij prof. dr. J.M.J. van Leeuwen aan het Instituut-Lorentz van de Rijksuniversiteit te Leiden aan een promotie-onderzoek te beginnen.

Tijdens mijn promotieperiode bezocht ik verscheidene conferenties, namelijk de "International Conference on Thermodynamics and Statistical Mechanics, Statphys 17" die in 1989 in Rio de Janeiro plaatsvond, en, in 1991, de "Rencontre de Physique Statistique" te Parijs. Ook nam ik in 1989 deel aan de "International Summer School on Fundamental Problems in Statistical Mechanics VII" te Altenberg, West-Duitsland, en de "Workshop on Computational Physics and Cellular Automata" in Ouro Preto, Brazilië.

Stellingen

1. Om een juist beeld te krijgen van het effect van een onzuiverheid op het gedrag van geleidingselektronen in een metaal is het wenselijk een zelf-consistent berekende onzuiverheidspotentiala te gebruiken.

A. Lodder et al., J. Phys. F 18 (1988) 1057

2. Het feit dat bij het toepassen van de paar-benadering van de cluster-variatiemethode op klassieke spinsystemen bij lage temperaturen geen terugkeer naar de ongeordende fase optreedt, wijst erop dat het wel optreden van dit effect bij quantumspins een gevolg is van het quantummechanische karakter van de spins.

3. De eis dat een real-space renormalisatie-transformatie de symmetrie van de Hamiltoniaan behoudt, maakt het onmogelijk voor het XXZ-model een dergelijke transformatie te construeren die in het hele fasediagram toegepast kan worden.

R.C. Brower et al., Phys. Rev. Lett. 38 (1977) 1231

4. De door Matsubara en Matsuda geconstateerde afname van de kritische temperatuur bij het toenemen van de dichtheid van een quantum-roostergas treedt slechts op bij dichtheden groter dan $1/2$. Vanwege de deeltje-gat symmetrie neemt de kritische temperatuur beneden deze waarde juist toe bij toenemende dichtheid.

T. Matsubara en H. Matsuda, Prog. Theor. Phys. 16 (1956) 569

5. De term XY-model zou uitsluitend gebruikt moeten worden voor modellen van quantumspins. Het gebruik van deze term voor klassieke spins met twee vrijheidsgraden geeft aanleiding tot verwarring.
6. Maarten 't Hart heeft geen gelijk met zijn bewering dat de meeste wetenschappelijke experimenten ongecontroleerd blijven omdat zij nooit gedupliceerd worden.

M. 't Hart, 1^e Albert Verwey-lezing, Leiden, 3 november 1989

7. Beschouw een vierkant $2 \times N$ rooster met periodieke randvoorwaarden. Op elk roosterpunt wordt een tweezijdige spiegel geplaatst zodanig dat een lichtstraal afkomstig uit een naaste-buurpunt over een hoek van 90 graden naar links of rechts afgebogen wordt. De twee mogelijke oriëntaties van de spiegels komen voor met waarschijnlijkheden p en $1 - p$. Een baan is een gesloten pad waarin een lichtstraal rond beweegt. Door het plaatsen van de spiegels wordt het rooster in banen verdeeld, zodanig dat in de limiet $N \rightarrow \infty$ het aantal banen per roosterpunt gelijk is aan $p(1 - p)$.
8. Zoals het woord hoogleraar al aangeeft zijn de didactische kwaliteiten van een hoogleraar minstens even belangrijk als zijn wetenschappelijke kwaliteiten.
9. De intelligentietests waarvan in sommige selectieprocedures gebruik wordt gemaakt zeggen vaak meer over het gebrek aan intelligentie bij degenen die deze tests toepassen dan over de geschiktheid van de kandidaten.
10. Indien het aantal bij een proefschrift te voegen stellingen werd teruggebracht tot één, zoals in België gebruikelijk is, zou dat de kwaliteit van die stelling ten goede komen.

Dirk Jan Bukman, februari 1992.